NOVEL SCHEMES FOR TIME–DIVISION–MULTIPLEXING OF HIGH–SPEED OPTICAL SIGNALS

A THESIS SUBMITTED
TO THE BOARD OF STUDIES
IN ELECTRONIC ENGINEERING AND THE GRADUATE SCHOOL
OF THE CHINESE UNIVERSITY OF KONG HONG
IN PARTIAL FULFILLMENT OF THE REQUIREMENTS
FOR THE DEGREE OF
MASTER OF PHILOSOPHY

By: Ka Suen LEE
Supervisor: Dr. C. T. SHU

August 1995

Acknowledgments

It is a pleasure to thank my supervisor Dr. C. T. Shu for his invaluable advice and guidance throughout this research project. I am grateful to Dr. L. K. Chen and C. K. Chan in the Department of Information Engineering at The Chinese University of Hong Kong for valuable suggestions and technical supports, respectively. The technical assistance from W. S. Chan and H. S. Choy are also highly appreciated. I am particularly grateful to my parents and all members of my family for their continuous encouragement throughout the whole period of my studies.

Ka Suen LEE

Abstract

Two novel multiplexing schemes for the generations of high-repetition-rate optical pulse train and array of spatial channels for the high speed time-division multiplexing (TDM) communications have been realized and experimentally demonstrated. The first scheme is constructed by using the optical loop mirrors for fiber based communications, and the second scheme is designed with the free space optics for high speed operations of two-dimensional array devices. We called these schemes "Optical Loop Mirror Multiplexer (OLMM)" and "Optical Matrix," respectively. In the OLMM, the multiplying configuration consisting of a parallel connection of several optical loop mirrors has been investigated. This scheme is shown to has higher reliability and can produce more even output pulses. It is suitable to be used as an all-optical clock multiplier and will has potential applications in space-division multi-channel parallel processing. With the use of fiber switches, the configuration can be converted into a high speed optical bit pattern generator. A mathematical series describing its operation is also derived. In the optical matrix, a two-dimensional array of sequentially delayed optical pulses has been generated. The required time delays among the optical elements can be precisely adjusted and each output has the same state of polarization as the input pulse train. The physical dimension of this matrix can be controlled for matching with the photodetector and switching arrays and there is no time jitter among the matrix elements. This optical matrix is suitable to be used in SDMA, TDMA and WDMA for high speed optical communications, parallel processing, and the waveguide or free-space optical interconnects under three proposed operation modes.

CONTENTS

Chapter I Introduction

In this chapter, the evolution of transmission medium, from copper coaxial cable to optical fiber, in the physical layer of a communication network is introduced in section 1.1. Two approaches in the use of lightwave technologies for optical networks are also described. In section 1.2, the historical developments in the lightwave systems, and the corresponding technical improvements for supporting such developments are briefly described. In section 1.3, several basic architecture of a network are discussed. Finally, the motivation of the researches in this thesis is described in section 1.4.

1.1 The evolution of communication networks

The evolution of the physical level in a communication network which underpins all the other functions of the system has undergone three stages. In the first generation, the fiber is not used. In the second generation, the optical fiber is used as replacement for copper wire. In the third generation, the fiber characteristics are exploited. The first two stages represent the "classical" evolution, whereas the third represents the "nonclassical" step. In the first-generation network, the bitrate is from few kilobits per second in the old commercial telephone systems up to a few megabits per second in the coax-based local area networks (LAN). In the second-generation network, the copper wires are directly replaced by the fiber-optic medium. The bandwidth in the system has been increased and the error rate has gone down. The typical example in this generation is the Fiber Digital Distribution Interface (FDDI) which is essentially a large 100 Mb/s LAN. In the third generation, the bandwidth, error-rate performance and propagation delays in the network are further improved by minimizing the number of electrical-to-optical and

optical-to-electrical conversions. Such network has been called "all-optical" network, because there are only two conversions between photons and electrons at the receiver and transmitter. Besides, the electronics in the node deals only with its own traffic, without regard to the traffic of other nodes in the network, therefore it can allow the extremely high throughput for the whole optical network with modest speed electronics, and without large amount of logical complexity and parallelism.

The *classical approach* in the use of lightwave technologies is to consider the detailed design already in the existence and to improve the performance of the network by using optical fiber. The network designers try to improve, for example, the point-to-point trunks and the token ring computer networks by upgrading the copper wire connections to the optical fiber connections for the growing traffic demands, whereas the scientists and engineers try to develop the high-speed lasers, the ultra-high bandwidth photodetectors, the faster time-division multiplex, demultiplex, and switch electronics to meet the network requirements. In the *nonclassical approach*, the viewpoint of the designers and engineers is on the higher-level network functions, which include the new possibilities of system capacity, reliability, and flexibility during the fiber-optic transmission. This required functions lead the scientists to exploit the characteristics and intrinsic parameters of the optical fibers for high-speed communications.

1.2 The development of lightwave communication systems

The lightwave communication is only 27 years old, but it has a great impact on all branches of information transmission, from spans of a few centimeters to intercontinental distances. This technology is expected to take over the role of guided transmission by copper wires and the unguided free-space radio and infrared

transmissions. This revolutionary technology has many unexploited opportunities for future communication networks: the greater bandwidth, the lower attenuation, the lower bit error rate, and potentially the lower costs. Figure 1-1 summarized the developments of the single link fiber optic transmission capability. The growth in system performance is caused by the introduction of new technologies.

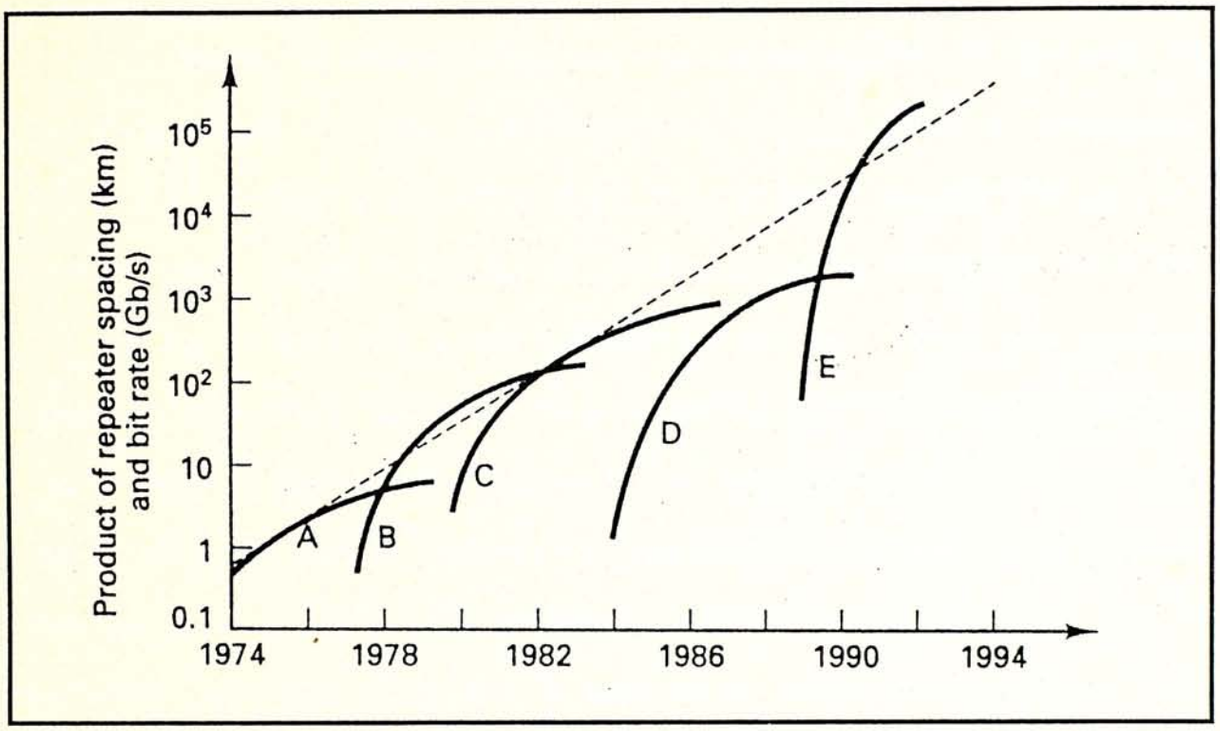

Figure 1-1. The growth history of the single link fiber-optic transmission capability expressed in product of inter-repeater spacing and bitrate [1].

(A) Multimode fiber with 0.85 μm laser,

(B) Single-mode fiber with 1.3 μm laser,

(C) Single-mode fiber with single frequency 1.55 μm laser,

(D) Coherent detection substituted for direct detection at 1.55 μm, and

(E) Erbium-doped fiber amplifiers (EDFA) substituted.

In the first-generation lightwave system, the optical sources were AlGaAs lasers and light-emitting diodes (LEDs) at operation wavelength of 0.85 μm, the photodetectors were PINs and avalanche photodiodes (APDs), and the transmission medium was the multimode optical fiber. The multimode fibers were extremely

attractive in this generation because their large core-diameter (about 50 μm) can make the optical coupling to LED or laser diode, and the fusion splicing in the fiber joints fairly easy, although its intrinsic loss and dispersion are greater than the performance of single-mode fibers. The most important dispersive mechanism in the multimode fiber is the modal dispersion.

In the second generation lightwave system, the single-mode fiber and 1.3 μm wavelength lasers were used. The transition to the longer operation wavelength was due to the lower loss in the optical fiber. Even in the multimode fiber used in the earliest system designs, increasing the operation wavelength from 0.85 μm to 1.3 — 1.6 μm can enhance the system transmission rate and increase the loss-limited transmission distance. The low fiber loss (about 0.6 dB/km) roughly compensated for the modest output power of LED at 1.3 μm wavelength, this LED system makes the loss-limited transmission distance comparable to that of laser system operated at wavelength of 0.85 μm. The advantages in this LED system are low cost, high reliability and simple design, so it is attractive for commercial applications. In the single-mode optical fiber, the optical loss is significantly lower than that of the multimode fiber even at the same wavelength, it is due to the reduction of Rayleigh scattering losses because of lower doping density in the fiber core. The typical spectral attenuation of single-mode fiber is shown in figure 1-2. In the consideration of the laser, the most important features are the capability of being directly modulated at high speeds and the oscillation in single transverse mode, preferably TEM_{00} mode, because higher order modes are different to be coupled to the fiber.

In the third-generation lightwave system, the operation wavelength of the optical sources was shifted to 1.55 μm in order to achieve the maximum loss-limited

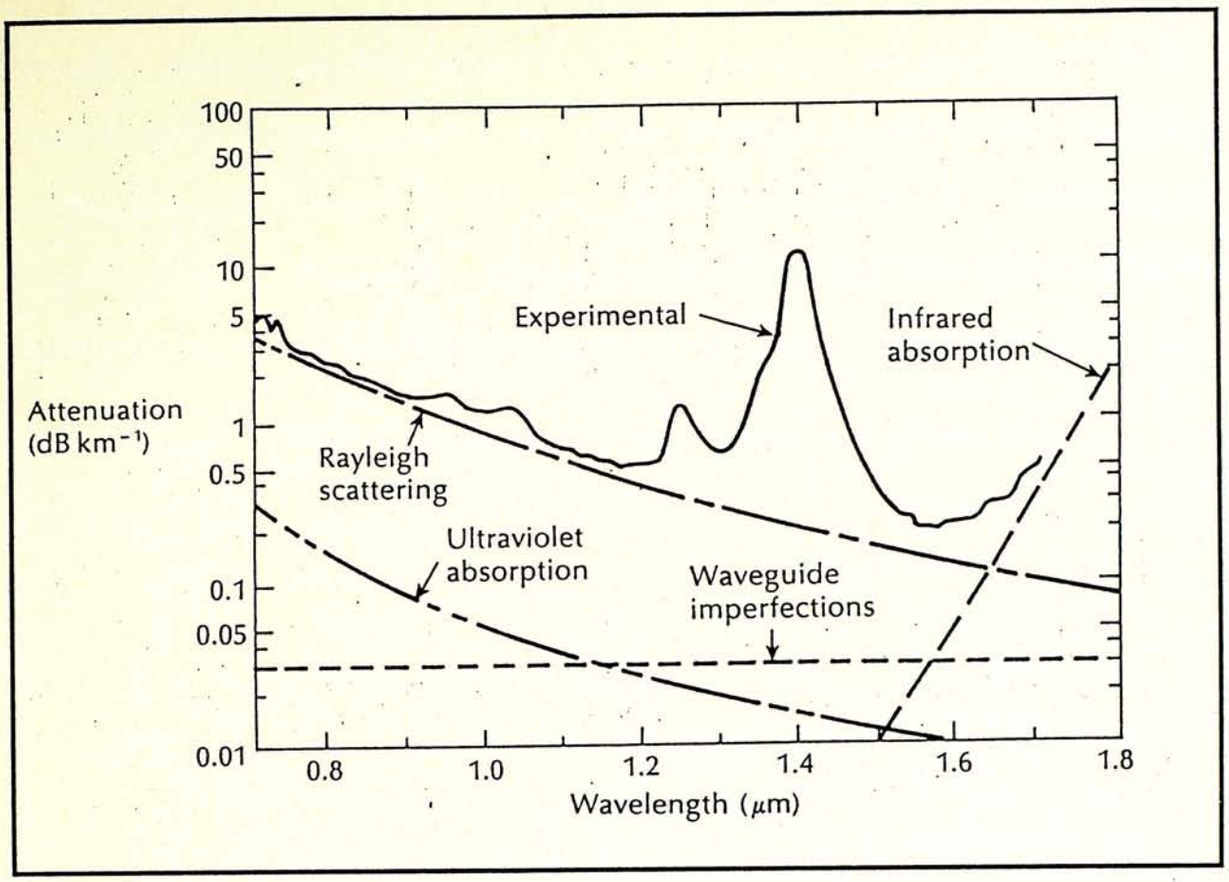

Figure 1-2. The spectral attenuation for high-quality single-mode optical fiber [2]. The fiber loss, which is dominated by Rayleigh scattering and vibrational absorption, reaches the minimum point in the wavelength of 1.55 μm. Two absorption peaks are due to the absorption of OH ions.

transmission distance. It is because the smallest attenuation in the fiber is at 1.55 μm. The attenuation constant is about 0.22 dB/km as shown in figure 1-2, which is about half as large as that at 1.3 μm. Therefore the loss-limited transmission distance can be simply doubled for the 1.55 μm systems. However, the dispersion problem is arisen in the optical fiber and the dispersion coefficient D is about 17 ps/km·nm. The controlled-dispersion fiber and single-frequency laser are the solutions for such problem. In the controlled-dispersion fiber, the waveguide dispersion can be enhanced with special fiber design, so the sign of this dispersion can become negative which is opposite to that of the material dispersion. With

precisely choosing the fiber parameters, the waveguide dispersion and the material dispersion can be made to cancel each other, and a special fiber called "dispersion-shifted fiber" is produced for 1.55 μm. In these fibers, both the attenuation and dispersion can be minimized at same operation wavelength. The typical refractive index profiles of them are shown in figure 1-3. Besides, the used lasers should have

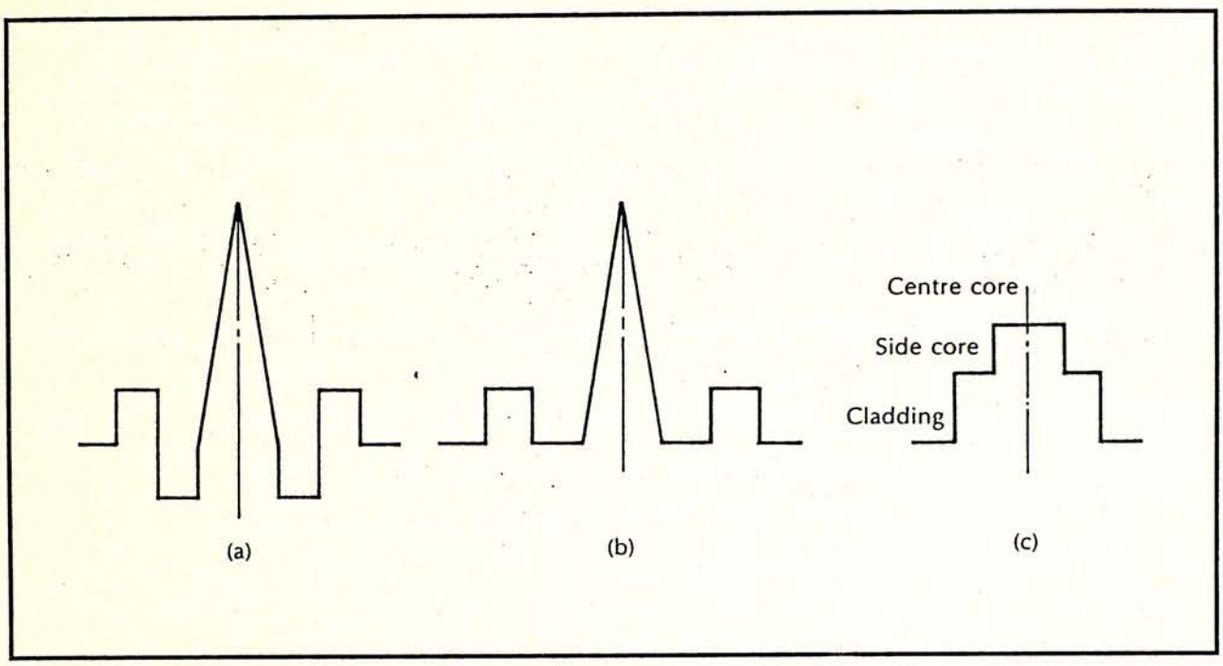

Figure 1-3. The refractive index profile of the fiber core in single-mode "dispersion-shifted" optical fiber [2]. (a) triangular profile multiple index design; (b) segmented-core triangular profile design; (c) dual-shaped core design.

a narrow spectral width; these lasers are called "single-frequency laser." It is because only one longitudinal mode in the laser cavity can be oscillated and amplified. This single-frequency effect can be obtained by some special laser structures shown in figure 1-4.

In the forth-generation system, besides using the single-mode fiber and 1.55μm lasers, the significant development in this stage is on the signal detection.

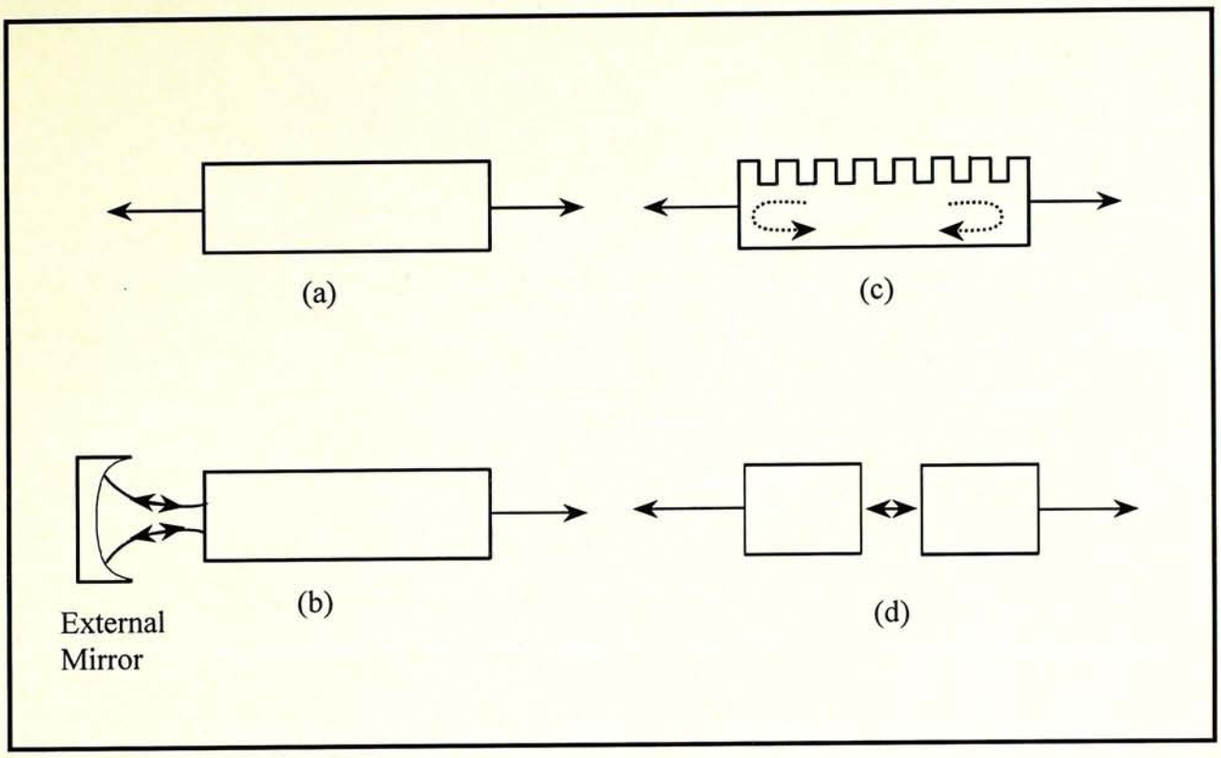

Figure 1-4. The structures for single-frequency lasers: (a) Basic Fabry-Perot cavity, (b) the External cavity, (c) Distributed feedback (DFB), and (d) Cleaved coupled-cavity (C^3).

methods. The coherent technique was used in the receivers to increase the sensitivity of detection. There are two fundamental processes for this technique: the homodyne (or heterodyne) detection and the direct optical detection [3]. In the direct-detection method, the optical input is detected by the photodetector directly and the detected signal is then amplified by the baseband amplifier. In the heterodyne detection, as shown in figure 1-5, the beam combiner or fiber coupler firstly adds the input optical signal a locally generated optical wave, and then the combined signals are detected with a photodetector. The optical frequency generated from the local oscillator, which is simply a cw laser source, is at about the same frequency of the carrier, so the optical interference is occurred at the beam combiner and both a high frequency and a intermediate frequency components are generated. Only the intermediate frequency is used, and the output photocurrent

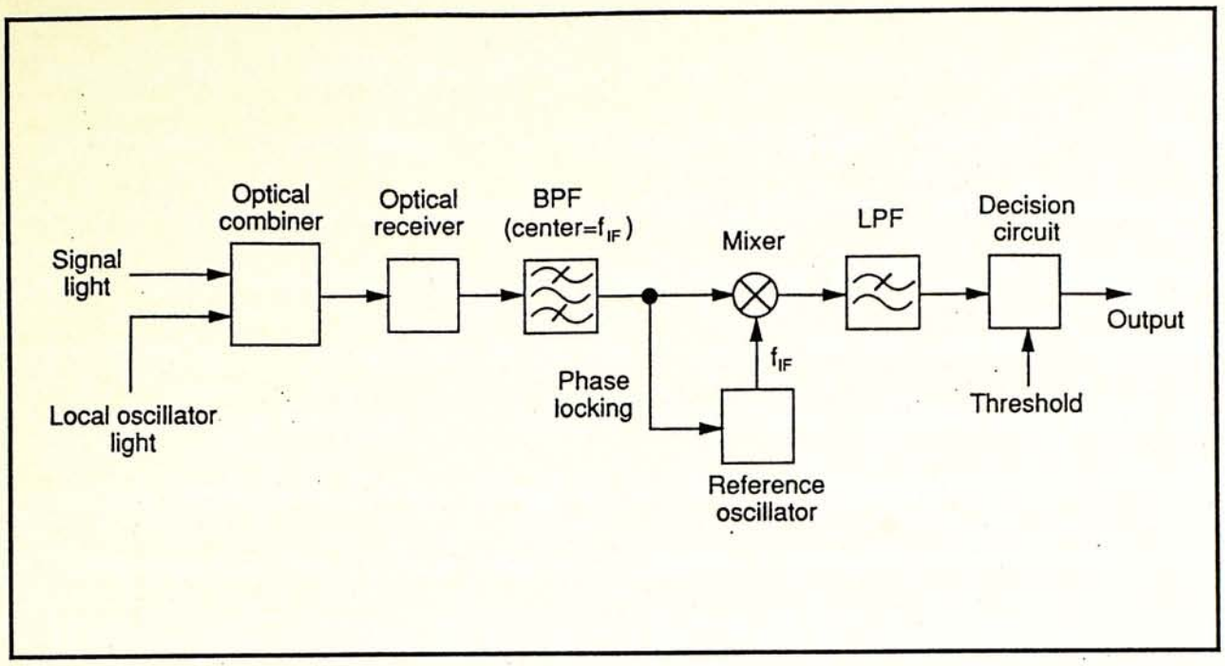

Figure 1-5. Basic configuration of amplitude shift keying (ASK) heterodyne synchronous detection system [4].

from the receiver is at frequency f_{IF}, which is low enough for signal amplification with electronic circuitry. The sensitivity in the detection can be further enhanced by using a phase-locked loop; and the noise in the signal is then removed by a low pass filter. So, finally, the signal can be recovered. Note that the phase-locked loop may not be required in other heterodyne detection methods. In the homodyne detection method, the main difference from the heterodyne detection is that the optical frequency in the local oscillator should be phase-locked to the incoming optical carrier, and the optical frequency of the local oscillator should be same as that in the incoming carrier $f_{LO} = f_s$. So the detected photocurrent is at the baseband frequency and the required signal can be extracted out.

In the fifth-generation system, the erbium doped fiber amplifiers (EDFA's) have been proposed to be used in the optical networks. Recently, numerous laboratories have already demonstrated the potential applications of the amplifier in

both digital and analog transmission systems. The EDFA's have the significant contributions in extending the unrepeatered, unamplified transmissions spanning several hundred kilometers, and will also become a important device in unrepeatered trans-oceanic transmission links spanning thousands of kilometers. The pumping wavelengths for the EDFA's are at 980 nm and 1.48 μm, and the corresponding optical sources are high-power InGaAs and InGaAsP semiconductor lasers which are commercially available. Moreover, the EDFA's are intensely used in the high-speed networks and the long-haul communications because its fluorescence band is at 40 nm centered around the 1.55 μm, which is the lowest attenuation wavelength in the single-mode optical fiber. Besides the lowest attenuation, the use of EDFA's can make the transmission system transparent in upgrading the modulation bitrate and increasing the channel wavelength capacity. These features have opened a new perspectives for future practical multi-gigabit, multi-wavelength, and soliton-based communication systems [5-7]. In addition, the continued improvements in design optimization for optical fiber can also support the developments of the innovative designs for EDFA's in various future optical network applications.

1.3 System architecture

The system architecture includes three different kinds of structure: (i) The *link* — point-to-point communication, for example, the telephone trunk, (ii) the *multipoint* — single station-to-multistation, such as the cable television distribution systems, and (iii) the *networks* — the any-to-any connections, as typified by the modern computer networks that any node has equal probability in access to any other node. The first two are the subsets of the third structure. The nodes, in general, can be the telephones, personal computers, workstations, terminals, or switches, etc.

With the *link* between two nodes, either unidirectional (simplex) or bi-directional (duplex), the transmitter at one end can send the messages to a receiver at the other end, so there are two parties in the system. The only requirement in the link is to pass the maximum possible optical bits over the greatest distance without the repeaters, and with the minimum possible error rate. The information in this transmission includes the voice bits, data bits, television bits, and those kinds of bits with great loss in the very large traffic aggregation. The link requirements and link technical solutions can be found in the reference [8]. For *multipoints*, there are N nodes or parties in the system, its main application is the one-to-many multimedia distribution. The functions of this distribution include the delivery of entertainment, stock quote information, home television, music, and education applications to the users. In consideration of the bitrate requirements, all digital video data have to be compressed before the transmission. Within 6 MHz channel bandwidth, the NTSC analog channel at bandwidth of 4.2 MHz, the PAL analog channel at 5 to 5.5 MHz, or the compressed High Definition Television (HDTV) digital channel at bitrate of 20 Mb/s with digital vestigial sideband modulation can be delivered to the end users through the network [9-11]. Thus, the multipoint serves the well-focused applications whereas the link only serves the totally unfocused application set. In *network*, the entire array of applications together with the technical requirements at various levels of the system have to be taken into account. The networks do not deliver the high bandwidth to a few users, but provide connectivity in an easy-to-use way to the widest possible community of users. "Easy-to-use" means accessible and affordable. In Ethernet the bandwidth is only 10 Mb/s, but it is needed to be shared for all the attached users in the network with a multiaccess protocol. However, it is ease of attachment, low cost, and with flexible access. In addition, in the recent gigabit applications, each user requires the bitrate up to 1 Gb/s for high-speed data transmissions in the network, for example, supercomputer visualization, medical imaging, multimedia conference, and CPU interconnects. The system

requirements of these applications are listed in the Table I. The available technology in the networks makes it possible to serve a large number of users at the same time within the large available bandwidth of the single optical fiber.

Applications	Bitrate (Gb/s)	Reachability	Packet switch requirement	Bit error rate
Supercomputer Visualization	>1	Low	No	10^{-9}
Medical Imaging	<1	Low	No	10^{-15}
Multimedia Conference	1	High	Yes	10^{-9}
CPU Interconnects	1	Low	Yes	10^{-15}

Table I. The Requirements for four important gigabit network applications.

1.4 The motivation of the researches

With the recently available technologies, one can build a multiple-access network in which the "dynamic" connections between the nodes can be performed by different wavelengths — wavelength-division multiple-access (WDMA), different time slots — time-division multiple-access (TDMA) or different signal waveforms — code-division multiple-access (CDMA) for the high bitrate network applications described in section 1.3. The "dynamic" means that the connectivity can be rapidly changed.

To date, the AT&T, Lincoln Labs. and IBM in U.S.A. have paid a large efforts in the development of WDMA technologies and the construction of the required network testbed [12,13], whereas the researches in NTT of Japan concentrates on the TDMA communications together with the optical soliton transmission [14]. Indeed, two multiple-access schemes can be used together in operation wavelength of 1.55 μm with EDFA's for high speed traffics in the future optical communication networks. In this thesis, I have tried to invent some methods for the time-division multiplexing schemes in high-speed communication systems. Two novel multiplying schemes for several optical channels have already been developed which are explained in the Chapter III and IV.

References

[1] Paul E. Green, JR., *Fiber Optic Networks*, Prentice-Hall, 1993.

[2] John M. Senior, *Optical fiber communications*, Prentice Hall, 1992.

[3] T. Okoshi and K. Kikuchi, *Coherent Optical Fiber Communications*, KTK Scientific Publishers, 1988.

[4] S. Ryu, *Coherent lightwave communication systems*, Artech House, 1995.

[5] M. Nakazawa, "Ultrahigh speed optical soliton communication and related technology," in *tenth international conference on Integrated Optics and Optical fibre Communication (IOOC'95)*, paper FD2-1, vol. 4, pp. 96-98, 1995.

[6] E. Yoshida, Y. Kimura and M. Nakazawa, "Generation of femtosecond pulse train at 20 GHz using an Erbium-doped fiber laser and a dispersion-decreasing Erbium-doped fiber amplifier," in *tenth international conference on Integrated Optics and Optical fibre Communication (IOOC'95)*, paper ThA1-1, vol. 3, pp. 2-3, 1995.

[7] P. Wan and J. Conradi, "Comparison of full duplex 622 Mb/s bidirectional transmission systems employing an open cascade of Erbium doped fiber amplifiers with systems employing isolators," in *tenth international conference on Integrated Optics and Optical fibre Communication (IOOC'95)*, paper ThC3-4, vol. 3, pp. 82-83, 1995.

[8] S. E. Miller and I. P. Kaminow, eds., *Optical Fiber Telecommunications II*, Academic Press, 1988.

[9] D. Anastassiou, "Digital television," *Proc. IEEE*, vol. 82, no. 4, pp. 510-519, 1994.

[10] C. Basile, A. P. Cavallerano, M. S. Deiss, R. Keeler, J. S. Lim, W. C. Luplow, W. H. Paik, E. Petajan, R. Rast, G. Reitmeier, T. R. Smith and C. Todd, "The U.S. HDTV standard: The Grand Alliance," *IEEE Spectrum*, pp. 36-45, April 1995.

[11] T. Chiang and D. Anastassiou, "Hierarchical coding of digital television," *IEEE Commun. Mag.*, vol. 32, no. 5, pp. 38-45, 1994.

[12] I. P. Kaminow and V. W. S. Chan, "Performance of an all-optical network testbed," in *tenth international conference on Integrated Optics and Optical fibre Communication (IOOC'95)*, paper ThC1-1, vol. 3, pp. 62-63, 1995.

[13] F. K. Tong, "Recent developments in optical computer networks," presented in *tenth international conference on Integrated Optics and Optical fibre Communication (IOOC'95)*, paper ThC1-2, 1995.

[14] M. Nakazawa, Y. Kimura, K. Suzuki, H. Kubota, T. Komukai, E. Yamada, T. Sugawa, E. Yoshida, T. Yamamoto, T. Imai, A. Sahara, H. Nakazawa, O. Yamauchi and M. Umezawa, "Field demonstration of soliton transmission at 10 Gb/s over 2,500 km and 20 Gb/s over 1,000 km in the Tokyo metropolitan optical network," in *tenth international conference on Integrated Optics and Optical fibre Communication (IOOC'95)*, paper PD2-1, vol. 5, pp. 21-22, 1995.

Chapter II Theories

The researches in this thesis are concentrated on the time-division multiplexing technologies for the high-speed optical communications. In this chapter, the theories of the time-division multiple-access is introduced in the first section, and the operations on a 2 × 2 fiber coupler acted as a basic building block of the multi-node optical network or the conventional time-division multiplexer is discussed in the second section.

2.1 The optical time-division multiple-access

In a high-speed optical time-division multiplexing communication network, each physical link can carry a number of access paths concurrently for a society of users, so these access paths should be distinguished from one to others. In figure 2-1, the capacity of the transmission medium is subdivided into several time slots, and each slot is assigned to one user. With the same bitrate, if the duration of each time slot is reduced by using the shorter optical pulses, more users can be connected to the network. The protocol based on this communication approach is called time-division multiple-access (TDMA). The signals agreed by the communication parties in the physical layer of a network is needed to be distinguished from other connections, so the users' time slots have to be well-defined and a good synchronization in the network is required. In the high speed communications or the recent gigabit applications, the TDMA approach can support their requirements on bitrate by using the high-repetition-rate optical pulse train with ultrashort pulses for these channels. Several methods for the generation of ultrashort pulses or compression of an optical pulse are proposed [1,2]. Although the nonlinear effects

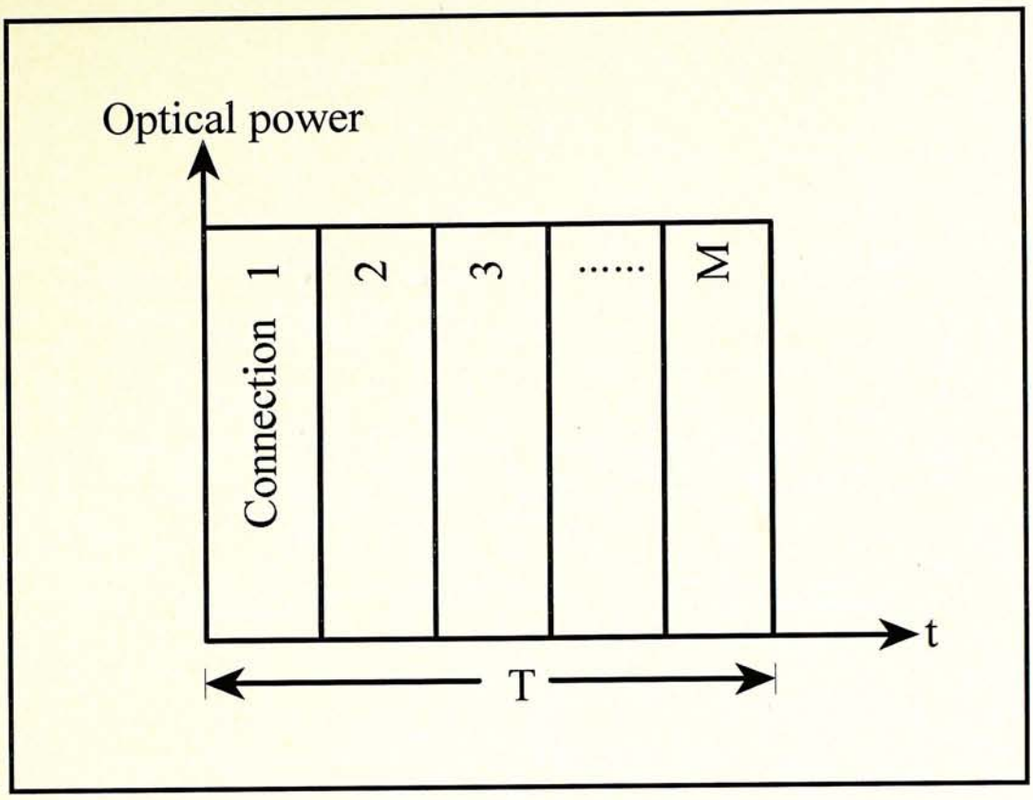

Figure 2-1 *The time-division multiaccess protocol (TDMA). There are M time slots in the time frame with duration T.*

in optical fiber can degrade the efficiency of TDMA communications, by using the self phase modulation together with the group velocity dispersion, an optical soliton can be generated and applied in this high-speed networks. Some soliton transmissions in the high-speed TDMA networks have also been demonstrated recently [3].

In the TDMA system architecture shown in figure 2-2, a system clock or a high-repetition-rate optical pulse train is distributed to the nodes and simultaneously provides the corresponding receiver synchronization. The users' time slots are defined in the provided time frame T, which is the time delay between two clock pulses. If the required duration τ of each time slot becomes shorter, more users can have access to the network. The relationship is given by

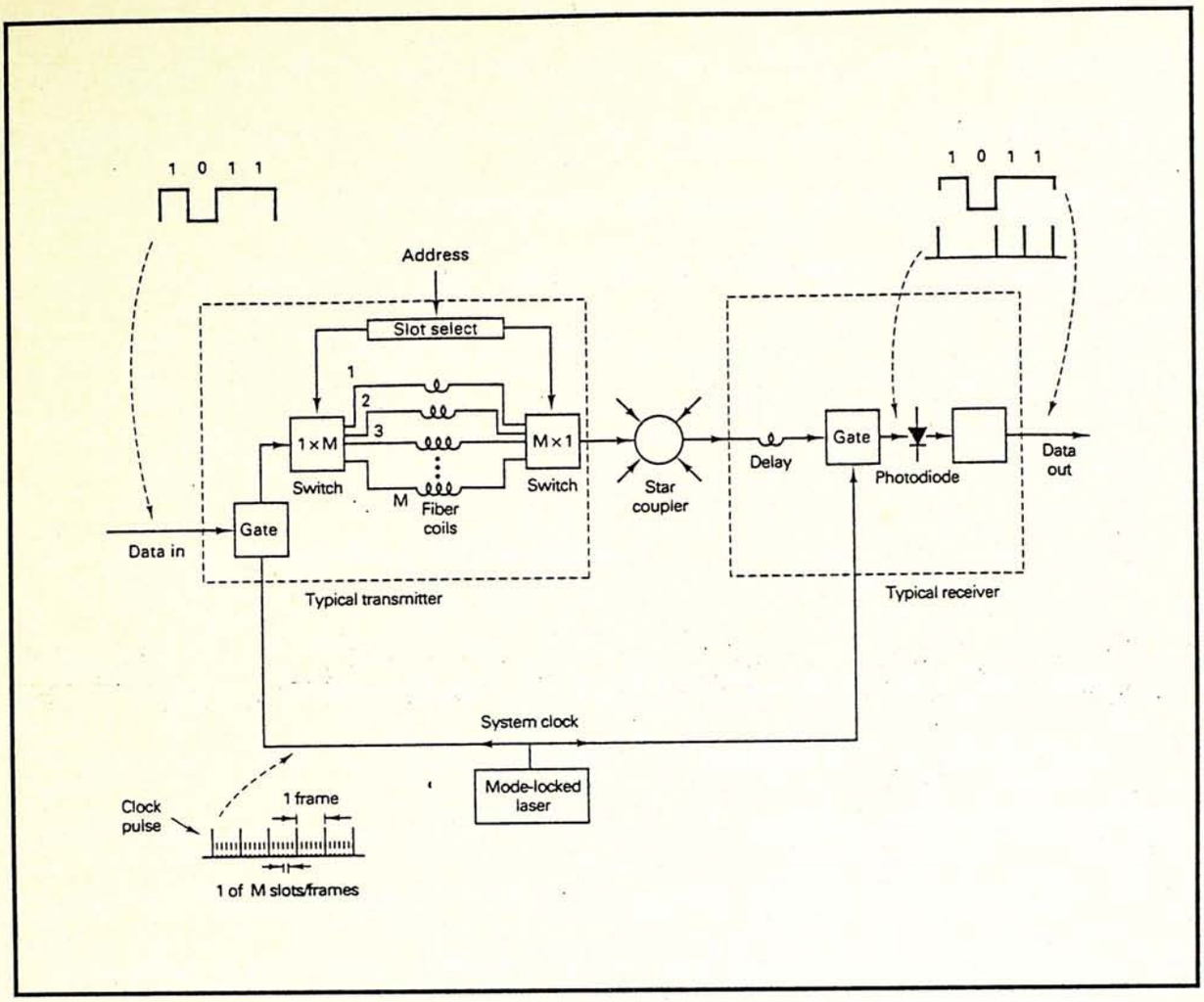

Figure 2-2 The time-division multi-access (TDMA) optical network [4].

$$M \leq \frac{T}{\tau} \tag{1}$$

where M is the total number of the time slots in one time frame T. In the transmitter shown in figure 2-2, a special time slot can be selected from M available optical channels by the input address, then the slot switch would connect the required optical path and the input data can be sent to the star coupler at this selected time slot. A time-division multiple-access coder has also been introduced recently [5], it can be used in the transmitter to select the appropriate time slot in a time frame by the input addresses. After a time delay for data transmission, the receiver can detect

the signals through the operation of the optical AND gate with an input of the synchronized system clock. Recently, the ultra-high speed all-optical time-division demultiplexer has been demonstrated for this purpose [6]. In synchronization of the network, the time jitter of optical pulses has to be controlled in order to increase the efficiency of the TDMA communications.

2.2 The operations of 2 × 2 fiber coupler

The 2 × 2 fiber coupler is a basic building block for a multi-node optical network and a large n × m coupler array. Its function is to divide the input optical powers into two optical outputs with the predetermined splitting ratio. It can be made by placing two single-mode fibers side by side in a flame and then drawing them away with precise controls. Under this manufacturing process, the optical device is called the fused biconical tapered 2 × 2 coupler. The figure 2-3 shows the configuration of the corresponding fiber coupler. As the tapers are very gradual, a negligible fraction of the input powers can be reflected back to the input ports, and this device is also called directional coupler. The power splitting ratio of the coupler can be varied from zero to unity by changing the length of coupling region Z, the core radius in the coupling region a, and the difference in the core radii in the coupling region Δa during the manufacturing process. Therefore, the power coupling coefficient is given by [7]

$$\alpha^2 = F^2 \sin^2\left(\frac{CZ}{F}\right) \tag{2}$$

where

$$F^2 = [1 + (234a^3 / \lambda^3)(\Delta a / a)^2]^{-1} \tag{3}$$

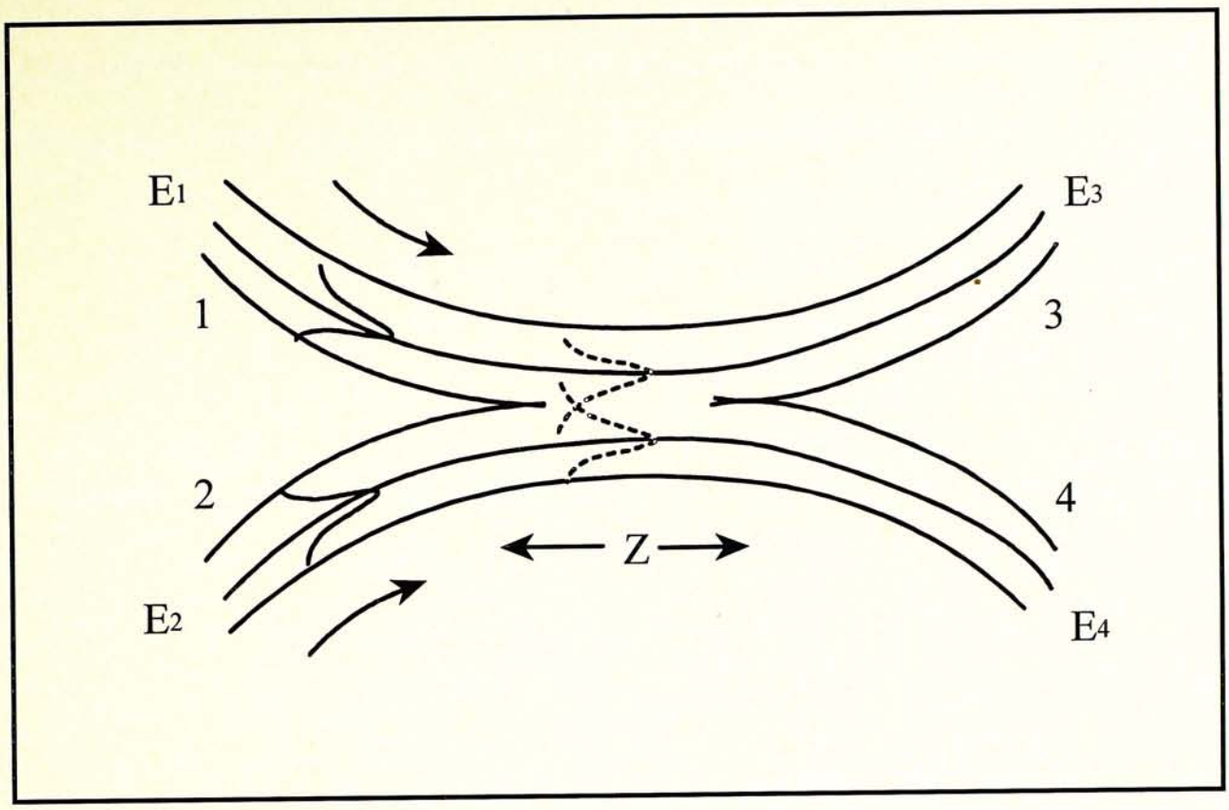

Figure 2-3 *The fused biconical coupler in which the length of the coupling region is Z. E_1 and E_2 are the input field strengths, and E_3 , E_4 are the output field strengths [7].*

and

$$C = 21\lambda^{5/2} / a^{7/2} \tag{4}$$

The parameters F and C indicate the effects on the core-diameter difference and the coupling between the fields of the two fibers, respectively. The α^2 is a sinusoidal function, so the output optical power from ports 3 and 4 can be controlled by properly choosing the parameters of Z, a, Δa and λ. Note that by making the peak of α^2 lie at 1.3 μm and the trough at 1.55 μm, this device can also become a wavelength division demultiplexer in which no optical power in 1.55 μm lightwave is coupled into the adjacent fiber whereas the optical power in 1.3 μm is totally coupled into the another fiber. Besides, to find the phase relationship between the

output field strengths E_3 and E_4 , the scattering matrix S is required to be introduced for the input field strengths E_1 and E_2. The operation of this matrix is

$$E_o = S\,E_{in}, \quad \text{where} \quad E_{in} = \begin{bmatrix} E_1 \\ E_2 \end{bmatrix} \quad \text{and} \quad E_o = \begin{bmatrix} E_3 \\ E_4 \end{bmatrix}. \tag{5}$$

The scattering matrix can be expressed as

$$S = \begin{bmatrix} \sqrt{1-\alpha} & j\sqrt{\alpha} \\ j\sqrt{\alpha} & \sqrt{1-\alpha} \end{bmatrix} \tag{6}$$

where α is coupling ratio for the optical power of an input wavelength in the fiber coupler. If α is equal to 0.5, a 50/50 coupler is then constructed and S becomes

$$S = \frac{1}{\sqrt{2}} \begin{bmatrix} 1 & j \\ j & 1 \end{bmatrix} \tag{7}$$

Therefore, the 90° phase shift is introduced in the output field strengths E_3 and E_4 in this 50/50 coupler. Recently, the theories and fabrication processes on the single-mode 4×4 fused fiber coupler and the single-mode wavelength flattened $1 \times N$ couplers have also been introduced [8,9], the quality controls in their manufacturing process are more complex. In addition, in the multimode couplers, the coupling mechanism is different from that of the single-mode configuration, because the coupling coefficient α in one mode is different from others in the multimode configuration even at the same wavelength.

References

[1] Eiji Yoshida, Tomoki Sugawa, Yasuo Kimura and Masataka Nakazawa, "A new femtosecond erbium-doped fiber laser with nonlinear polarization rotation," *Optical Amplifiers and Their Applications*, vol.14, paper PD12, pp.384–388, 1993.

[2] J. A. R. Williams, I. Bennion and L. Zhang, "The compression of optical pulses using self-phase-modulation and linearly chirped Bragg-gratings in fibers," *IEEE Photon. Technol. Lett.*, vol. 7, no. 5, pp. 491-493, 1995.

[3] M. Nakazawa, Y. Kimura, K. Suzuki, H. Kubota, T. Komukai, E. Yamada, T. Sugawa, E. Yoshida, T. Yamamoto, T. Imai, A. Sahara, H. Nakazawa, O. Yamauchi and M. Umezawa, "Field demonstration of soliton transmission at 10 Gb/s over 2,500 km and 20 Gb/s over 1,000 km in the Tokyo metropolitan optical network," in *tenth international conference on Integrated Optics and Optical fibre Communication (IOOC'95)*, paper PD2-1, vol. 5, pp. 21-22, 1995.

[4] P. R. Prucnal, M. A. Santoro and S. K. Sehgal, "TDMA fibre-optic network with optical processing," *Electron. Lett.*, vol. 22, no. 23, pp.1218-1219, 1986.

[5] P. R. Prucnal, M. F. Krol and J. L. Stacy, "Demonstration of a rapidly tunable optical time-division multiple-access coder," *IEEE Photon. Technol. Lett.*, vol. 3, no. 2, pp.170-172, 1991.

[6] J. P. Sokoloff, I. Glesk, P. R. Prucnal and R. K. Boncek, "Performance of a 50 Gbit/s optical time domain multiplexed system using a terahertz optical asymmetric demultiplexer," *IEEE Photon. Technol. Lett.*, vol.6, pp.98–100, 1994.

[7] Paul E. Green, JR., *Fiber Optic Networks*, Prentice-Hall, 1993.

[8] D. B. Mortimore, "Theory and fabrication of 4 × 4 single-mode fused optical fiber couplers," *Appl. Opt.*, vol. 29, no. 3, pp. 371-374, 1990.

[9] D. B. Mortimore and J. W. Arkwright, "Theory and fabrication of wavelength flattened 1 × N single-mode couplers," *Appl. Opt.*, vol. 29, no. 12, pp. 1814-1818, 1990.

Chapter III Optical loop mirror multiplexer

A novel configuration for the generation of high-repetition-rate optical pulse train is experimentally demonstrated. The set-up consists of a parallel connection of optical loop mirrors. This multiplexer has potential applications in multi-channel parallel processing and in high speed optical communications. With the use of fiber switches, the multiplexer can be converted into an optical bit pattern generator.

3.1 Self Phase Modulation in optical fiber

The self-phase modulation (SPM) is a nonlinear effect in the optical fiber which is caused by the intensity-dependent refractive index change of the optical path. The phase shift of an optical pulse thus becomes intensity-dependent during propagating through this path. In a single-mode optical fiber, as the core has a tiny cross-section area, the light intensity in it is very strong even for a modest input laser power. When the interaction length is long, the SPM becomes significant. The refractive index of an optical fiber is

$$n = n_0 + n_2 I \tag{1}$$

where n_0 is the linear refractive index which is independent on the input intensity I, and n_2 is the Kerr coefficient. Consider a square optical pulse with constant amplitude, when it travels through the fiber with length L, its phase shift is

$$\Delta\phi = \frac{2\pi}{\lambda} L n_2 I \tag{2}$$

respect to the phase with low input intensity. Therefore, for a gaussian-shaped optical pulse, as its intensity profile is a function of time, the transmission phase of the pulse peak should be different from that of the leading and trailing pulse edges. If take the optical frequency of the pulse peak as reference, the frequencies in the leading half of the pulse are reducing, whereas the optical frequencies in the tailing half are increasing. So, the variable frequency shift or chirp is caused and the frequency spectrum of the pulse is broadened [1]. The self phase modulation is very important in the nonlinear-optical loop mirror and the nonlinear amplifying loop mirror.

3.2 Current developments of the optical loop mirror

The nonlinear-optical loop mirror was firstly demonstrated in 1988 [2]. In the following few years, it has found a wide range of applications in high speed communications and optical signal processing. This device is based on the nonlinear lightwave propagation in the optical fiber loop which is formed by connecting the output ports of a 2 × 2 coupler. Its construction is simple and the setup does not require the precisely interferometric alignment in free space. In the operation of the device, when an optical pulse is launched into the 2 × 2 coupler, it is split into two pulses with different intensities, in general. These pulses are then propagated in the opposite directions but with the same optical path. As the optical fiber is a nonlinear medium and the effect of self-phase modulation (SPM) depends on the launched optical power as explained in section 3.1, the nonlinear effect on two pulses will no longer be identical. Therefore, their intensity-dependent phase velocities or phase shifts due to SPM are different after passing through the same fiber length. When these pulses travel back to the fiber coupler, the interference occurs at the coupling region. The emerged power from the output ports depends on

the differences in the accumulated phase shifts between two overlapping fields. So, this device is phase sensitive and the output optical power in two output ports can be adjusted by controlling the phase shifts in two propagating fields. Note that an extra phase shift between two fields is also introduced by the coupling mechanism of the fiber coupler. For the exactly 50/50 coupler, as described in chapter II, the relative phase difference between two output fields is 90° [3].

Figure 3-1 shows the basic configuration of the optical loop mirror. The power-coupling ratio in the fiber coupler is α : (1-α). With the nonlinear effect of SPM, the phase shift acquired on the pulses with field E after propagating the optical fiber with length of L is [2]

$$\phi = \frac{2n_2\pi |E|^2 L}{\lambda} \tag{3}$$

where n_2 is the Kerr coefficient and λ is the input wavelength. The typical value for

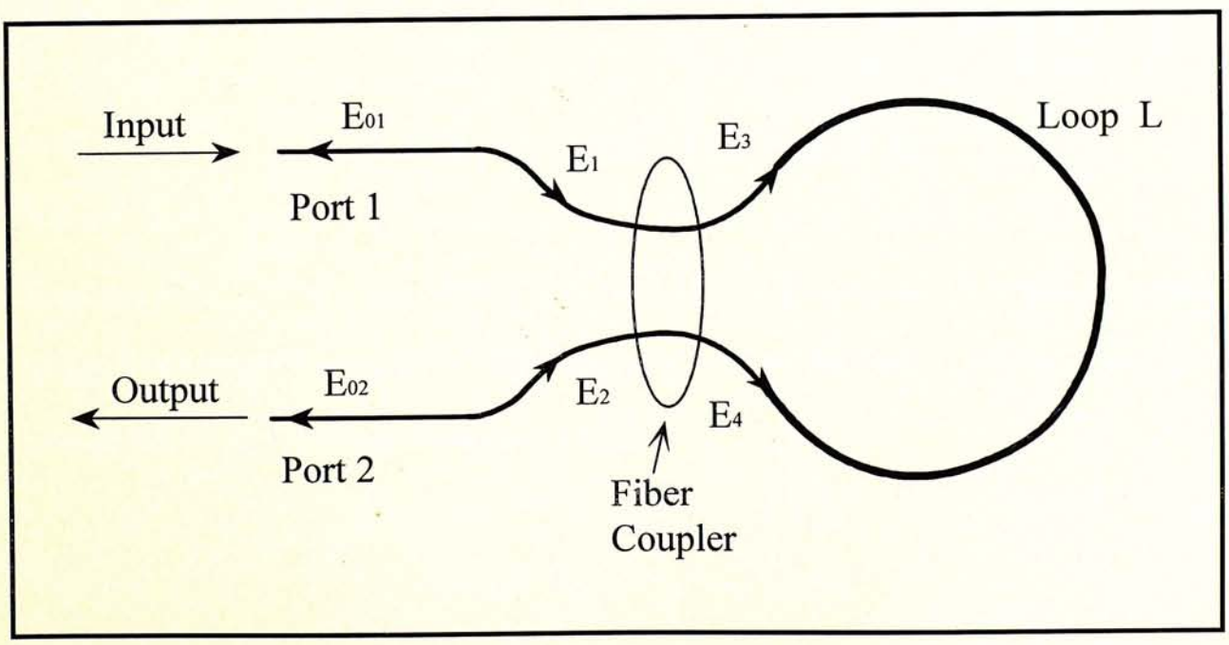

Figure 3-1 The basic configuration of the optical loop mirror [2]. The power coupling ratio of the fiber coupler is α : 1-α.

n_2 is 3.2×10^{-20} m^2W^{-1} in the silica fiber. The relation between the input fields E_1 , E_2 and the output fields E_3 , E_4 of the 2 × 2 fiber coupler is given by

$$E_3 = \alpha^{1/2} E_1 + i(1-\alpha)^{1/2} E_2 \tag{4a}$$

$$E_4 = i(1-\alpha)^{1/2} E_1 + \alpha^{1/2} E_2 \tag{4b}$$

When assuming only one input field E_{in} launched into the fiber loop from port 1, by equations (3) and (4), the optical output power from port 2 is

$$|E_{02}|^2 = |E_{in}|^2 \{1 - 2\alpha(1-\alpha)\{1 + \cos[(1-2\alpha) \times \phi]\}\} \tag{5}$$

To find the boundary cases for the output power, ϕ is defined to be

$$\phi = \frac{2n_2\pi |E_{in}|^2 L}{\lambda} = m\frac{\pi}{1-2\alpha} \tag{6}$$

So the equation (5) becomes

$$|E_{02}|^2 = |E_{in}|^2 \{1 - 2\alpha(1-\alpha)[1 + \cos(m\pi)]\} \tag{7}$$

where m = 0, 1, 2, 3, ……. When m is odd, $|E_{02}|^2$ is equal to $|E_{in}|^2$ and all optical power is emerged from port 2. Whereas if m is even, the output power from port 2 is reduced to the minimum value and equal to

$$|E_{02}|^2 = |E_{in}|^2 [1 - 4\alpha(1-\alpha)] \tag{8}$$

The output power switches from low-value to 100% every when the power increase by λ / [2(1-2α)Ln_2], and the best switching ratio occurs at α closest to 0.5 but the

switching energy increases correspondingly. This switching characteristics in the nonlinear loop mirror is shown in figure 3-2. It should be noted that if a polarization controller is used in the fiber loop, the additional and variable intensity-independent phase changes between two fields can be obtained.

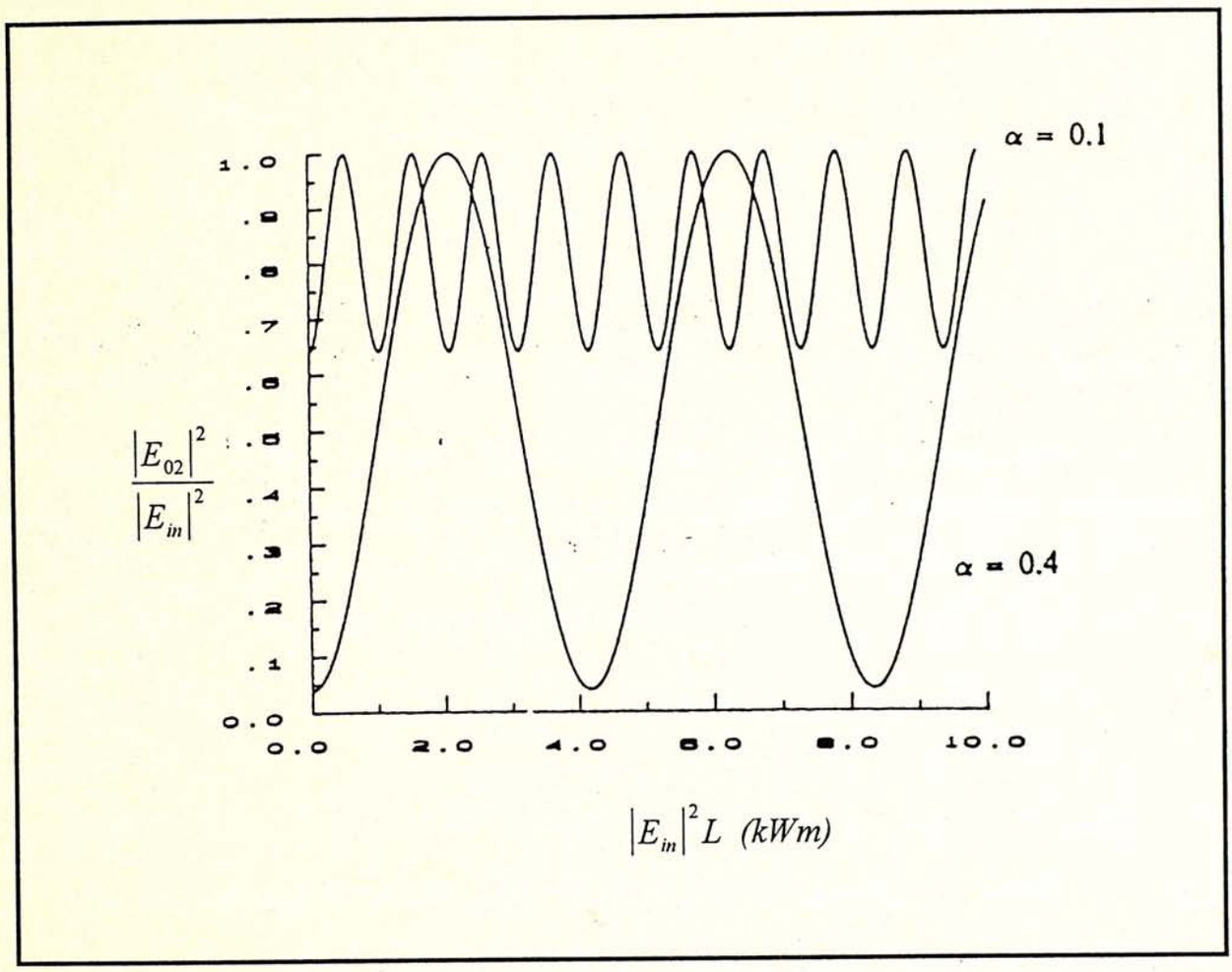

Figure 3-2 The transfer function of the nonlinear-optical loop mirror [2].

In 1990, the another configuration of the nonlinear loop mirror was introduced [4]. It is called the nonlinear amplifying loop mirror (NALM). In this setup, the power-coupling ratio of the fiber coupler is exactly 50:50 but an optical amplifier is inserted into the fiber loop that is located near one end of the coupler. Figure 3-3 shows the corresponding configuration. The switching effect of NALM can be independent on the input power, because the amplifier can generate the high

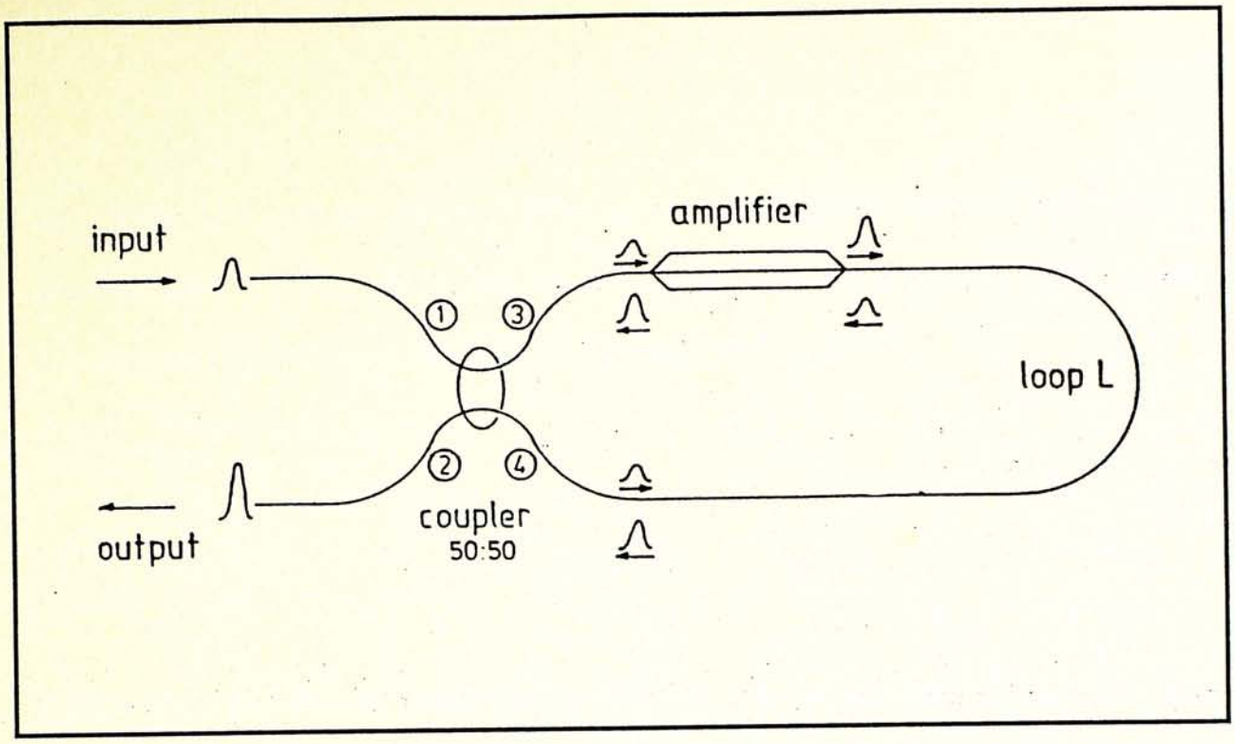

Figure 3-3 *The basic part of the NALM [4]. The signal is launched at port 1, split equally at the 50:50 fiber coupler, and experienced a different phase delay along the two propagation directions owing to the asymmetrically located amplifier.*

optical power to asymmetrically change the nonlinearity of the optical paths for the light propagating clockwise and counterclockwise around the loop. The phase changes in the clockwise and counterclockwise components are determined by

$$\delta\phi_c = \frac{n_2 \pi L}{\lambda} I_{in} g \tag{9a}$$

$$\delta\phi_{cc} = \frac{n_2 \pi L}{\lambda} I_{in} \tag{9b}$$

respectively, where I_{in} is the pulse intensity launched into the fiber port 1, g is the gain of the optical amplifier, L is the fiber loop length and λ is the input wavelength. Therefore, the clockwise-propagating pulse experiences a g-times higher phase delay than the counterclockwise component, and the equations (9) can be expressed as

$$\delta\phi_c = g\delta\phi_{cc} \tag{10}$$

By varying the gain of the amplifier, the phase difference between two pulses can be controlled. Besides, the maximum switching of the pulse peak power from port 1 to port 2 can be occurred with the input intensity of

$$I_s = \frac{\lambda}{n_2 L(g-1)} \tag{11}$$

Again, the polarization controller in the fiber loop can also change the phase difference between two pulses.

On the whole, based on the developed theories [2-4], this nonlinear optical loop mirror has been proposed to function as an ultrafast switch [5-8], an optical pulse shaping and compression device [8-10], an optical modulator [11], an extinction ratio improvement device and noise filter [12-13], a bandpass switch [14], a wavelength converter [15-16], and a saturable loss element [17]. Recently, in optical time-division-multiple-access (TDMA) communications, the optical loop mirror has been successfully demonstrated as an ultrahigh speed all-optical demultiplexer in the terahertz domain [18-20]. In this chapter, we try to use a combination of the optical loop mirrors to construct a novel time-division multiplexer to multiply the repetition rate of optical pulses. This multiplexer can overcome the intrinsic problems in the conventional configuration which include the low reliability and the uneven splitting ratio in the output pulses. An optical bit pattern generator based on our new configuration is also proposed. A mathematical series governing the operation of the multiplexer is derived.

3.3 The principle of the novel time-division multiplexer

Our multiplying configuration is shown in figure 3-4. Four optical loop mirrors AC, AD, BC and BD are connected in parallel using single-mode 2 × 2 and 4 × 4 fiber couplers. An optical pulse is launched into the primary 4 × 4 coupler and is split into four equal pulses. Each pulse, after passing through the secondary 2 × 2 coupler, is further split into two pulses. By choosing proper delay paths in the loop mirrors, the eight pulses will travel back to the 4 × 4 coupler at four different

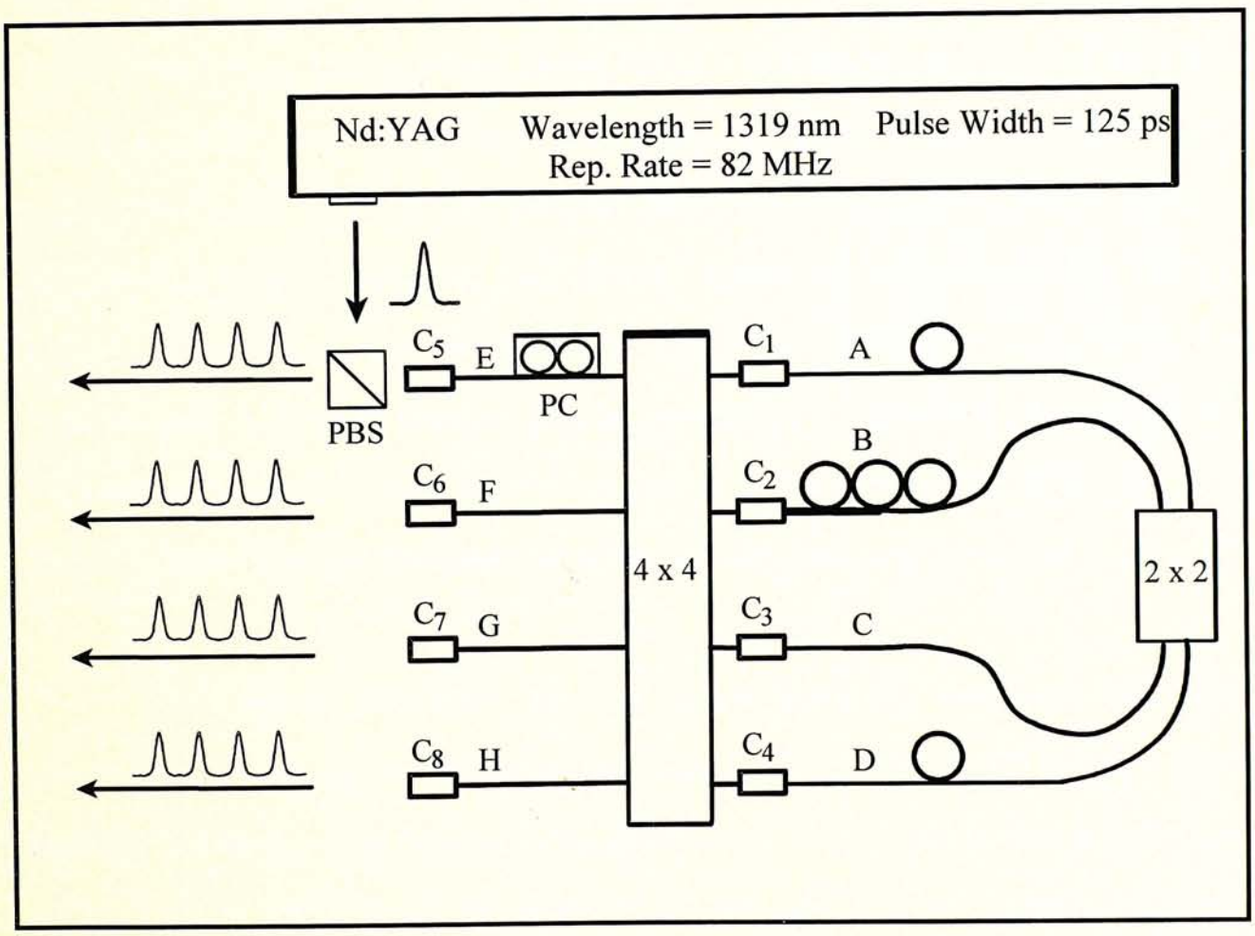

Figure 3-4 *Configuration for the generation of high-repetition-rate optical pulses.*
PBS - polarization beam splitter
PC - polarization controller
C_1 to C_8 - Fiber connectors.

moments. Each of the ports E, F, G and H will carry the same output of four sequentially delayed optical pulses. It is worth to note that the interference effect between the optical pulses in the primary coupler may result in output pulses of different amplitudes. It can be solved by using polarization controllers in the loop mirrors.

3.4 The experiment and results

The optical loop mirror multiplexer (OLMM) is experimentally demonstrated using 125 ps optical pulses from a 1319 nm cw mode-locked Nd:YAG laser at 82 MHz. The theories, operations and setup of this laser are described in the Appendices 1 and 2. The pulses are detected using a 25 GHz photodetector and are displayed on a digital sampling oscilloscope. Figure 3-5(a) shows the four optical pulses generated from the set-up. Four such outputs from ports E, F, G, H are available and they can be used for parallel processing. To generate different optical bit patterns, one can simply disconnect one or more arms in the fiber couplers. Figure 3-5(b)–(f) shows the experimental results obtained with our set-up.

When the signals from the four output ports are combined after the introduction of suitable optical delays, an optical pulse train with 0.3 ns delay time between the neighboring pulses can be generated. The output is shown in Figure 3-6(a). Slight variations in the pulse amplitudes are believed to be caused by imperfect coupling and splitting ratios in the loop mirrors. With the incorporation of high speed optical switches, the pulse train can be converted into 16 data channels for high-bit-rate TDMA communications.

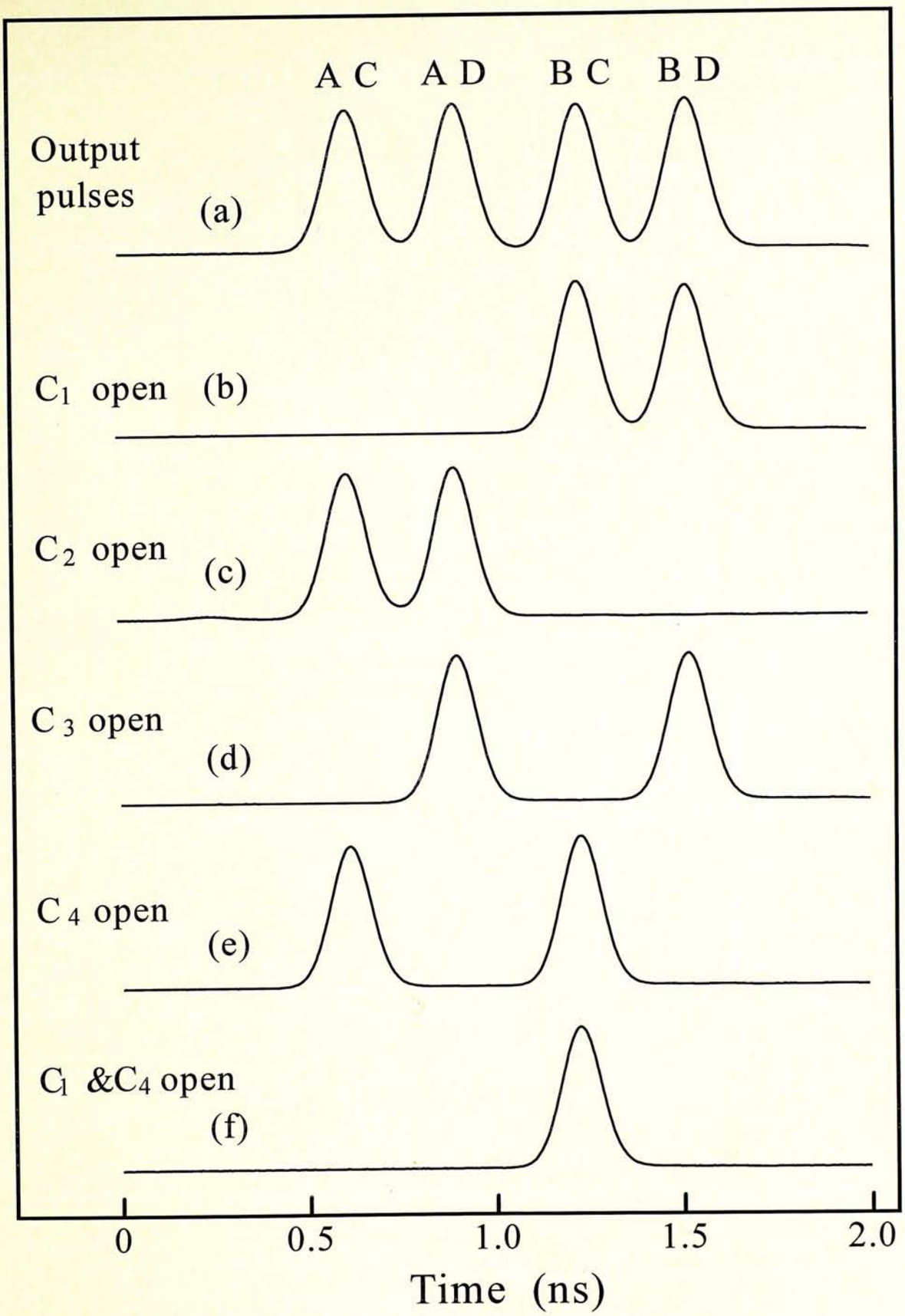

Figure 3-5 *(a) Optical pulse train obtained from an output port with a pulse separation of 0.3 ns. The labels AC, AD, BC, and BD refer to the optical paths of the pulses in the set-up. (b) – (f) Optical bit patterns generated by opening some of the fiber connectors.*

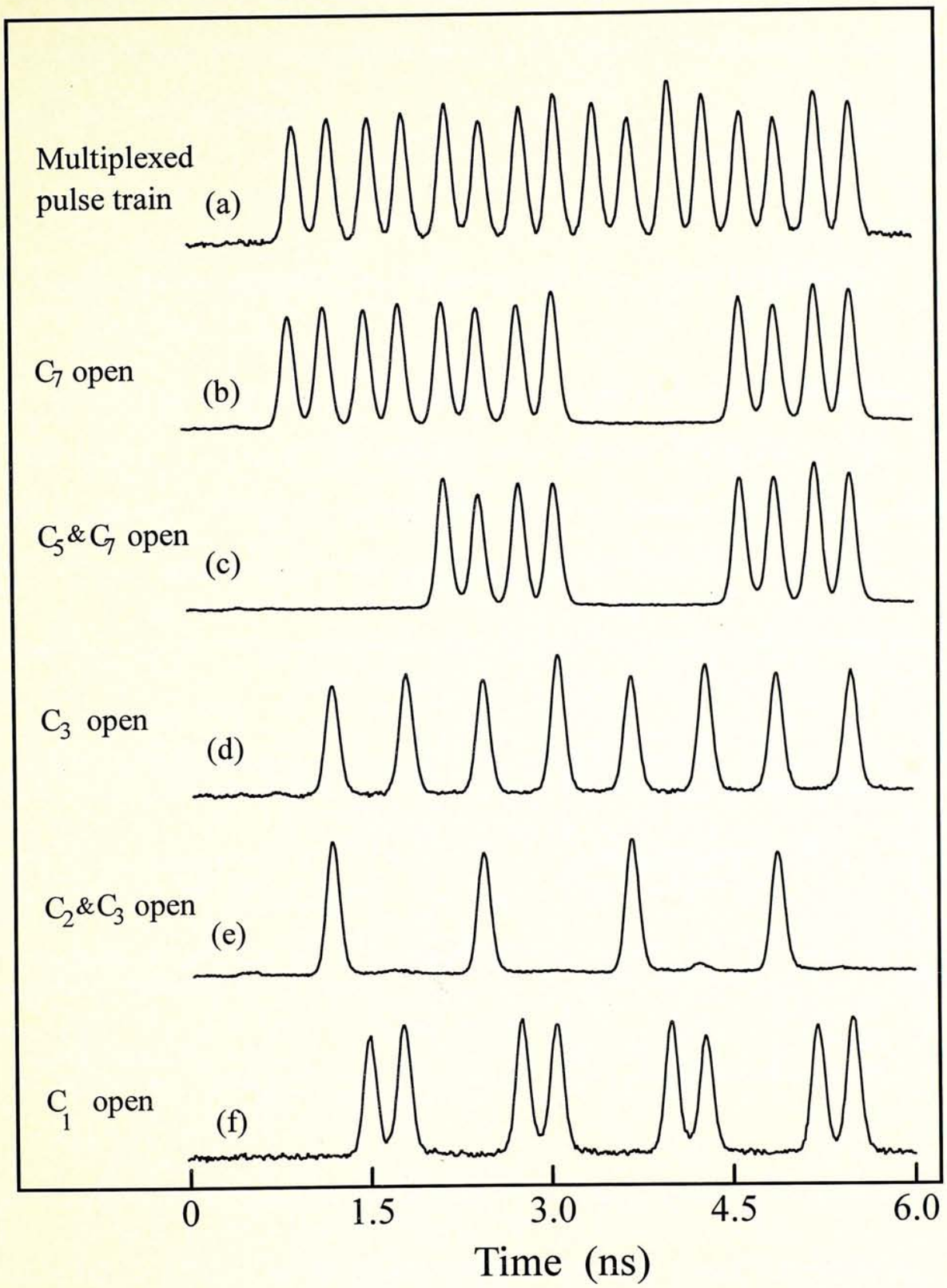

Figure 3-6 *(a) High-repetition-rate time-division-multiplexed pulse train for 16-channel data communications. (b) – (f) Output pulse trains with different burst lengths, bit rates, and bit patterns.*

Again, a number of optical bit patterns can be generated in the multiplexed pulse train. Figure 3-6(b)–(f) depicts the patterns obtained by opening some of the fiber connectors in the set-up.

3.5 Analysis on the splitting ratios of the optical loop mirror multiplexer

In general, the primary 4 × 4 fiber coupler of the OLMM is made by four 2 × 2 fiber couplers [21] or by the fusion process on four optical fibers [22]. The detailed analysis on 16 optical outputs from our novel scheme is shown in figure 3-7, and their optical outputs from the ports E, F, G and H are shown in Table I(a).

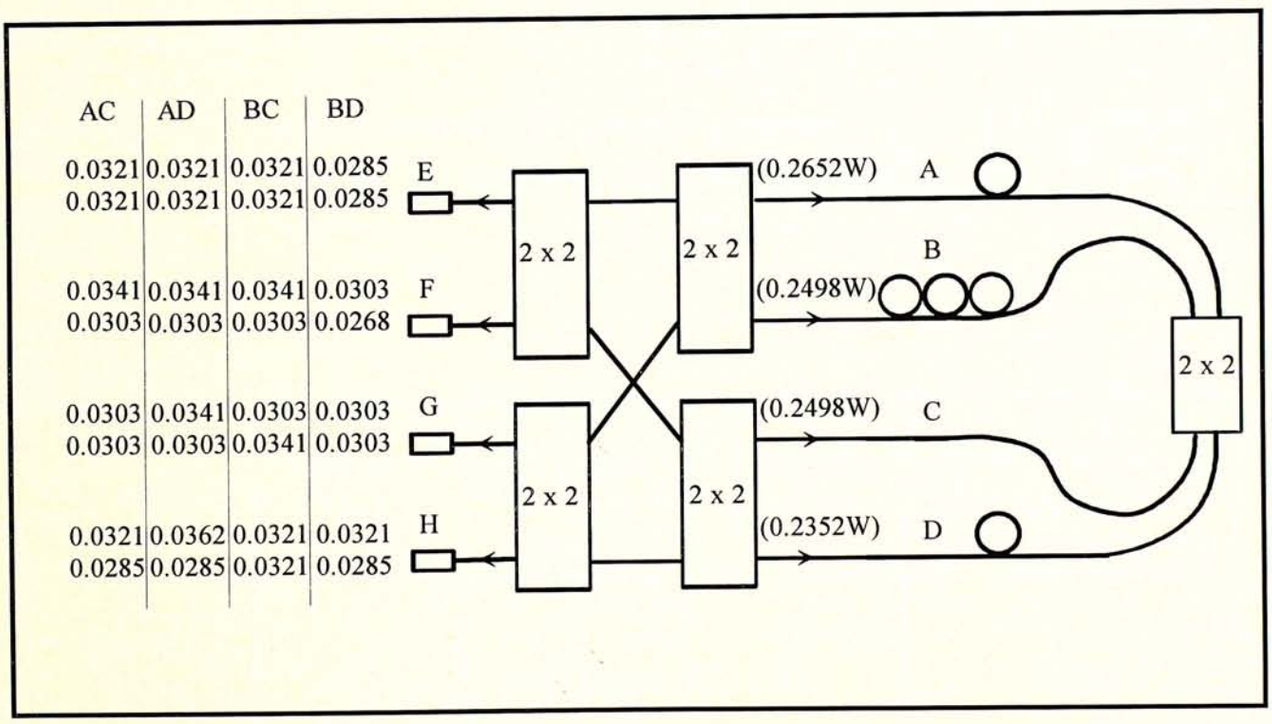

Figure 3-7 *Analysis on the splitting ratios of optical loop mirror multiplexer. Assumed that the optical input is from port E with 1 W peak power and the tolerance on the coupling ratio of each 2 × 2 fiber couplers is ± 3 % [21]. Each one of the 16 optical outputs is the sum of two peak powers from its clockwise and anticlockwise components, which are listed on the left side. The units for all outputs are in Watt and the phases of the pulses are not taken into consideration.*

Note that the maximum tolerance on coupling ratio in a single fused 4 × 4 fiber coupler is same as that used in figure 3-7.

Output Ports	AC	AD	BC	BD
E	64.259	64.259	64.260	**56.991**
F	64.375	64.375	64.375	57.087
G	60.516	64.375	64.375	60.516
H	60.625	**64.723**	64.259	60.625

Table 1(a) *The peak powers of the 16 optical outputs from OLMM. The bold values are the maximum and minimum output powers. All units are in mW.*

	Maximum Outputs (mW)	Minimum Outputs (mW)	Range of deviation (mW)	Range of deviation with power loss in fusion joints (mW)
Novel Scheme	64.7227	56.9907	7.7320	7.3080
Conventional Scheme (four 2 × 2 couplers)	70.3443	55.3308	15.0135	13.7957

Table I(b) *The comparison on the range of deviations in output peak powers between the optical loop mirror multiplexer and the conventional scheme.*

Table 1(b) shows that the range of deviation between the maximum and minimum optical outputs in the novel and the conventional schemes are 7.3080 mW and 13.7957 mW, respectively, and this deviation on the OLMM is only 53 % of that in the conventional scheme. Thus, our scheme can give the more even outputs for time-division multiplexing communications.

3.6 Analysis on the phase of the optical outputs

In consideration of the interference effects on the primary coupler of OLMM, the phase difference between the clockwise and counterclockwise propagating optical fields for each one of the 16 outputs should be taken into account. As the function of the polarization controller is to introduce the phase delay between the orthogonal components on x- and y- axes of an input optical field, the interference effects and the pulse splitting ratios of OLMM can be externally controlled. So, by using the polarization controllers in single-mode fiber loops, the more even output pulses can be simply obtained.

The operation of the polarization controller (PC) is shown as follows: To express the input optical field E as the orthogonal components E_x and E_y on the x- and y- axes in a column matrix

$$E = \begin{bmatrix} E_x \\ E_y \end{bmatrix} \tag{12}$$

the phase delay δ between these orthogonal components can be introduced by the transformation matrix of the PC which is expressed as [23]

$$H = \begin{bmatrix} e^{i\frac{\delta}{2}} & 0 \\ 0 & e^{-i\frac{\delta}{2}} \end{bmatrix} \tag{13}$$

In general, the coordinate system of the input optical fields is different from that of the polarization controller, so the coordinate system is needed to be rotated in order to match with that of the polarization controller. The rotational matrix is thus required and expressed as

$$R(\rho) = \begin{bmatrix} \cos\rho & -\sin\rho \\ \sin\rho & \cos\rho \end{bmatrix} \tag{14}$$

where ρ is the angle between the coordinate systems of the PC and the input optical fields. Therefore, the overall transformation matrix for the polarization controller with respect to the coordinate system of input optical fields is

$$P = R(\rho)HR(-\rho) \tag{15}$$

or in matrix form

$$P = \begin{bmatrix} \cos^2\rho e^{i\frac{\delta}{2}} + \sin^2\rho e^{-i\frac{\delta}{2}} & 2i\cos\rho\sin\rho\sin\frac{\delta}{2} \\ 2i\cos\rho\sin\rho\sin\frac{\delta}{2} & \cos^2\rho e^{-i\frac{\delta}{2}} + \sin^2\rho e^{i\frac{\delta}{2}} \end{bmatrix} \tag{16}$$

This is called the Jone's matrix of the polarization controller.

According to the intrinsic phase relationship on the 16 output pulses shown in figure 3-8, when certain phase delays are introduced on all optical pulses

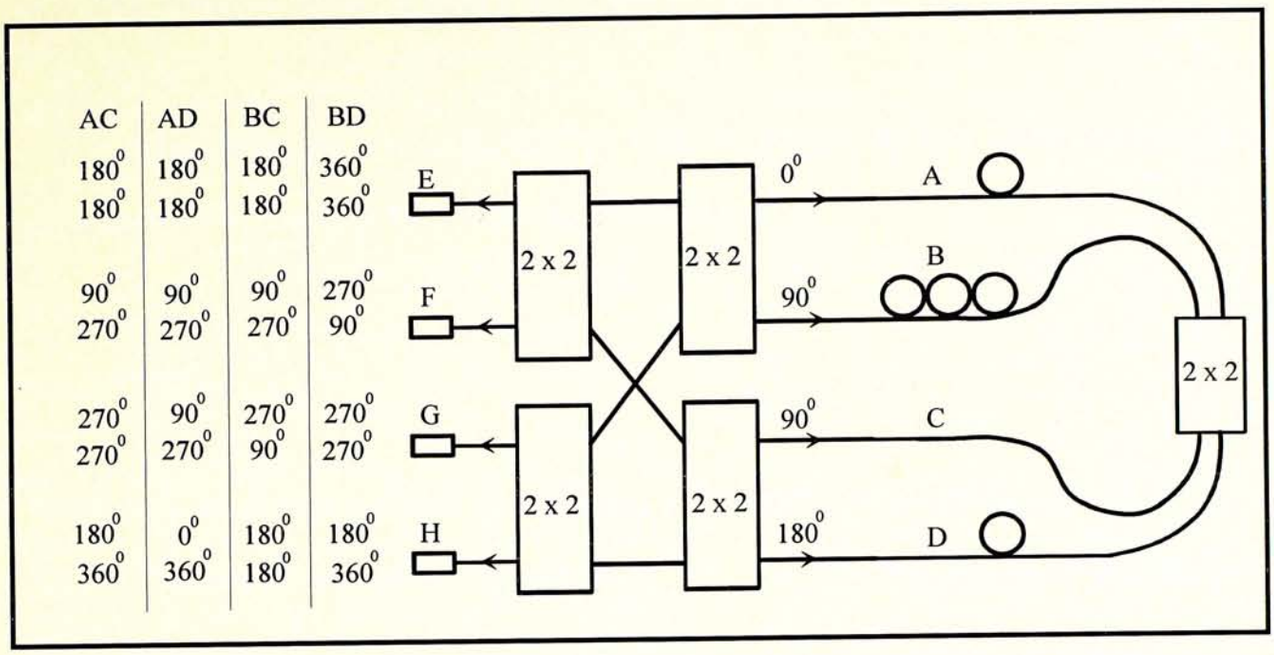

Figure 3-8 *The phase relationships between the clockwise and counterclockwise propagating fields of each one of the 16 optical outputs in the OLMM. The Self-Phase Modulation on the optical fibers is not taken into consideration.*

propagating through the single-mode fibers A and B by the polarization controllers, the amplitudes of the optical outputs can become even. It is because the interference effect of the clockwise and anticlockwise components in each outputs is adjustable. The temperature change and physical vibration are suggested to be minimized for this set-up because the small variation in phase or polarization of the propagating fields might be introduced in the optical fiber. It is worth to note that the polarization controllers on the optical loop mirrors can provide the function of "amplitude equalization" on the time-division optical channels in our novel multiplexer.

3.7 The theories of the optical loop mirror multiplexer

In general, for a $m_1 \times m_2$ primary and a $n_1 \times n_2$ secondary couplers, the input pulse repetition rate will be multiplied by a factor of

$$M = m_2 \times n_1 \times n_2 \tag{17a}$$

where m_1 , m_2 are the number of input and output ports respectively and $m_1 \geq (n_1 + n_2)$. In the special case of $m_1 = m_2 = m$, $n_1 = n_2 = n$, and $m = 2n$, the multiplication factor becomes

$$M = 2n^3. \tag{17b}$$

With the simple configuration, a relatively large multiplication factor can be achieved. The technique is most suitable for use in solid state lasers and in passively mode-locked fiber ring laser [24] which have demonstrated low repetition rates (less than 200 MHz) and high optical peak power (more than 20 W). In order to obtain a background-free pulse signal or the maximum extinction ratio, the time delay between the optical pulses should be equal to or longer than the pulse duration. Table II summarized the expected outputs for several combinations of the optical loop mirror multiplexer.

When m and n are replaced by A_{k+1} and A_k respectively, an optical loop mirror multiplexer series can be constructed as follows: the zeroth order multiplexer is represented by a primary $A_1 \times A_1$ and a secondary $A_0 \times A_0$ couplers, the 1 st order multiplexer is represented by a primary $A_2 \times A_2$ and a secondary $A_1 \times A_1$couplers, and so on. In general, the k th order multiplexer consists of a primary $A_{k+1} \times A_{k+1}$ and a

Primary Coupler m × m	Secondary Coupler n × n	Input Repetition Rate (GHz)	Input peak Power (W)	Multiplication factor $M = 2n^3$ (for m = 2n)	Output peak Power (W)	Output Repetition Rate (GHz)
4 × 4	2 × 2	0.1	100	16	6.250	1.6
6 × 6	3 × 3	0.1	100	54	1.852	5.4
8 × 8	4 × 4	0.1	100	128	0.781	12.8
12 × 12	6 × 6	0.1	100	432	0.231	43.2
16 × 16	8 × 8	0.1	100	1024	0.098	102.4

Table II. *A summary on the optical outputs for several loop mirror configurations*

secondary $A_k \times A_k$ couplers. The corresponding multiplication factor M_k is given by $2A_k^3$. By defining $A_k = 2^k \times A_0$, the multiplication factor of the series becomes

$$M_k = 2^{3k+1} \times A_0^3 \tag{18}$$

where $k = 0, 1, 2, 3, \cdots\cdots$ is the general order of the OLMM series. The whole series is shown in figure 3-9. This equation holds for any integer $A_0 \geq 1$. Assume $A_0 = 1$, the zeroth order multiplexer will simply consists of a 2 × 2 coupler, the 1 st order multiplexer is constructed by a primary 4 × 4 and a secondary 2 × 2 couplers, and the 2 nd order multiplexer is constructed by a primary 8 × 8 and a secondary 4 × 4

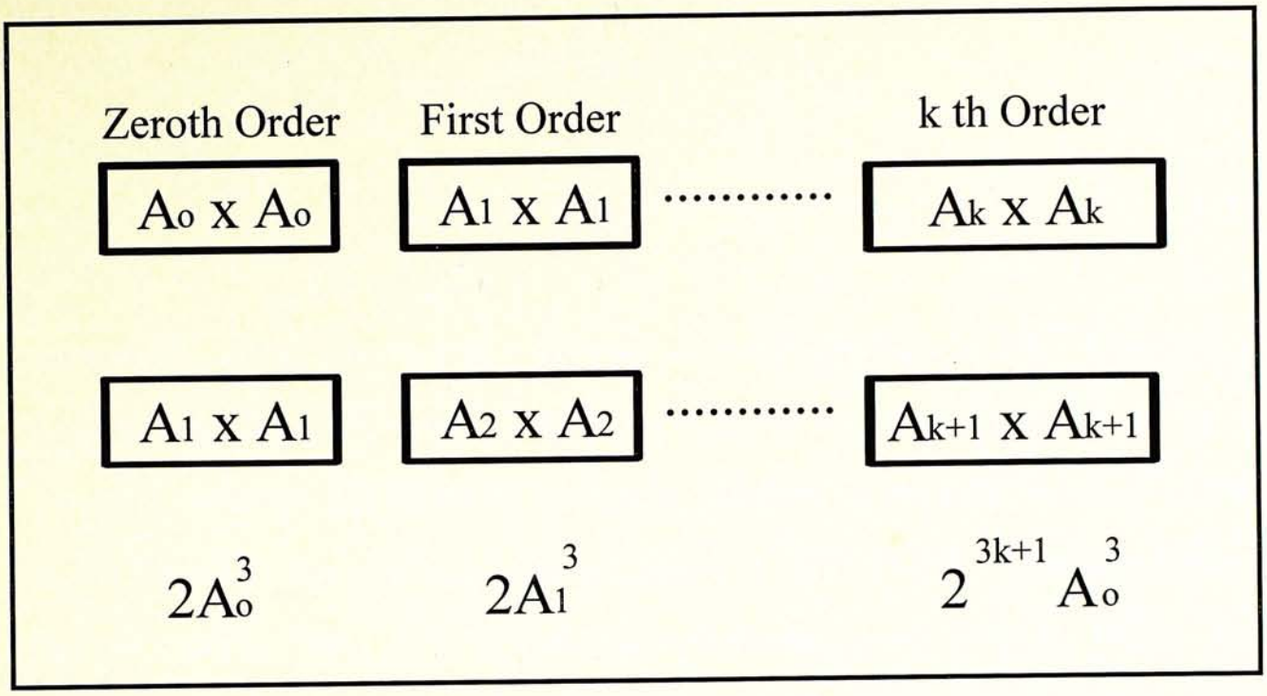

Figure 3-9 The optical loop mirror multiplexer series, where $A_{k+1} = 2A_k$.

couplers, and so on. The multiplication factors are given by 2 ($M_0 = 2^1 \times A_0^3$), 16 ($M_1 = 2^4 \times A_0^3$), 128 ($M_2 = 2^7 \times A_0^3$), ····· , respectively. Note that the whole series of optical loop mirror multiplexers are constructed by commercially available standard star couplers.

3.8 The advantages on the optical loop mirror multiplexer

In the view point of system applications, the network components with higher reliability and better performance are highly desired, so a series of tests should be done for the newly developed devices according to the special network requirements. For the optical loop mirror multiplexer, in consideration of its reliability, if n_b is the number of broken fibers, the maximum penalty in the multiplication factors in equations (17a) and (17b) are

$$M = m_2 \times n_1 \times (n_2 - n_b) \tag{19a}$$

and

$$M = 2n^2 \times (n - n_b) \tag{19b}$$

respectively, where $n_1 \geq n_2 \geq n_b$. Suppose an 8 × 8 primary and a 4 × 4 secondary couplers are used for the multiplying process, as the configuration shown in figure 3-10(a), a multiplication factor of 128 can be obtained. If the input is at 1 GHz, the output repetition rate will be dramatically increased to 128 GHz. In the case when a pair of optical fibers are broken, the maximum penalty is to reduce the multiplication by a factor of 2. Comparing with the conventional technique of concatenating 2 × 2 couplers in series, shown in figure 3-10(b), which in the worst case will not produce any output, our configuration is shown to be more reliable. Higher reliability means lower reduction in the multiplication factors in this multiplexer. The described advantage is also held in the whole OLMM series.

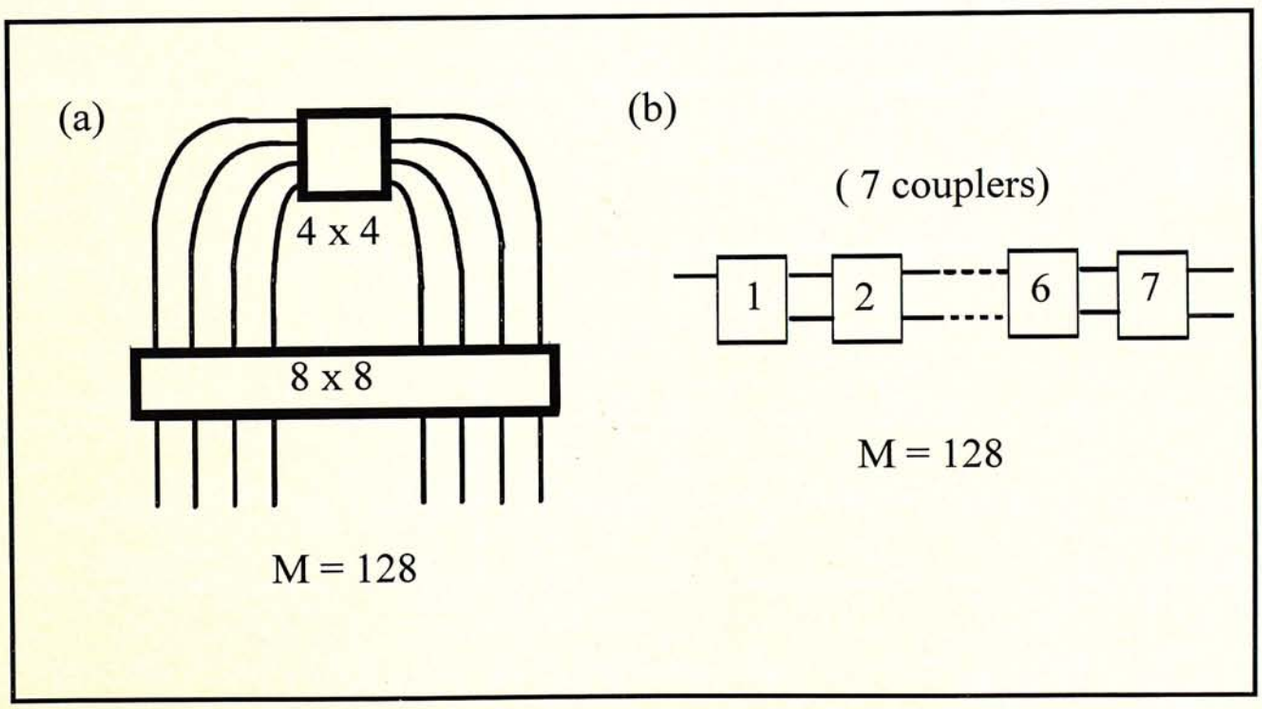

Figure 3-10 The configurations of the novel (a) and the conventional (b) time-division multiplexers with multiplication factor of 128.

In general, the probability of ceasing the multiplying process or reducing the multiplication factor to zero in the novel scheme can be determined by

$$\text{P (no output)} = A \times p^{n_b} (1-p)^{h-n_b} \tag{20a}$$

whereas the corresponding probability in the conventional technique is

$$\text{P (no output)} = B \times p^{n_b} (1-p)^{l-n_b} \tag{20b}$$

where p is the probability of breaking one optical fiber; A , B are the number of cases for ceasing the multiplying processes and h , l are the total number of used fiber in the novel and the conventional schemes, respectively. Table III and figure 3-11 show the comparison on the reliability for two different schemes. Figure 3-11 shows that the reliability of OLMM series is increased quickly when the required multiplication factors become larger, whereas in the conventional scheme, the

	Multiplication factor	2	16	128	1024
Novel scheme	P (no output)	2.97×10^{-4}	1.88×10^{-4}	0	0
Conventional scheme	P (no output)	1.00×10^{-4}	3.77×10^{-4}	6.20×10^{-4}	8.35×10^{-4}

Table III *The probability of ceasing the multiplying processes in the novel and the conventional schemes. Assumed that the probability of breaking* 1 *fiber (p) is 0.01 and the number of broken fibers (n_b) is 2.*

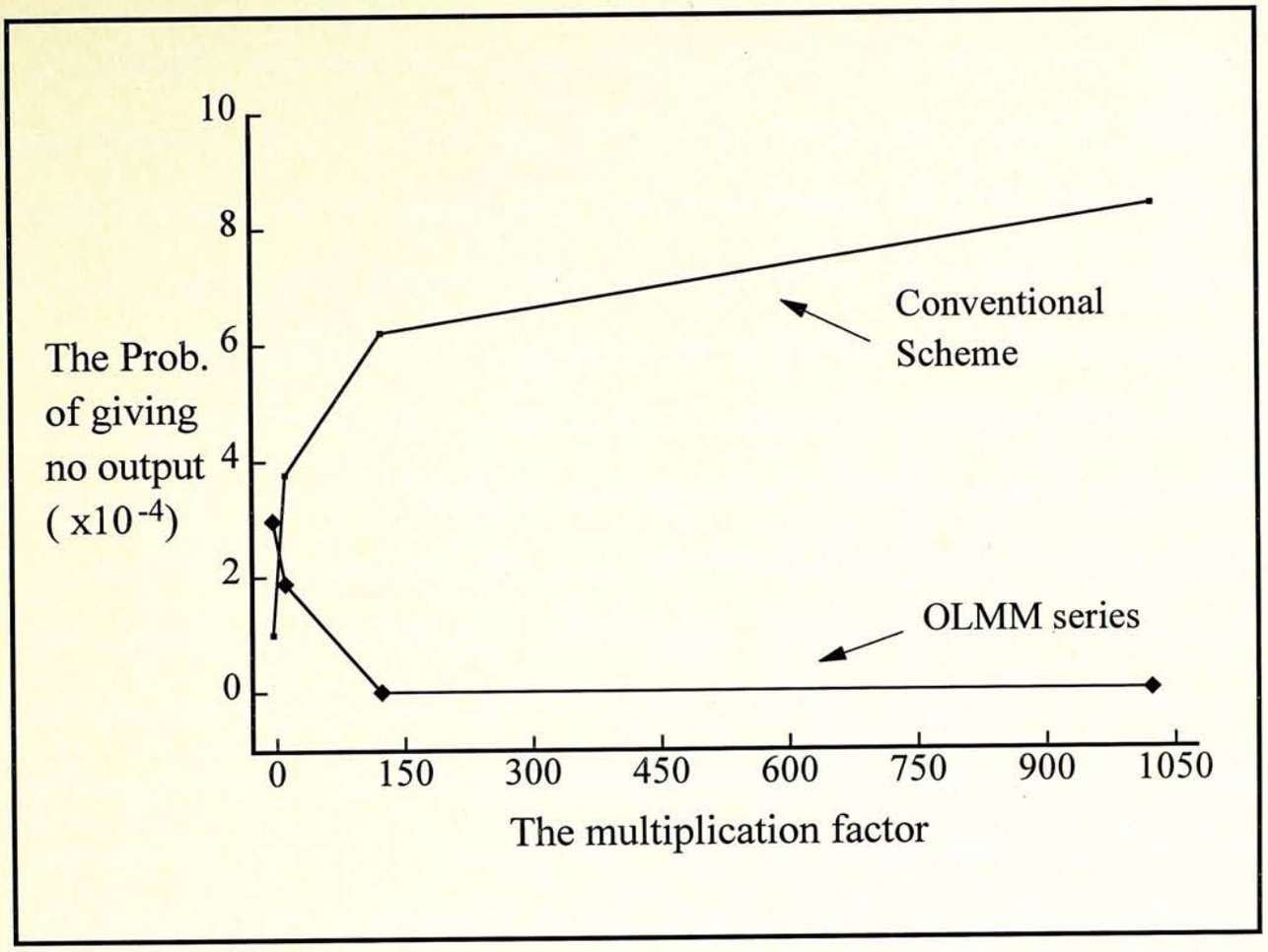

Figure 3-11 Comparison on the reliability of the novel and the conventional multiplying schemes. Assuming that the probability of breaking 1 fiber (p) is 0.01 and the number of broken fibers (n_b) is 2.

reliability is decreasing with increasing the multiplications. So the OLMM series is more reliable.

Besides the reliability, the generation of uneven outputs is also the intrinsic problem of the conventional scheme. In the practical systems, optical pulse train with even outputs is highly desired in the TDMA applications, because if the more uneven pulses are used, higher amplifier gain is needed to preserve the smallest pulse. As the result, the extra amplifier noise will be introduced in the system and the bit error rate (BER) performance will then be degraded. For the conventional multiplexer configuration, as each output pulse should pass through all 2 × 2 fiber

couplers and a large number of fusion spliced joints at the fiber delay paths, the total power loss in the fiber joints together with the accumulated imperfect coupling ratios in a series of couplers would reduce the pulse amplitudes and cause the more uneven outputs. The imperfect splitting ratios on the output pulses can not be externally adjusted and is highly dependent on the qualities of all 50:50 couplers. It should be noted that during the introduction of delay paths, both the quality of fiber splicing and the accuracy of fiber lengths should be precisely controlled at the same moment, so that the average power loss in the fusion splicing should be greater than the mean value of 0.06 dB (P_{out} = 98.6% of the original input) [25]. In our novel scheme, the pulse splitting ratios can be externally controlled by using the polarization controllers in the single-mode fiber loops, the more even output pulses can then be obtained. Even in the multimode configuration, in which no polarization controller is used, the pulse splitting ratio is also more even than the conventional scheme. It is because all output pulses only pass through three fiber couplers and four spliced joints, fewer accumulated imperfect-coupling effects from couplers and less power loss in fiber joints are contributed to the output pulses.

To find the tendency in the deviation of splitting ratios in optical outputs, we take the smallest output pulse into consideration as it is the first bit to be lost in the practical applications. Assuming unity input power, the output power of this pulse is

$$P_S = 2 \times [R_1 \times (1 - T_1)]^2 \times [R_2 \times (1 - T_2)] \times P_{out}{}^4 \tag{21a}$$

and

$$P_S = [R \times (1 - T)]^q \times P_{out}{}^{2(q-1)} \tag{21b}$$

in the novel and the conventional schemes respectively, where *R's* are the ideal power-coupling ratios in the couplers, *T's* are the manufacturing tolerances in the coupling ratios, P_{out} is the average power transmission in fusion spliced joints, q is

the number of 2×2 couplers used in the conventional technique, and the numerical subscripts at the symbols R's and T's indicate the corresponding multiplying stages in the novel scheme. Note that the smallest output estimated in the equation 21(a) for the novel scheme is slightly less than the actual one, because the smallest output pulse is not necessary to be composed with two smallest optical fields as shown in figure 3-7. The factor P_{out} is determined from the average loss L in the fiber fusion joints which is expressed as

	Multiplication factors	2	16	128	1024
	Ideal output power P_{ideal} (W)	0.5	625×10^{-4}	78.1×10^{-4}	9.8×10^{-4}
Novel scheme	Smallest output P_s (W)	0.474	534×10^{-4}	62.7×10^{-4}	7.4×10^{-4}
	P_s / P_{ideal} (%)	94.7	85.5	80.3	75.3
Conventional scheme	Smallest output P_s (W)	0.49	531×10^{-4}	57.5×10^{-4}	6.2×10^{-4}
	P_s / P_{ideal} (%)	98	84.9	73.5	63.7

Table IV *The smallest optical output at various multiplication factors in the novel and the conventional multimode schemes. Assuming that the input peak power = 1 W, the loss in each fusion joint = 0.06 dB (98.6% power transmission), and the tolerances in the coupling ratios of 2×2, 4×4, 8×8, and 16×16 couplers are 2%, 4%, 6% and 8%, respectively [26].*

$$L(dB) = 10\log\frac{P_{in}}{P_{out}} \tag{22}$$

where P_{in} is the input optical power. The comparison in the splitting ratios for two schemes are shown in Table IV and figure 3-12. The normal coupling tolerance in 2 × 2 coupler is ±3% or ± 5%, whereas the premium one has ± 2% tolerance [26]. The tolerance in the premium coupler is used in our estimation. Figure 3-12 shows that in the OLMM series, when the multiplication factor become higher, the deviation in output power of the smallest pulse from the ideal one is increasing slowly. However, in the conventional scheme this deviation is increasing quickly,

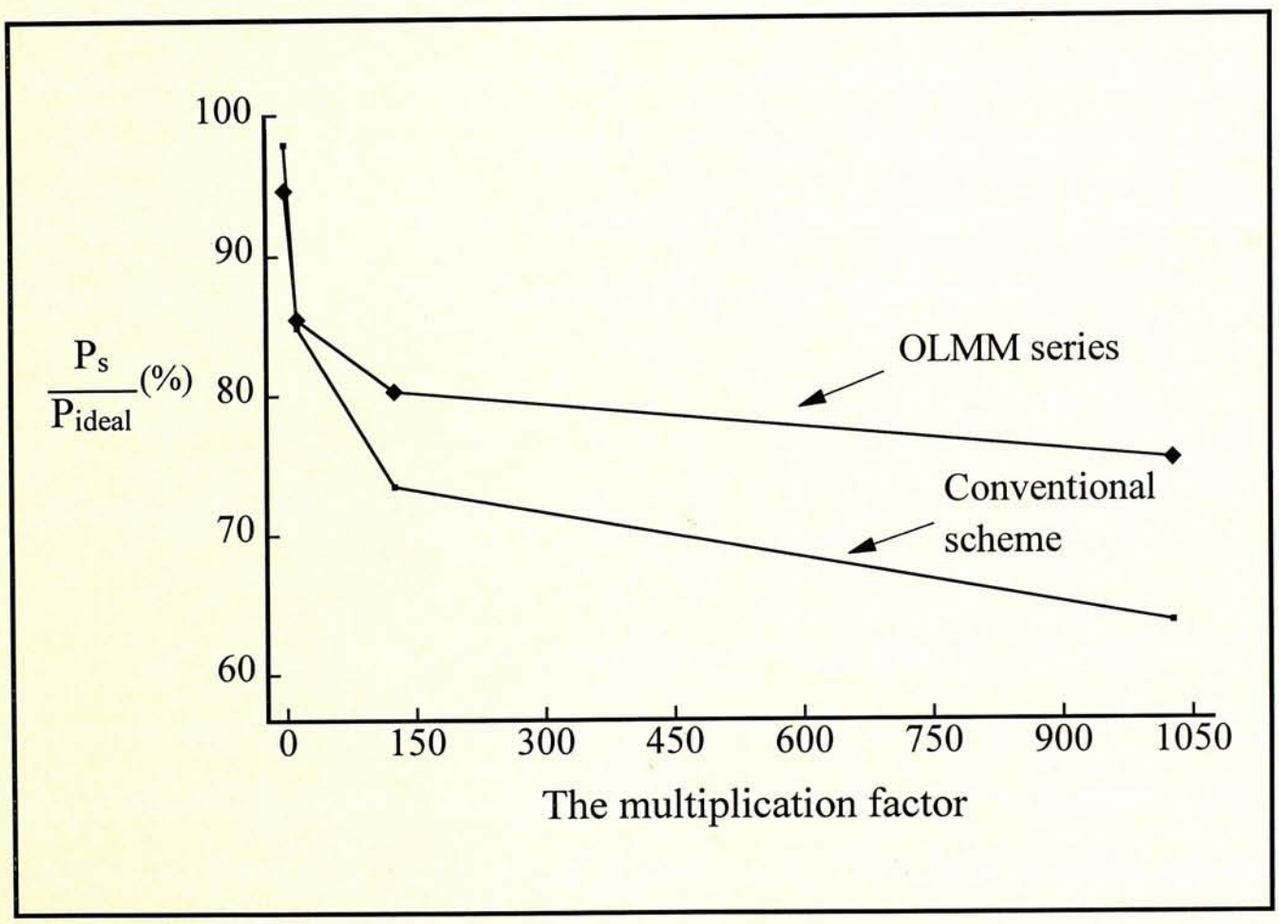

Figure 3-12 Comparison in the splitting ratios of the OLMM series and the conventional schemes. Assuming that the input peak power = 1 W, the loss in each fusion joint = 0.06 dB (98.6% power transmission), and the tolerances in the coupling ratios of 2 × 2, 4 × 4, 8 × 8, and 16 × 16 couplers are 2%, 4%, 6% and 8%, respectively [26].

thus the smallest output may be disappeared when large multiplications are required. Therefore, together with the results described in section 3.5, the optical pulses generated from the OLMM series are shown to be more even as expected, and on the whole, the overall performances of the optical loop mirror multiplexer are better than the conventional configuration.

In addition, when comparing our configuration with the more conventional scheme, which is constructed with the 1 × M and M × 1 star couplers for the multiplication factor of M, although its reliability is greater, its splitting ratios on the output pulses can not be externally controlled and are highly dependent on the coupling tolerance of the fiber couplers. Moreover, when combining the M split pulses to a single output port by the M × 1 coupler for time-division multiplexing operations, the high power loss should be observed in this combiner. This loss is much greater than that in the OLMM because the novel scheme do not require the M × 1 combiner for the multiplying process with multiplication factor of M.

3.9 The optical bit pattern generation

Our set-up can also be converted into an optical bit pattern generator by replacing the fiber connectors with fiber switches. With a primary 4 × 4 and a secondary 2 × 2 couplers, nine possible optical bit patterns can be generated from each of the four output ports. Several selected patterns have been demonstrated and depicted in figure 3-5. In general, with a $m \times m$ primary and a $n \times n$ secondary couplers ($m = 2n$), the number of output bit patterns from an output port or the combinations of the switches being in "off" state is $[\ {}_{2n}C_0 + {}_{2n}C_1 + \cdots\cdots + {}_{2n}C_{2n}\ ]$. However, the combinations with all n switches turned off at one side of the

secondary coupler will produce no output. Thus, the number of possible bit patterns generated from an output port should become

$$N(n) = ({}_{2n}C_0 + {}_{2n}C_1 + \cdots\cdots + {}_{2n}C_{2n-2}) - 2 \times ({}_nC_0 + {}_nC_1 + \cdots\cdots + {}_nC_{n-2}) \qquad (23a)$$

When the signals from all the ports are combined with suitable time delays, the total number of output bit patterns will be

$$N_t(n) = N(n) \times [\, {}_{2n}C_0 + {}_{2n}C_1 + \cdots\cdots + {}_{2n}C_{2n-1} \,] \qquad (23b)$$

In our experiment, 135 possible output bit patterns can be generated. Some of the outputs have been depicted in figure 3-6. If an 8 × 8 primary and a 4 × 4 secondary couplers are employed, a total of 57375 bit patterns can be produced. The repetition rate of the pulse train and the length of the optical bursts can both be controlled by the fiber switches. The features provide added flexibility for applications in high-bit-rate optical communication systems.

3.10 The conclusions of the optical loop mirror multiplexer

In conclusion, a novel configuration for the generation of high-repetition-rate optical pulse train is developed and is experimentally demonstrated. This scheme can be used in both single-mode and multimode fiber couplers. A mathematical series describing the operation of the optical loop mirror multiplexer is also derived. The novel scheme has higher reliability and can produce more even output pulses. This multiplexer is suitable to be used as an all-optical clock multiplier. It will have potential applications in ultrahigh speed TDMA communications and in space-

division multi-channel parallel processing. With the use of fiber switches, the configuration can be converted into a high speed optical bit pattern generator.

References

[1] D. Cotter, "Fiber nonlinearity on optical communication," *Optic. and Quantum Electron.*, vol. 19, pp. 1-17, 1987.

[2] N. J. Doran and David Wood, "Nonlinear-optical loop mirror," *Opt. Lett.*, vol.13, pp.56–58, 1988.

[3] D. B. Mortimore, "Fiber loop reflectors," *J. Lightwave Technol.*, vol. 6, no. 7, pp. 1217-1224, 1988.

[4] M. E. Fermann, F. Haberl, M. Hofer and H. Hochreiter, "Nonlinear amplifying loop mirror," *Opt. Lett.*, vol.15, pp.752–754, 1990.

[5] D. A. Pattison, P. N. Kean, W. Forysiak, I. Bennion and N. J. Doran, "Soliton switching using cascaded nonlinear optical loop mirrors," *Conference on Lasers and Electro-Optics/Europe*, paper CFG3, pp.404–405, 1994.

[6] K. J. Blow, N. J. Doran and B. K. Nayar, "Experimental demonstration of optical soliton switching in an all-fiber nonlinear Sagnac interferometer," *Opt. Lett.*, vol. 14, no.14, pp.754-756, 1989

[7] N. J. Doran, D. S. Forrester and B. K. Nayar, "Experimental investigation of all-optical switching in fiber loop mirror device," *Electron. Lett.*, vol. 25, no.4, pp.267-269, 1989.

[8] B. K. Nayar, N. Finlayson and N. J. Doran, "Concatenated all-optical loop mirror switches," *J. Modern Opt.,* vol.40, pp.2327–2332, 1993.

[9] K. Smith, N. J. Doran and P. G. J. Wigley, "Pulse shaping, compression, and pedestal suppression employing a nonlinear-optical loop mirror." *Opt. Lett.*, vol.15, pp.1294–1296, 1990.

[10] K. Smith, E. J. Greer, N. J. Doran, D. M. Bird and K. H. Cameron, "Pulse amplification and shaping using a nonlinear loop mirror that incorporates a saturable gain," *Opt. Lett.,* vol. 17, no. 6, pp. 408-410, 1992.

[11] K. J. Blow, N. J. Doran, B. K. Nayar and B. P. Nelson, "Two-wavelength operation of the nonlinear fiber loop mirror," *Opt. Lett.,* vol.15, 248–250, 1990.

[12] Bengt-Erik Olsson and Peter A. Andrekson, "Extinction ratio improvement using the nonlinear optical loop mirror," *IEEE Photon. Technol. Lett.*, vol.7, pp.120–122, 1995.

[13] B. E. Olsson and P. A. Andrekson, "Noise filtering with the nonlinear optical loop mirror," *J. Lightwave Technol.*, vol. 13, no. 2, pp. 213-215, 1995.

[14] P. N. Kean, D. A. Pattison, W. Forysiak, I. Bennion and N. J. Doran, "Bandpass switching based on a nonlinear optical loop mirror and an in-fibre grating reflector," *Conference on Lasers and Electro-Optics/Europe*, paper CFG1, p.403, 1994.

[15] D. Mahgerefteh and M. W. Chbat, "All-optical 1.5 μm to 1.3 μm wavelength conversion in a walk-off compensating nonlinear optical loop mirror," *IEEE Photon. Technol. Lett.*, vol.7, no.5, pp.497-499, 1995.

[16] K. A. Rauschenbach, K. L. Hall, J. C. Livas and G. Raybon, "All-optical pulse width and wavelength conversion at 10 Gb/s using a nonlinear optical loop mirror," *IEEE Photon. Technol. Lett.*, vol.6, no.9, pp.1130-1132, 1994.

[17] I. N. Duling, III, C. J. Chen, P. K. A. Wai and C. R. Menyuk, "Operation of a nonlinear loop mirror in a laser cavity," *IEEE J. Quantum Electron.*, vol.30, no.1, pp.194-199, 1994.

[18] J. P. Sokoloff, P. R. Prucnal, I. Glesk and M. Kane, "A terahertz optical asymmetric demultiplexer (OTAD)," *IEEE Photon. Technol. Lett.*, vol.5, pp.787–790, 1993.

[19] J. P. Sokoloff, I. Glesk, P. R. Prucnal and R. K. Boncek, "Performance of a 50 Gbit/s optical time domain multiplexed system using a terahertz optical asymmetric demultiplexer," *IEEE Photon. Technol. Lett.*, vol.6, pp.98–100, 1994.

[20] I. Glesk, J. P. Sokoloff and P. R. Prucnal, "Demonstration of all-optical demultiplexing of TDM data at 250 Gbit/s," *Electron. Lett.*, vol.30, pp.339–341, 1994.

[21] Catalog on *Optoelectronic Components*, Acrotec Optoelectronics, p.8, Nippon Mining Co., Ltd., 1992.

[22] D. B. Mortimore, "Theory and fabrication of 4 × 4 single-mode fused optical fiber couplers," *Appl. Opt.*, vol. 29, no. 3, pp. 371-374, 1990.

[23] R. C. Jones, "A new calculus for the treatment of optical systems I. Description and discussion of the calculus," *J. Opt. Soc. Am.*, vol. 31, pp. 488-493, 1941.

[24] Eiji Yoshida, Tomoki Sugawa, Yasuo Kimura and Masataka Nakazawa, "A new femtosecond erbium-doped fiber laser with nonlinear polarization rotation," *Optical Amplifiers and Their Applications*, vol.14, paper PD12, pp.384–388, 1993.

[25] S. E. Miller and I. P. Kaminow, eds., *Optical Fiber Telecommunications II*, Academic Press, 1988.

[26] Catalog on singlemode fiber optic couplers: Type SF3 and SF4, Canstar, 1992.

Chapter IV Optical matrix for high-speed operation in two-dimensional array devices

A novel scheme for the generation of an optical matrix with an adjustable dimension has been experimentally demonstrated. The matrix consists of sequentially delayed optical pulses suitable for use with two-dimensional array optoelectronic devices. Each output pulse has same state of polarization and there is no time jitter among the matrix elements. This optical matrix can be used in time-division and space-division multiple-accesses. Three operation modes: multiplexing mode, independent mode and broadcasting mode are proposed in this scheme for high speed optical communications and optical parallel processing.

4.1 Recent developments in two-dimensional array devices

The optical fiber has demonstrated many advanced performances in the long-haul communications and the high-speed networks, because it can support several multiple-access schemes for a society of users as described in chapter I. If the optical data bits are transmitted inside a computer, other transmission media and optical sources may be required instead of the fibers and edge emitting laser diodes. It is because the distance of data transmission is short and the parallel data processing is needed for the future high-capacity communication and computational systems. For the optical data transmission between the very-large-scale-integrated (VLSI) chips or several processor layers [1], the proper transmission media are the directly optical interconnections because the electronic interconnections are limited by the speed and power consumption bottlenecks [2].

The optical interconnections can be classified into two types: the waveguide interconnects and the free-space interconnects. In the waveguide interconnects, the dielectric pathways are used for several parallel channels, while in the free-space interconnects, no physical pathway is required. The free-space technique is suitable to be used for parallel processing architectures, such as the plane-to-plane and chip-to-chip connections [3,4], because no mutual interference is introduced in the light beams when they crossed over each other in the free space. Recently, the efficient methods for optical interconnections between several layers of processor arrays have been investigated [5]. These two-dimensional array devices can be used in both waveguide and free-space optical interconnects to replace their electronic counterparts for future high speed computers. In the optical sources, the arrays of surface-emitting lasers integrated with electrical driver circuits are often used. The hybrid integration technology for them has also been developed recently [6]. If the wavelength-division multiple-access (WDMA) applications are required, the surface-emitting lasers can also support its special requirement because they can emit different wavelengths and be fabricated together in a small area [7]. These lasers are expected to be operated at the exact single-longitudinal mode because their ultra-short laser cavities, about 1 μm for wavelength of 0.85 μm, can increase the mode spacing in the laser oscillation. The mode-spacing which is the function of cavity length can be designed to be wider than the gain profile of the active medium, so only one optical frequency can exist in the laser cavity.

With the proposed optical interconnects and the surface emitting laser arrays, the microlens array is also a key component for the multistage optical interconnection networks, because it can collimate the optical outputs from an array of surface-emitting lasers to the array of processors or photodetectors. Several architectures of multistage optical interconnections by array of microlens have been

introduced [8], and the Table I summarized the proposed hierarchy levels for the optical interconnections in parallel processing systems.

Interconnection Level	Techniques
Racks	Optical Fiber
Modules	Optical Fiber/Free-Space
Board	Free-space
Chips	2-D Waveguide

Table I. Interconnections for massively parallel processing [8].

Besides the wavelength-division multiplexing technique, the time-division multiple-access (TDMA) is also very efficient and useful for high-speed data communications. If the TDMA is used in a surface-emitting laser array, the lasers should be operated under a sequential order and the multiple time-delayed electrical pulses for the electrical connections to the laser pixels are required. Thus, the high precision in electrical delay is important in the electrical circuitry for its actual operation. Moreover, as the pulse time jitter is the intrinsic problem of the semiconductor lasers, the delay time in the optical pulses is very difficult to be adjusted and this effect will reduce the efficiency of the time-division multiplexing communications. In this chapter, we proposed a new scheme to generate the sequentially delayed optical pulses with precise time adjustment in a two-dimensional array. There is no time jitter among all the elements in the array. This

optical matrix can be operated in three different modes: multiplexing mode, independent mode and broadcasting mode for high speed optical computing and communications in an optical system.

4.2 The principle of the novel optical matrix

Figure 4-1 shows the setup of the optical configuration. From the top view, when an optical pulse is incident onto the first 50/50 beam splitter, it will be divided into two pulses with equal optical intensities. The first pulse passes through the beam splitter directly, and the second pulse is reflected back to the 100% reflecting mirror M_1. A time delay is introduced in the reflected pulse along the optical delay path ABC. If the angle of incidence at the medium with refractive index of n_1 is θ, the optical delay path will be $2l_1 cos\theta$, where l_1 is the separation between the splitter and the mirror. The corresponding delay time is determined by

$$\Delta t = \frac{2n_1 l_1 \cos\theta}{c} \tag{1}$$

where c is the speed of light in free space. After the reflection, these two pulses will propagate in the same direction and will be further split by a second 50/50 splitter. Therefore, four optical pulses with equal intensities and time delays can be obtained. The sequential order is shown in the output array of the first stage. The multiplying process can be continued to generate a large number of optical pulses in one dimension, the spatial separation between neighboring outputs is governed by

$$\Delta s = 2l_1 \sin\theta \tag{2}$$

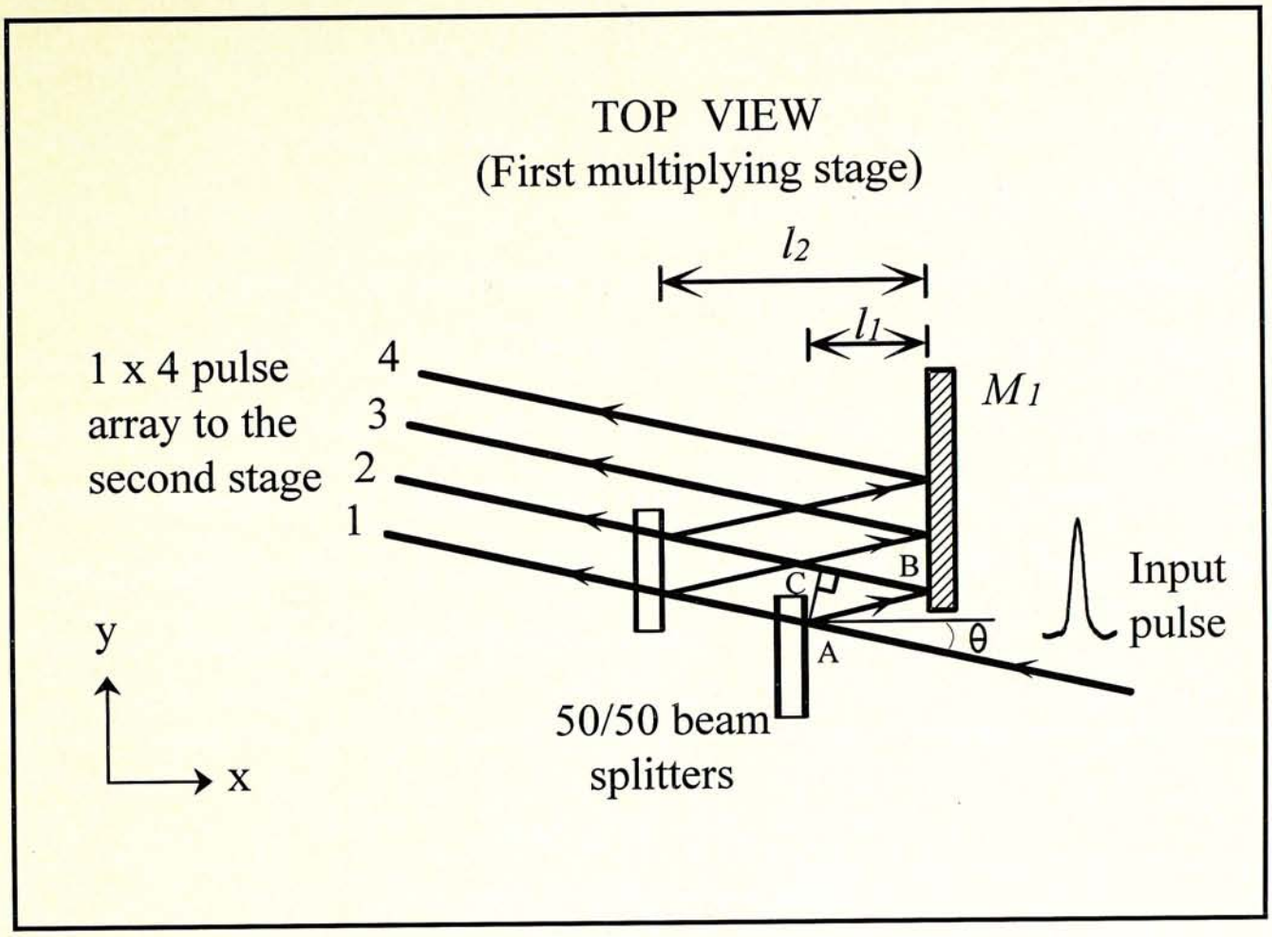

Figure 4-1 *Scheme for the generation of sequentially delayed elements in a 1 × 4 optical array on x-y plane. The sequential order is shown in the output array.*

The relationship between the separations of the splitters and that with the mirror M_1 is given by

$$l_n = 2l_{n-1} \tag{3a}$$

where $n = 2, \ldots\ldots, N_1$. The mirror M_1 provides a reference position in defining the distances and N_1 is the total number of 50/50 beam splitters used in the one-dimensional multiplying scheme.

To construct a two-dimensional matrix, another set of beam splitters and 100% reflecting mirror are employed. The second multiplying stage is illustrated on

the side view of the setup in figure 4-2. The input is now composed of an array of sequentially delayed optical pulses in the horizontal plane. The input array is incident on the (N_1+1) th splitter at the same angle θ. Each of the inputs will be split into two pulses. The set of transmitted pulses forms the first row of the matrix, whereas the reflected pulses are on the second row after they have propagated through the delay path DEF. The time delay is introduced by the separation l_{N1+1} between the splitter and the mirror M_2. The number of rows in the matrix can be further multiplied by using additional 50/50 beam splitters. The distances of the 50/50 splitters from the mirror M_2 are given by

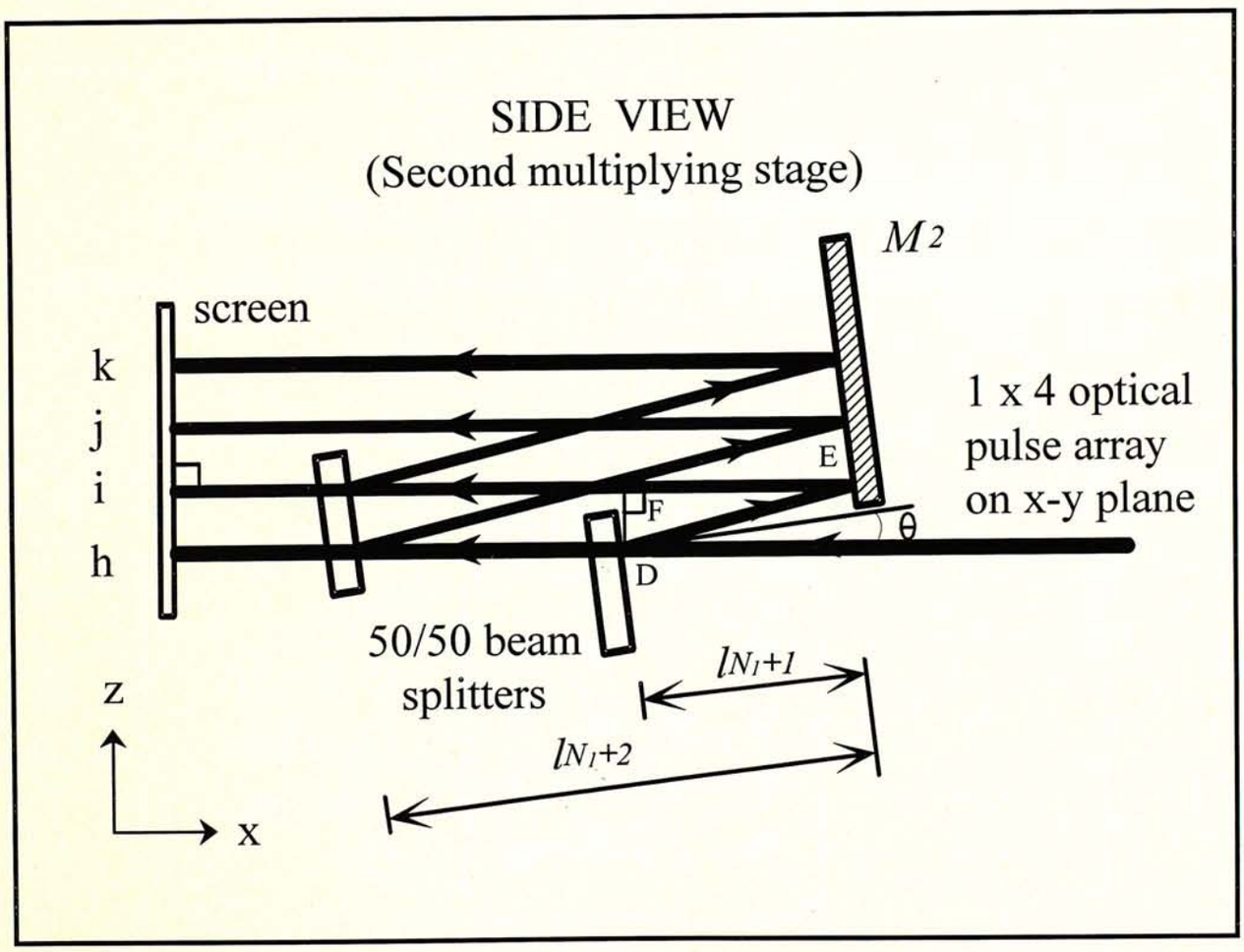

Figure 4-2 *The second multiplying stage on x-z plane, which is oriented in an orthogonal direction to the first stage. Symbols h, i, j and k indicate the sequential order of the formation of the rows in an optical matrix.*

$$l_m = 2l_{m-1} \tag{3b}$$

where $m = N_1+1, N_1+2, \ldots\ldots, N_2$, and N_2 is the total number of splitters used in the overall scheme. A two-dimensional optical array is thus constructed and the sequential order is indicated in the front view of the setup, shown in figure 4-3. The total number of pixels in the matrix is 2^{N_2}. Accordingly, assuming no optical power loss in the splitters and the mirrors, the output power of each pulse is $1/2^{N_2}$ of the original input. Note that the output sequence of the pulses can be inverted by using a pair of converging lens with the same focal length, and the physical dimension of the matrix can be adjusted by the collimating optics to match with the photodetector or switching array.

The delay time of the elements will be reduced if the overall physical dimension of the configuration become smaller. So, the optical matrix has an

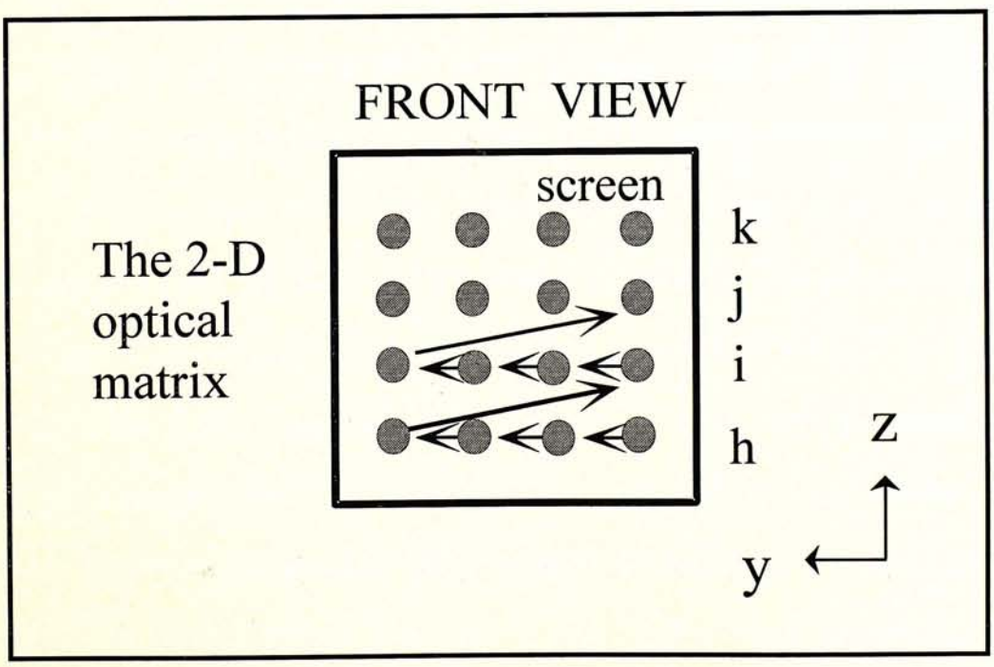

Figure 4-3 The front view of the optical matrix, in which h, i, j and k indicate the sequential order of the matrix rows.

advantage in supporting the high bitrate operations for the two-dimensional array devices with occupying only a little space. The pixel size on the matrix depends on the divergent angle of the optical input, therefore the input laser beam is suggested to be collimated before entering the first multiplying stage; and the diameter of the pixel is assumed to be equal to or smaller than the spatial separation between the neighboring elements.

4.3 The experiment and results

Our configuration is experimentally demonstrated with 150 ps optical pulses from a cw mode-locked Nd:YAG laser. The wavelength is 1.319 μm, the repetition rate is 82 MHz and the average optical power is about 2 Watts. The operation of this laser is described in Appendices 1 and 2. The 50/50 beam splitters used in the experiments were manufactured by depositing multi-layer dielectric thin films on BK 7 glass substrates. An anti-reflection coating has been applied at the back surface to suppress undesirable reflections at the glass-air interface. The metallic 50/50 beam splitters are not preferred in our setup because about 33% optical power will be lost in each beam splitter [9]. The visible He-Ne laser is superimposed with the 1.319 μm laser for the alignments of the experiment. The incident angle θ and the splitter separations l_1, l_2 and l_3 are selected to be 4°, 5 cm, 10 cm and 20 cm, respectively. The first multiplying stage consists of 2 splitters and generates a 1 × 4 array of optical elements. The second multiplying stage is placed at an orthogonal orientation. It consists of a single splitter and translates the 1 × 4 array into a 2 × 4 two-dimensional array. With a focusing lens and a high speed photodetector connected to the sampling scope, the sequentially delayed pulses can be observed and is depicted in figure 4-4. The delay time and the spatial separation between the optical elements are 332 ps and 7 mm, respectively. The fluctuation in the pulse

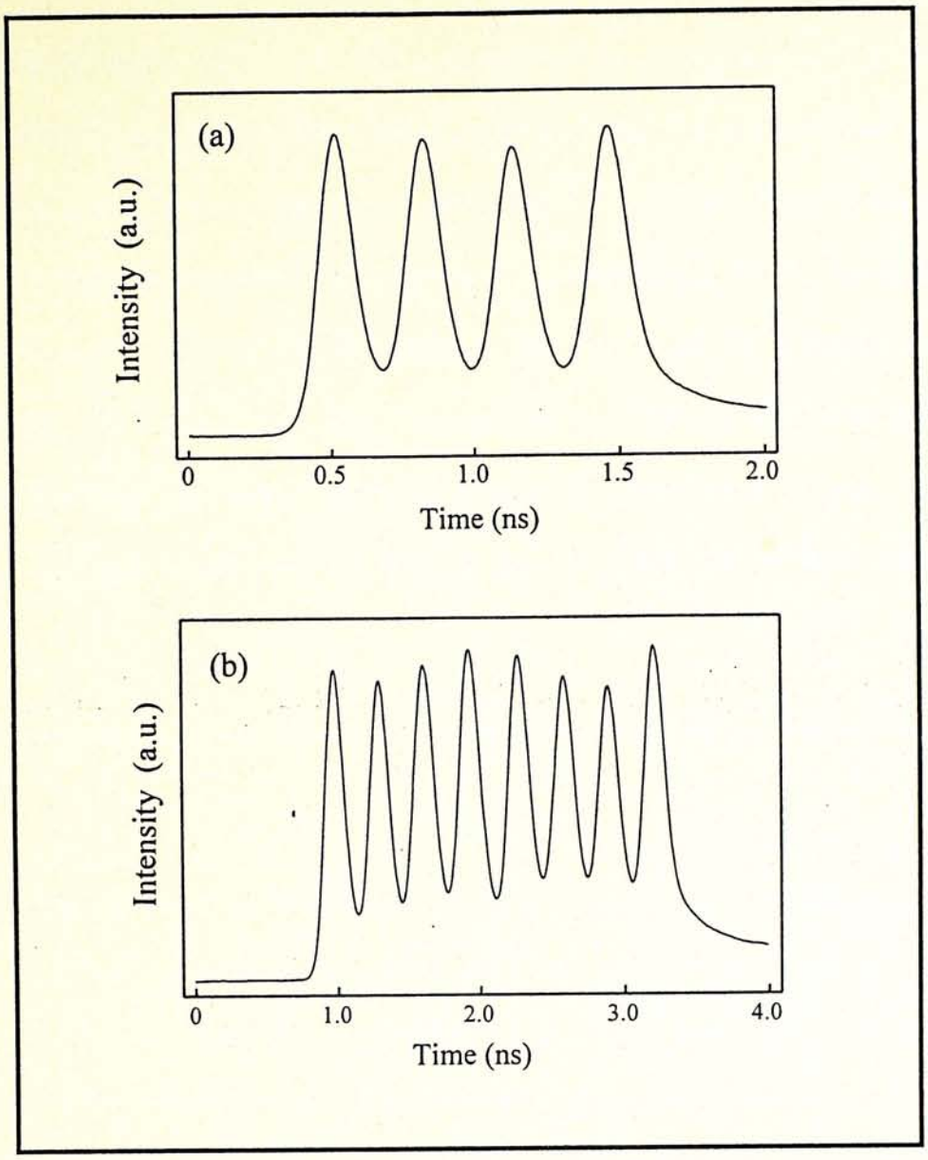

Figure 4-4 *Sequentially delayed optical outputs from (a) one matrix row and (b) two matrix rows. The time delay between the neighboring pulses is 332 ps.*

amplitude was attributed to the tiny dimension (25 μm diameter) of the photodetector which might have non-uniform sensitivity over its detection window. Slight offset from a completely parallel optical arrangement also made it difficult to focus the matrix elements to the same spot on the photodetector. Each output pulse has no time jitter among all matrix elements because mechanical vibrations are minimized on the beam splitters. Whereas the semiconductor surface-emitting laser can not avoid this effect because pulse time jitter is intrinsic problem of

semiconductor lasers. The multi-layer dielectric beam splitters can also keep the state of polarization in both the transmitted and the reflected pulses as that in the input pulses if the angle of incidence is within ±5° of the normal, shown in figure 4-5. The polarization state of each element is maintained to be linearly vertical in the experiment. These optical pulses can be used in polarization-dependent modulations. The setup can also be used in wavelength-division multiple-access (WDMA) because the wavelength tolerance for the beam splitters and the total reflecting mirrors is at least 50 nm, it can support the WDM channels with

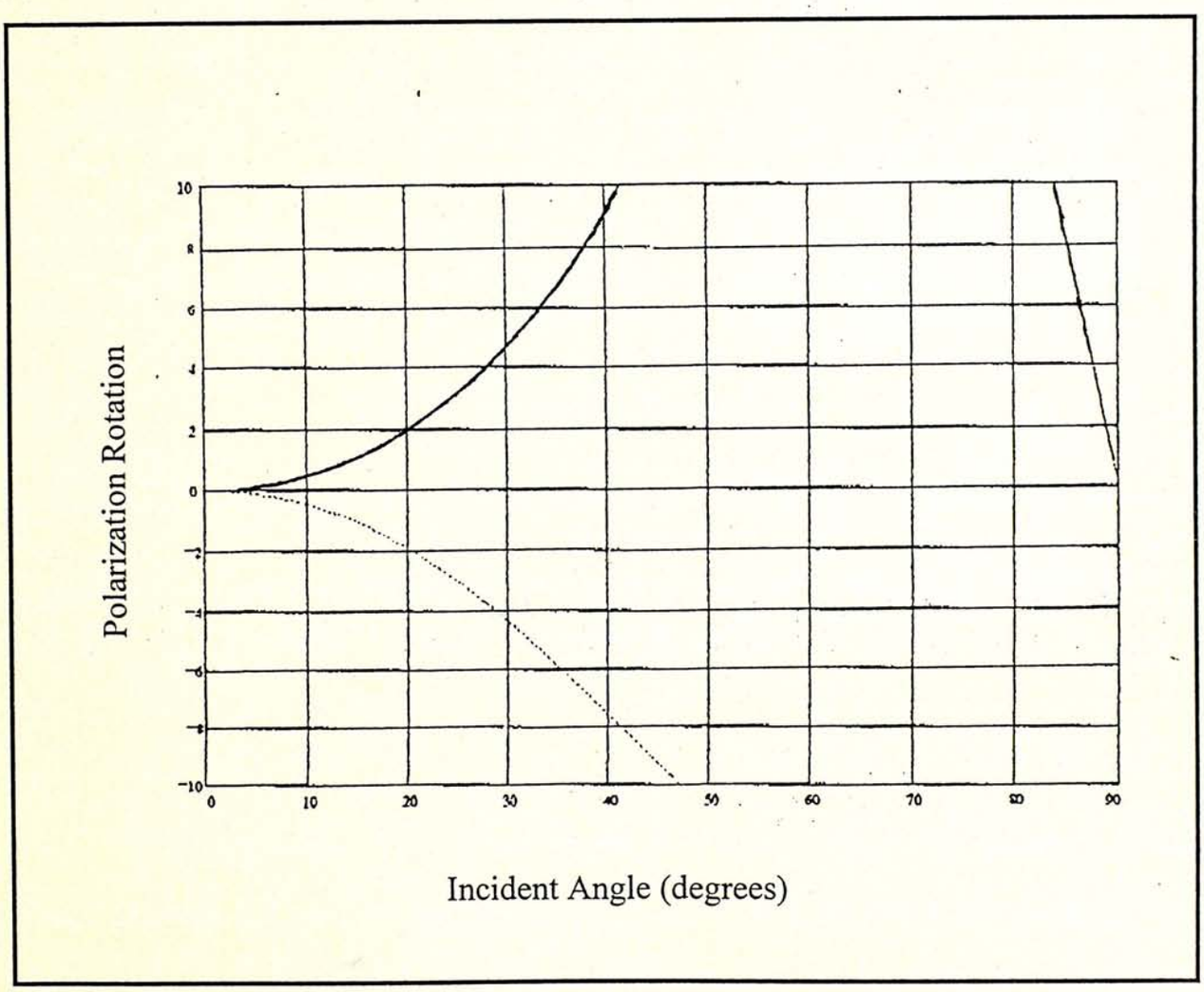

Figure 4-5 Polarization rotation against angle of incident on the dielectric multilayer 50/50 beam splitters [10].

——— *Reflected beam polarization rotation.*

····· *Transmitted beam polarization rotation.*

wavelengths inside this range. The transmittance characteristics as a function of wavelengths in the splitters is shown in figure 4-6.

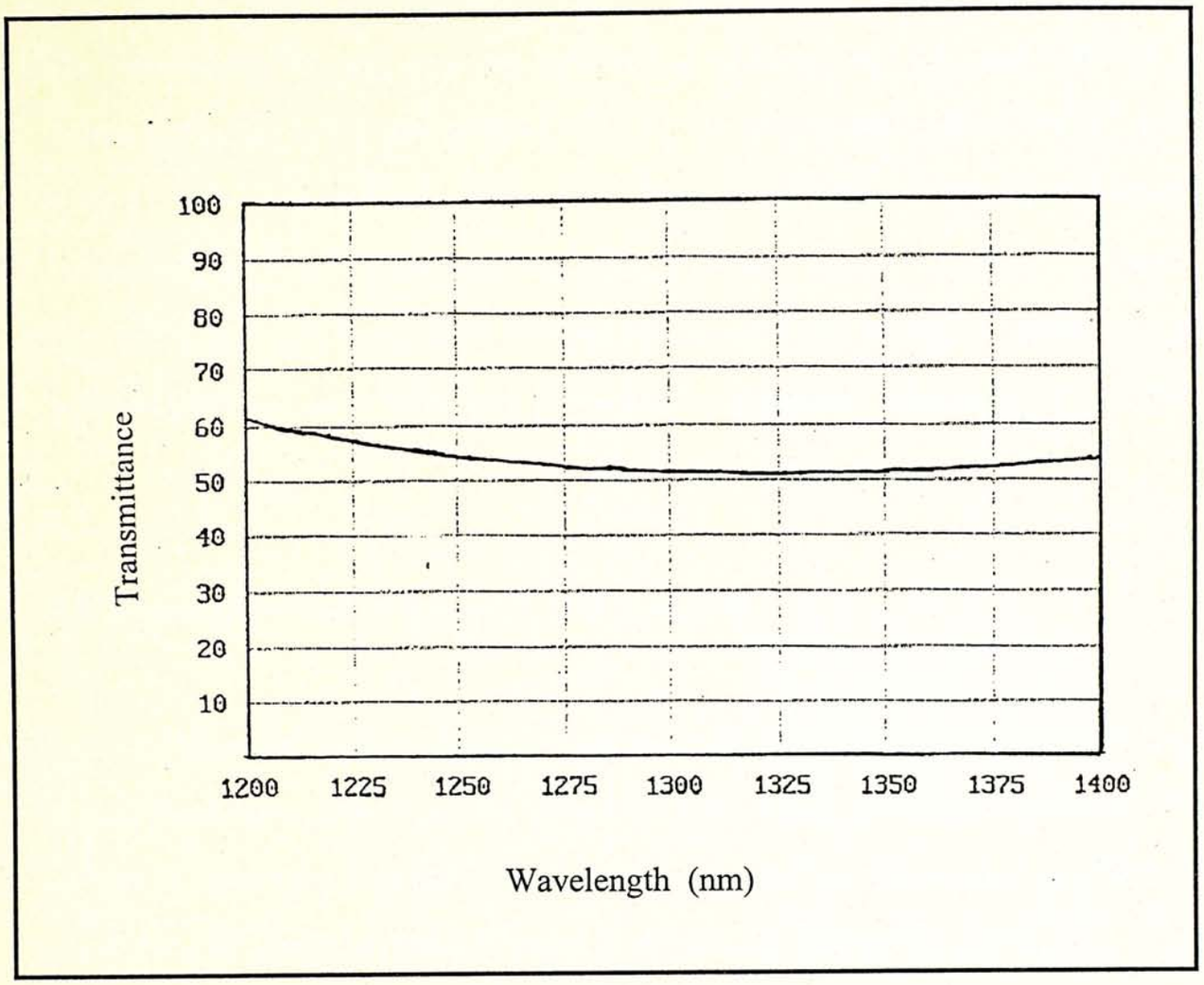

Figure 4-6 *The transmittance characteristics as a function of wavelengths in the 50/50 dielectric multilayer beam splitters [10].*

If the separation l_1 is chosen as the thickness of the beam splitter and the space between the splitters and the mirror is filled with an index matching oil, the delay time and the spatial separation of adjacent optical pulses can be reduced significantly. In our case, the pulses will be separated by 29 ps (corresponding to 34 GHz) and will be 523 μm apart for $\theta = 5°$ and $l_1 = 3$ mm. Thus the new configuration has a potential application in the area of integrated optics. Moreover,

this optical matrix may also be constructed on the recently developed silicon optical bench in which the micromirrors or beamsplitters are assembled on a silicon chip [11]. The positions and separations of these micromirrors can be predetermined in the fabrication process, and the required alignments can be accomplished by incorporating movable and micromechanical structures fabricated directly on the silicon chip. The micromechanical structure is able to be electromechanically controlled for providing the high alignment accuracy in the whole setup. Therefore, the optical matrix is possible to be constructed at a small area on a silicon chip for providing the optical interconnects in the future high-speed computational systems.

4.4 The applications of the novel optical matrix

Three operation modes for the optical matrix are proposed for the high-speed applications in an optical system. The first mode relates to time-division multiple-access (TDMA) communications or processing, whereas the second and the third modes can be applied to space-division multiple-access (SDMA) scheme.

1) *Multiplexing Mode*: The optical matrix with sequentially delayed elements can be focused into a light-guide or an optical fiber through the combined lens, so a high repetition rate optical pulse train can be generated for high speed TDMA communications. Therefore, the scheme performs the function of a time division multiplexer in this mode. The optical configuration is shown in figure 4-7. The multiplication factor of the pulse train is given by

$$M = 2^{N_2} \tag{4}$$

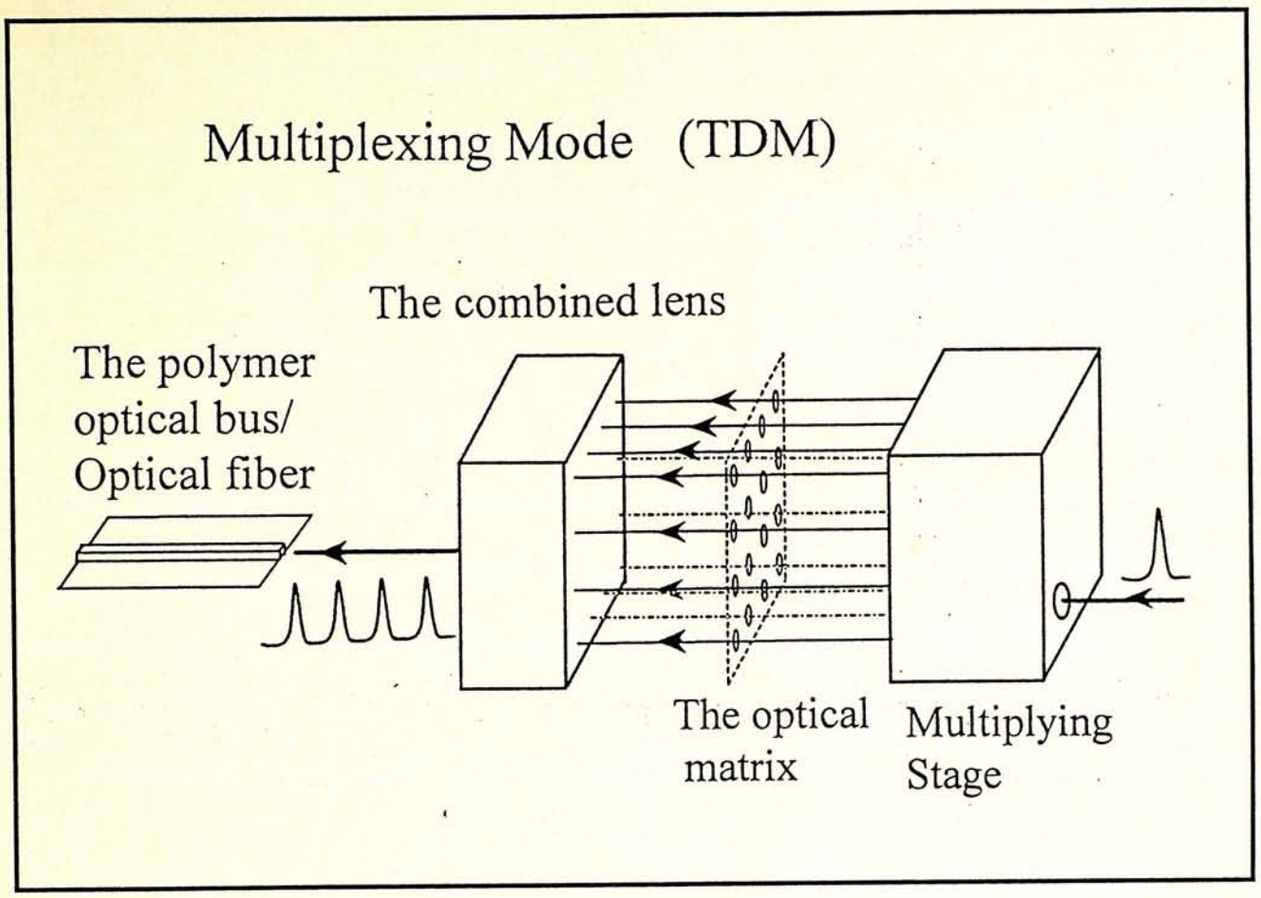

Figure 4-7 The optical configuration of the multiplexing mode.

where N_2 is the total number of beam splitters used in the overall multiplying scheme. In our experiment, the multiplication factor and the delay time between the output pulses in the pulse train are 8 and 332 ps, respectively. The result is shown in figure 4-4(b). When this pulse train is used together with high speed switching arrays, the efficient optical time-division multiplexing and demultiplexing can be demonstrated. The data stream can also be transmitted between chips or broads in optical systems through the polymer optical buses [12]. The delay time between the pulse in the output train can be further reduced with using the shorter optical pulses. The passively mode-locked fiber ring laser which have demonstrated the femtosecond optical pulses with low repetition rates (less than 200 MHz) and high optical peak power (more than 20 W) can be employed in this mode [13].

2) *Independent Mode*: Each optical element represents a spatial channel which can be individually encoded with a modulator. Altogether 2^{N_2} independent channels are generated in the scheme. The bitrate of each channel is the same as that of the input pulse train, shown in figure 4-8. In our demonstration, the bitrate of each channel is 82 Mbit/s and eight spatial channels are created in the setup. By using two-dimensional masks of different patterns, the spatial channels can be encoded with different signals, shown in figure 4-9, the sequential order and the corresponding outputs of these channels are shown in figure 4-10. Therefore these channels can be used in high-speed parallel processing in an optical system.

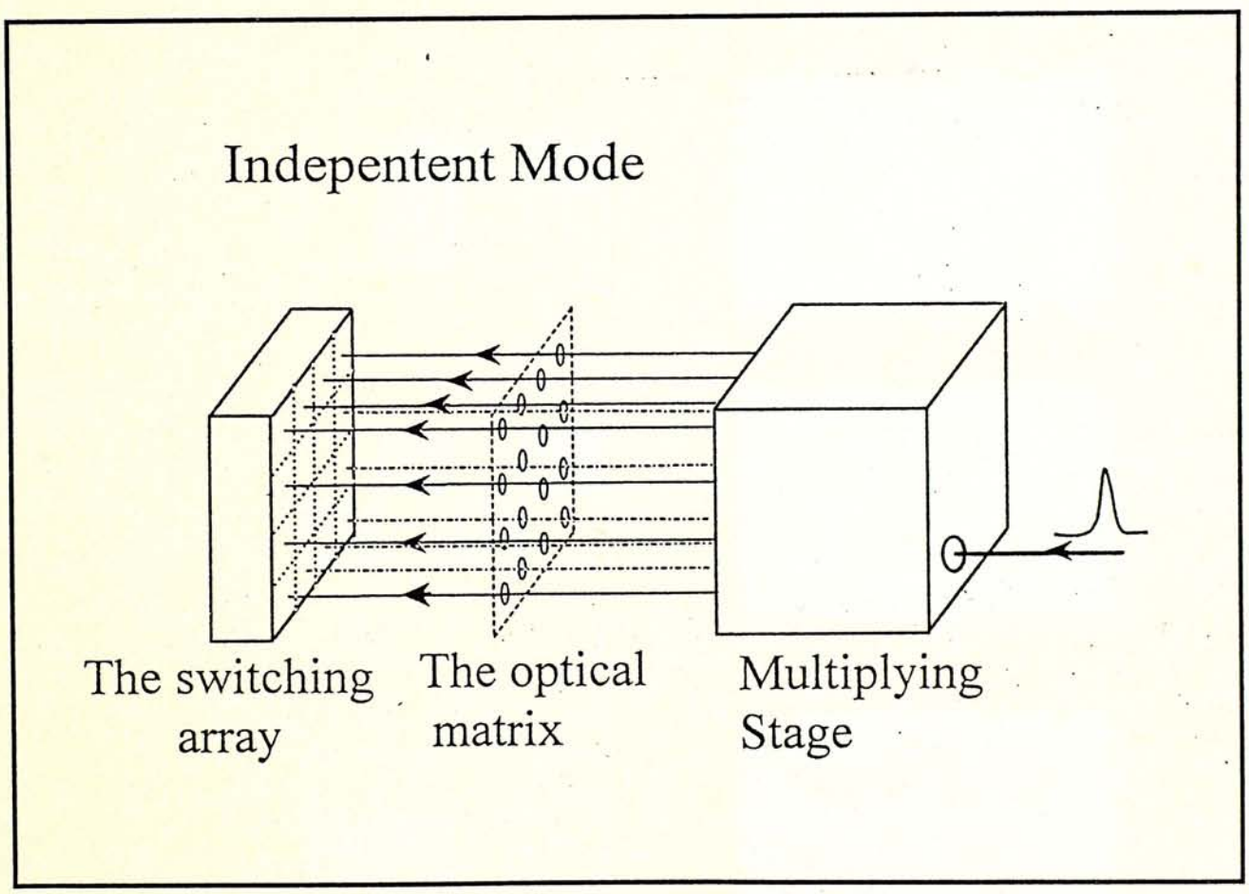

Figure 4-8 The optical configuration of the independent mode.

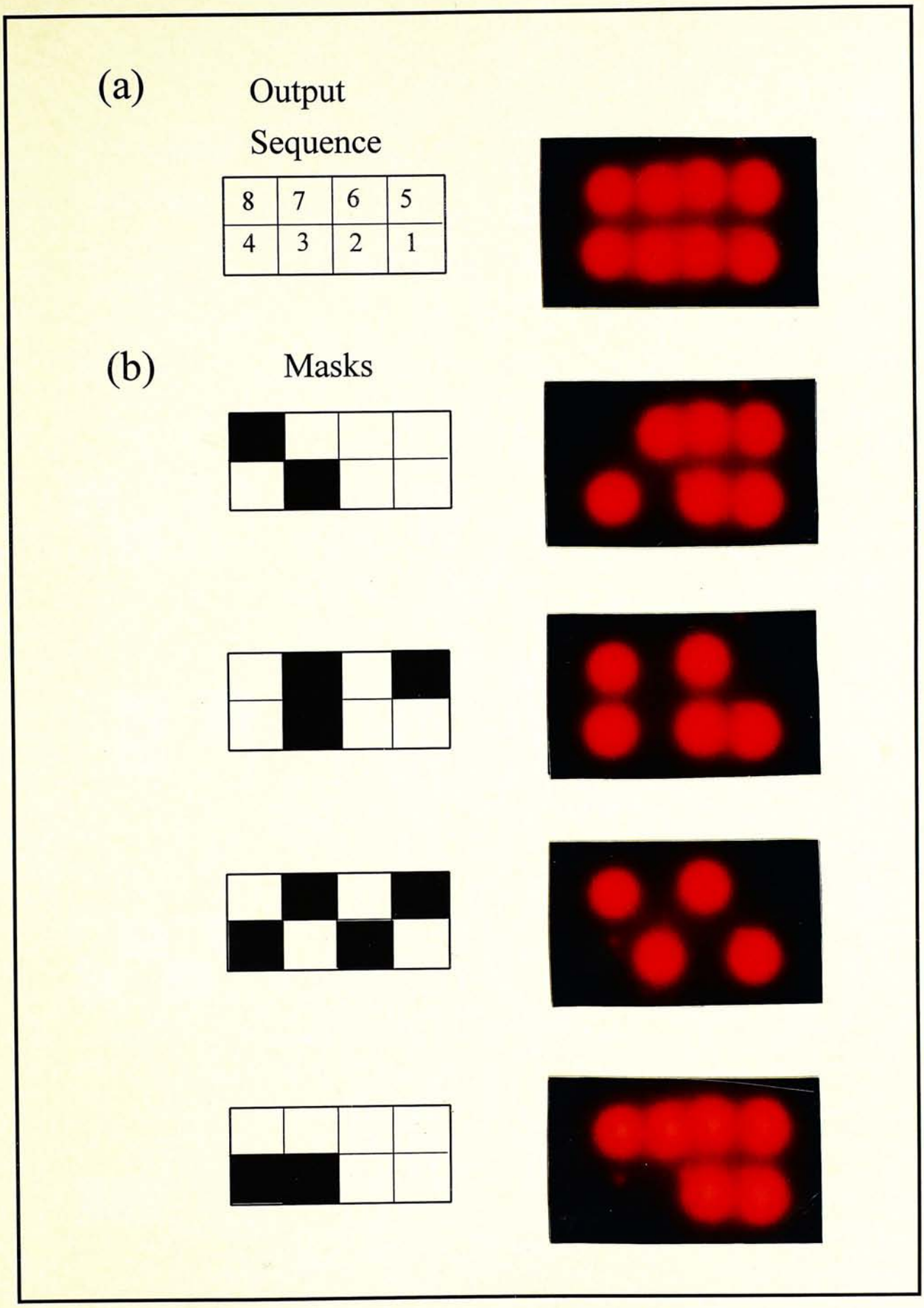

Figure 4-9 *(a) The optical matrix with eight sequential elements. (b) Eight optical pulse elements encoded with different photomask patterns. The images are captured on an infrared screen.*

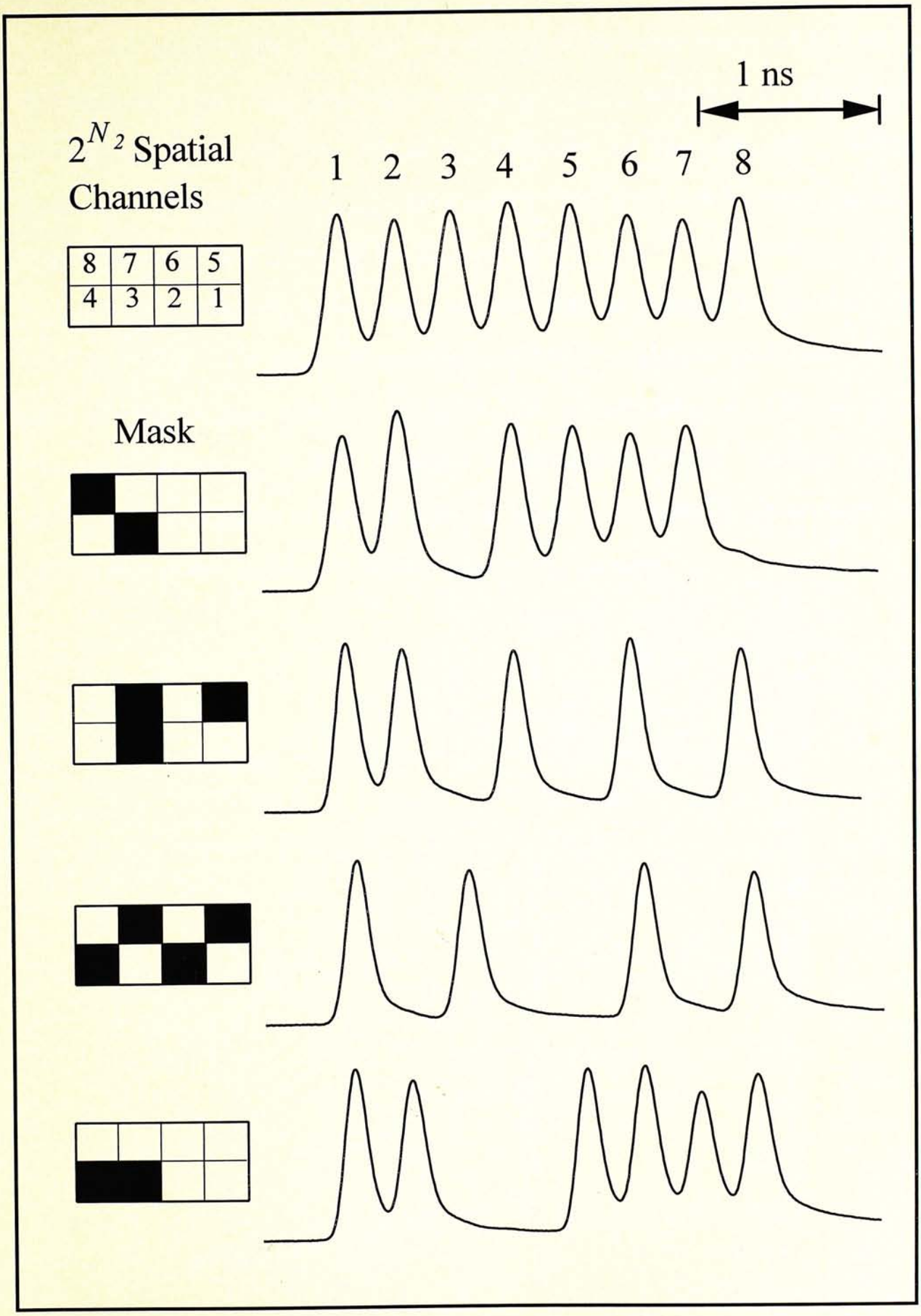

Figure 4-10 The sequential order and encoded outputs from eight spatially separated optical channels.

The optical matrix can also be tailored to generate pulses with several different amplitudes. The outputs can be used in logic operations with high-speed photodetector arrays [14,15]. Figure 4-11(a) shows an interesting experimental result in which the separation l_{N1+1} between the splitter and the mirror in the second multiplying stage was chosen to be the same as l_1 (5 cm). Two rows of spatially separated matrix elements were again generated. With the arrangement, it should be noted that three of the pulses in each row overlapped temporally with those of the other row, but the pulse pairs 2-5, 3-6 and 4-7 are spatially separated. These pulses have been combined to produce outputs with twice the amplitude. Together with a coding scheme as shown in figure 4-11(b), different output patterns representing the combination of two optical data streams have been generated.

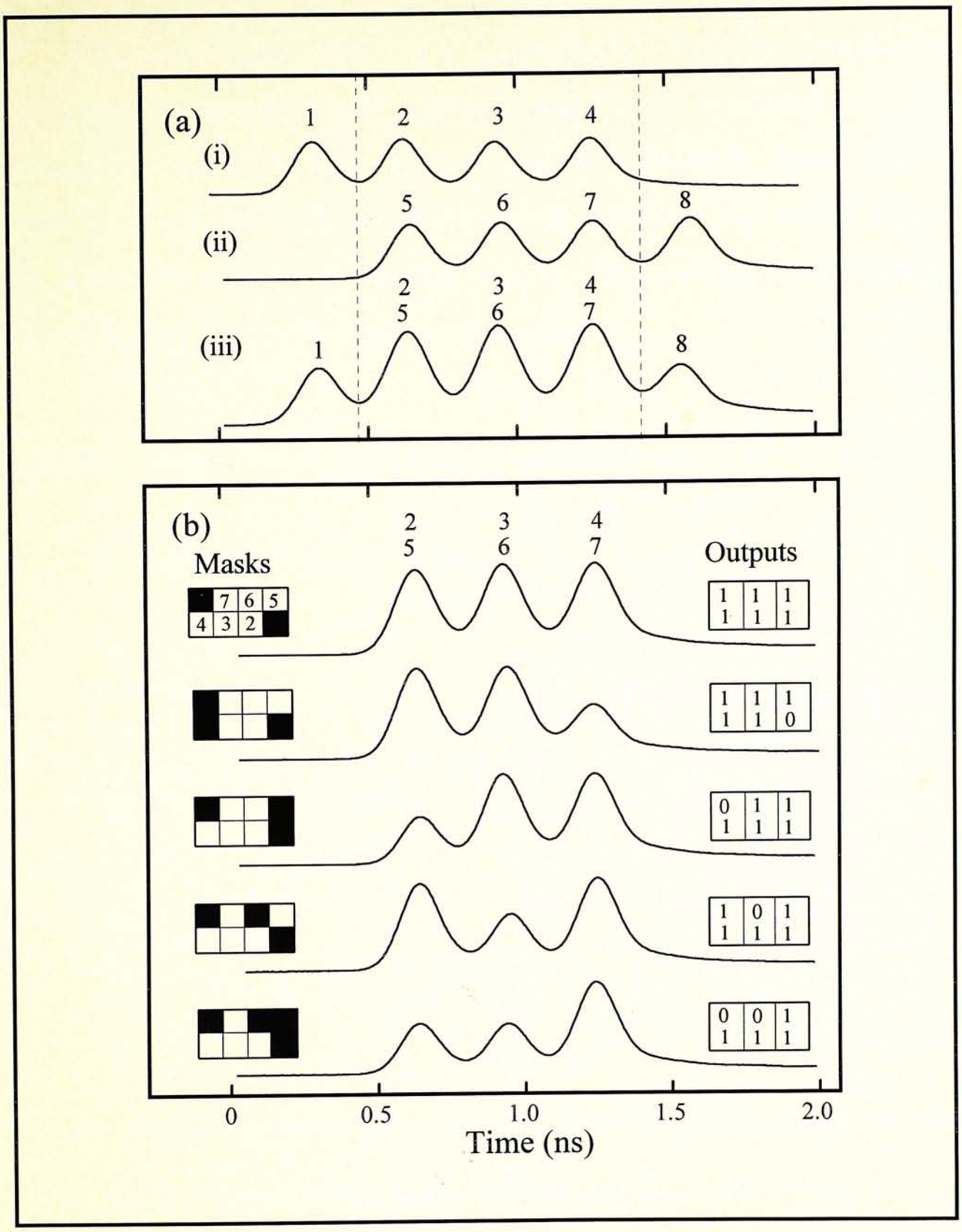

Figure 4-11 *Generation of an optical signal representing the combination of two synchronized data streams. (a) (i) optical output in the first row of the matrix, (ii) optical output in the second row with one bit shifted from that in (i), (iii) combined outputs of (i) and (ii). Note that the pulse pairs 2-5, 3-6, and 4-7 overlap temporally but are spatially separated. (b) Combined outputs of the two optical data streams.*

(3) *Broadcasting Mode*: The optical matrix enjoys the advantage of multiplying one input pulse to 2^{N_2} matrix elements in a two-dimensional array. The setup is shown in figure 4-12. The input can be modulated by acousto-optic or electro-optic devices. It will then be converted to multiple output channels carrying the same information for broadcasting purpose. Thus, the optical matrix can be applied for data distribution in future optical systems.

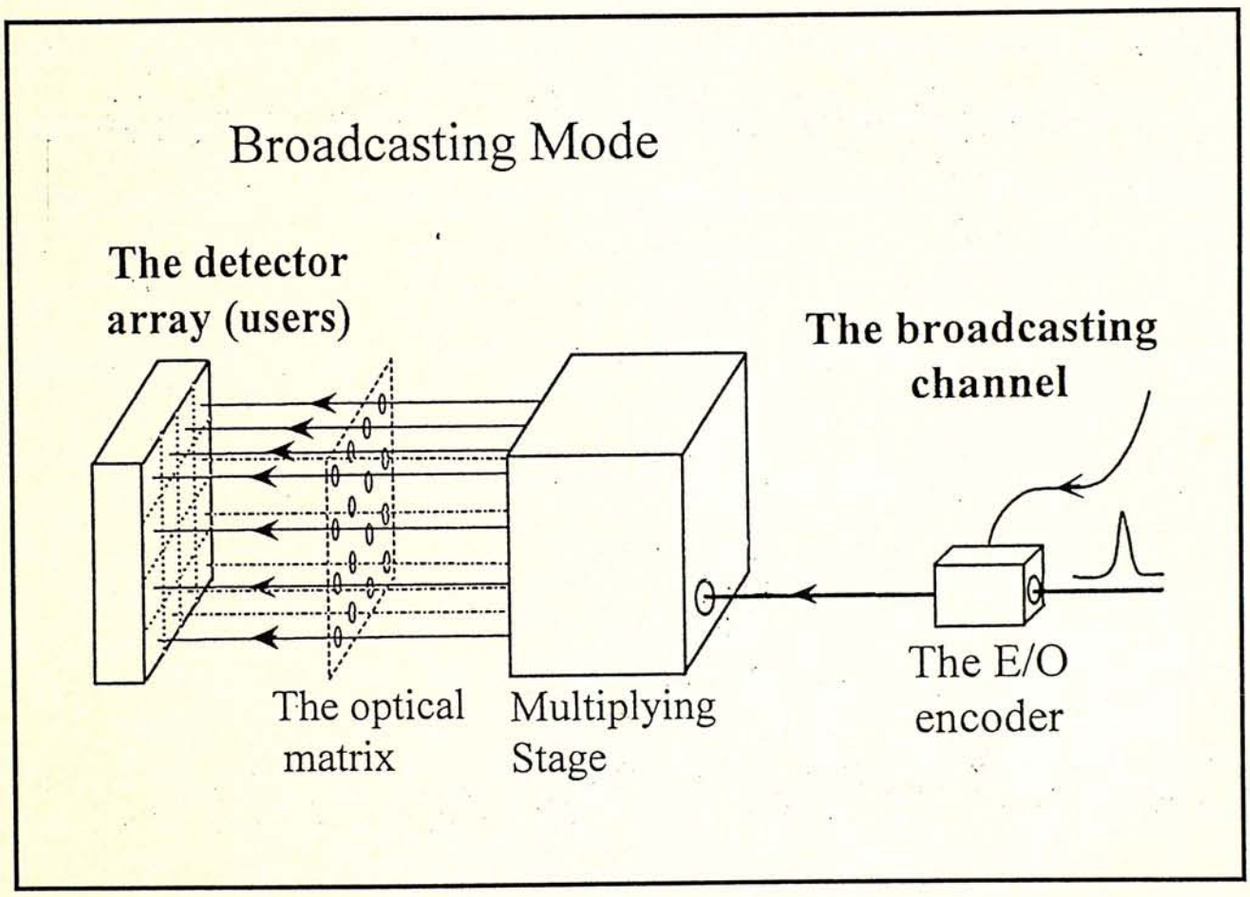

Figure 4-12 The optical configuration of the broadcasting mode.

4.5 Comparison on the operation modes of the optical matrix

In the comparison on operation modes of the optical matrix, the recently developed wavelength-division multiplexing (WDM) interconnect is taken into our consideration. It is because this technique is efficient for the large-capacity parallel data processing in the future high-speed computers and computational systems. Figure 4-13 shows the three-dimensional view of the WDM one-to-many plane optical interconnect constructed by a two-dimensional laser-pixel array and several detector planes [7]. In this configuration, only the first plane is comprised with the vertical-cavity surface-emitting lasers (VCSELs). The N^2 identical laser pixels, in which each one of them consists of three spatially separated VCSELs with different

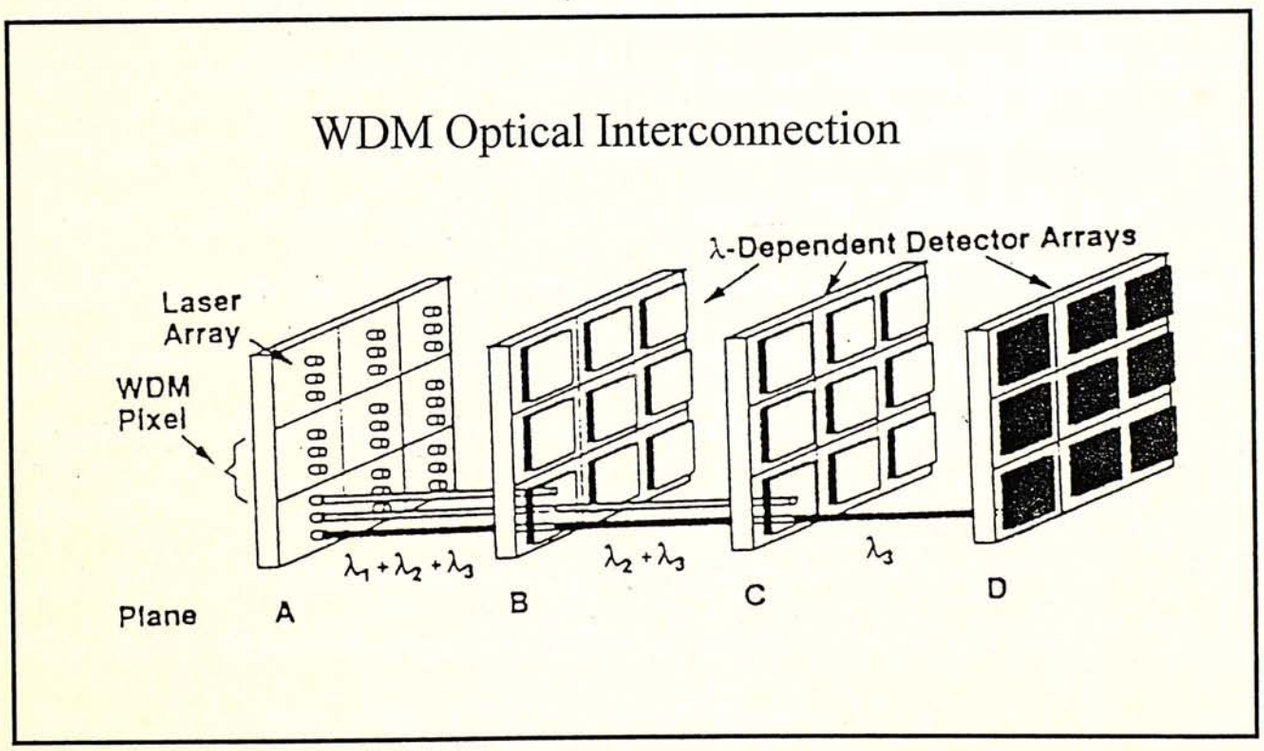

Figure 4-13 The two-dimensional pixel array of identical 3-λ vertical cavity surface-emitting laser (VCSEL) mini-arrays and three λ-selective detector arrays [7].

operation wavelengths, are used to construct the N × N transmitter array. So, this laser pixel array can be used for WDM communications. Besides, in each one of the detector planes, all the pixels have the same and specified spectral response which is slightly offset from the corresponding pixels on the next plane. Thus the cutoff wavelengths of the detecting planes are increasing for each subsequent plane. As the result, each plane only detects the shortest wavelength signal remaining in the laser beam and is transparent to all the longer wavelength signals. The wavelength-selective detection for the WDM communications can be obtained in these special detecting planes.

The two-dimensional WDM interconnect can be used in three operation modes: independent mode, broadcasting mode and individual mode. Their encoding and operation principles are similar to that of the optical matrix described in section 4.4. In the *Independent Mode*, the lasers can be turned on simultaneously and independently for transmission of different data streams to different receiving planes. The $3N^2$ electrical drivers are then required for operating all the VCSELs. In the *Broadcasting Mode*, all lasers are simultaneously turned on with the same input data from a single driver. Such data stream can be transmitted to the photodetectors on N planes for broadcasting purpose. In the *Individual Mode*, only one of three VCSELs in each pixel can be turned on at a time from the same electrical driver, so only one detecting plane can receive the transmitted data from a laser pixel. Therefore, these three operation modes are dependent on the electrical inputs, and the bandwidths of VCSEL and photodetector arrays.

If the VCSEL array is operated under the sequential order, its performance will depend on the precision of electrical delay in the connected circuitry at its actual operation. However, as the pulse time jitter is the intrinsic problem of the semiconductor lasers, the delay time in the optical outputs is very difficult to be

adjusted and this effect will reduce the efficiency of the time-division multiplexing applications.

In the optical matrix, as no time jitter is on the output pulses of the matrix, its performance in the time-division multiplexing applications is expected to be better than the WDM interconnect. Moreover, the three described operation modes in WDM interconnect can also be accomplished by using several input lasers with different wavelengths and a switching array. It is because the wavelength tolerance of the beamsplitters in our scheme is at least 50 nm, which can be employed for WDM channels within this range. Besides, the pulse generation schemes for the lasers used in the matrix is more flexible than that of VCSELs because several techniques, such as the passive and active mode locking described in Appendix 2, can be employed. So, the pulse width of the optical outputs can be shorter than that from gain switching and the required modulation frequency of the switching array can be at the repetition rate of the input pulse train. In such scheme, the relatively low-speed electrical inputs can be used in the switching array for ultrahigh speed TDM communications.

4.6 Comparison on the construction of the optical matrix

The plate beamsplitter has been recently proposed for generation of the ultrafast pulse stream and the multiple equal-intensity beams [16,17]. Figure 4-14 shows the technique to produce the multiple time-delayed optical pulses by using a plate beamsplitter and a total reflecting mirror, whereas in figure 4-15, a glass plate with coatings on both sides is used to produce four equal-intensity beams with spatial separation of 6.8 mm. Two multiplexing schemes are similar except the

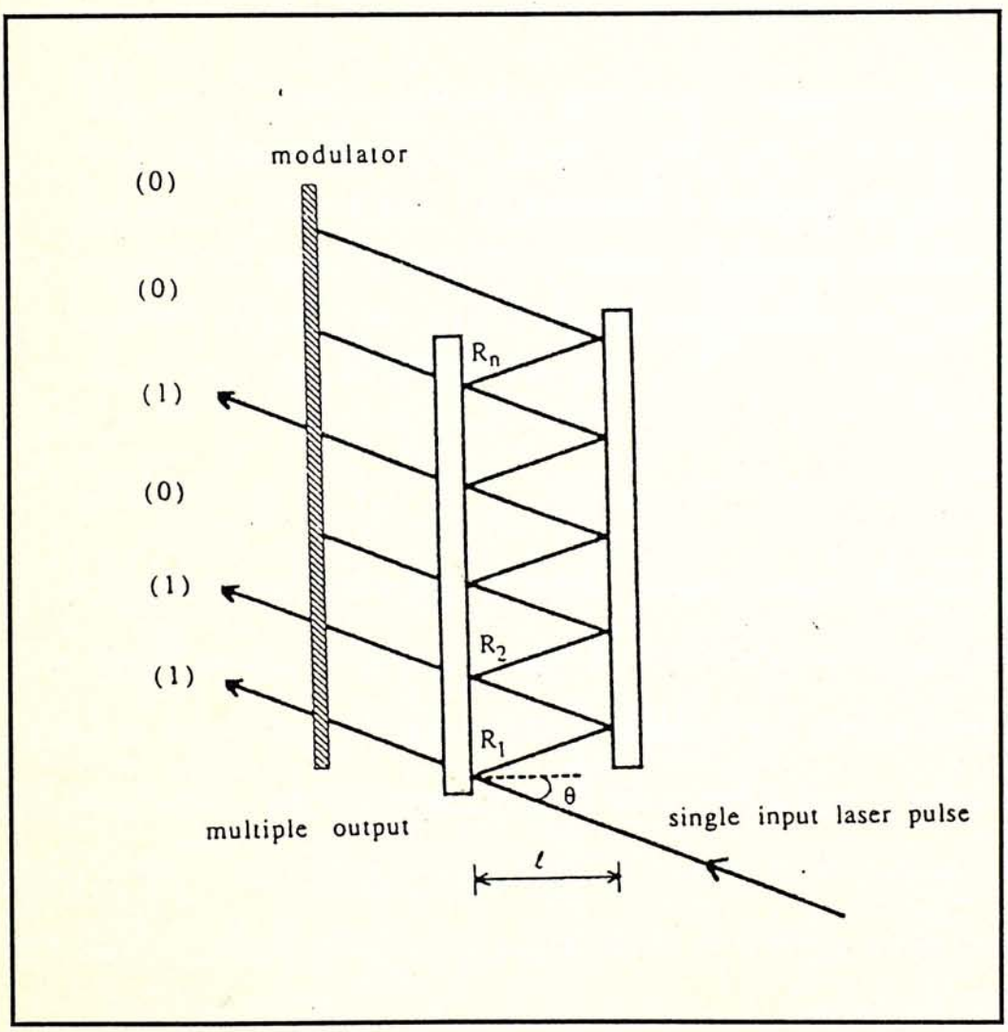

Figure 4-14 The schematic illustration of the technique to generate the time-delayed beams with equal intensities. The reflectivities of R_1, R_2 and R_3 are 75, 67 and 50 %, respectively [16].

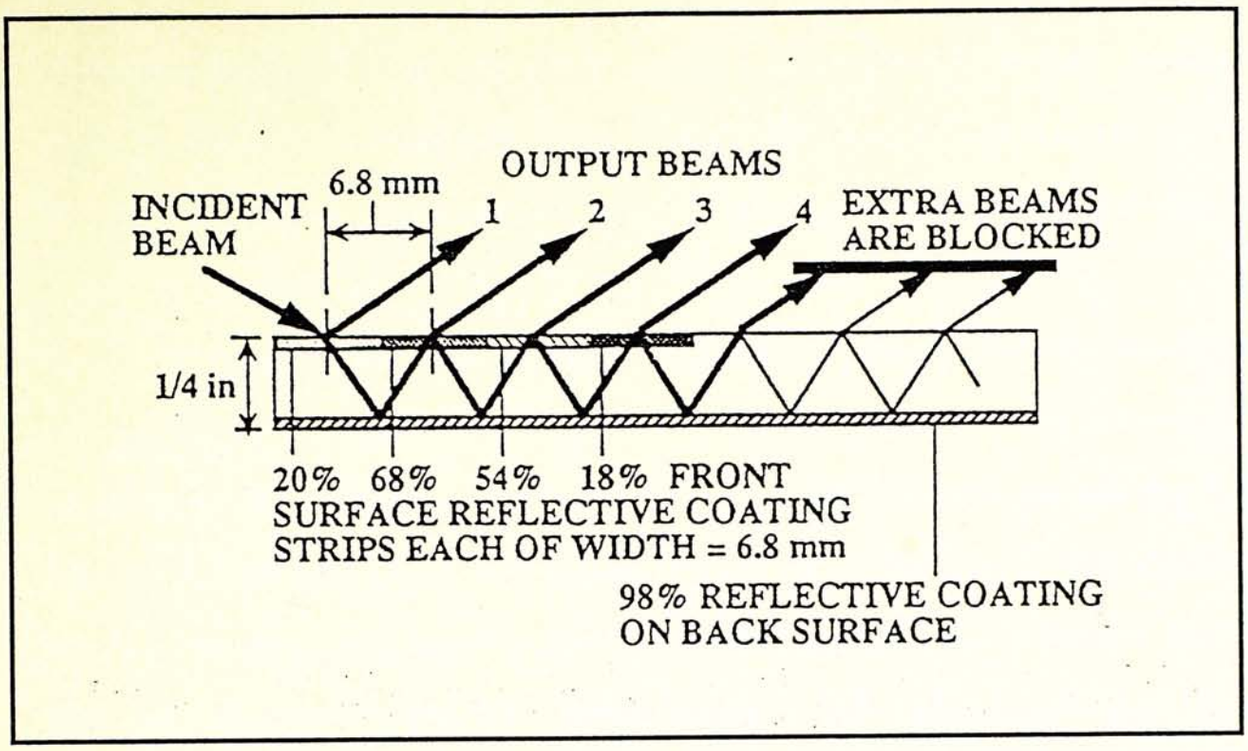

Figure 4-15 *The practical design of the plate beamsplitter to produce four equal-intensity beams. Each output beam is of intensity 20 % relative to the input beam intensity. The front surface has four step reflectances of 20 %, 68 %, 54 %, and 18 % provided by strips of reflective coating, each of width equal to lateral beam spacing of 6.8 mm. The back surface has 98 % reflective coating [17].*

medium used between two reflecting surfaces. Their operation principle is as follows: The configurations consist of 2 mirrors, a total reflecting mirror and a partially reflecting mirror with discrete steps of coatings. To obtain the multiple outputs with equal intensities, the reflectances of the multiple step coatings should be determined before the actual fabrication. In figure 4-14, three steps of coatings are used and the corresponding reflectivities are 75, 67 and 50 %, respectively. In the configuration shown in figure 4-15, four steps of coatings are required and the reflectivities are 20, 68, 54 and 18 %, respectively. Four light beams in a one-dimensional array are generated in both schemes and their output intensities are dependent on the fabrication tolerance of the multiple steps. Note that to keep the

absorption loss small in the partially reflecting surface, the discrete steps should be made by the dielectric coatings. It is because the metallic coatings have higher absorption on optical power and can reduce the obtainable maximum intensities.

In comparing with the optical matrix, these single-plate-beamsplitter designs are specific for a predetermined number of output beams because it cannot be extended for the additional beams when the partially reflecting surface has been fabricated. In the optical matrix, the number of output beams can be freely increased by simply introducing more 50/50 beamsplitters. So, it is more flexible than the single-plate-beamsplitter configuration in terms of multiplication factor. Moreover, in the scheme shown in figures 4-14 and 4-15, the output intensities are highly dependent on the fabrication tolerance of the discrete steps. If a large manufacturing deviation is introduced on the coating of a single step, for example the second step, the intensities of all four output beams will be affected. A new multiple step beamsplitter may be required to be made for the setup. In the optical matrix, such problem can be solved by simply replacing the imperfect beamsplitter by another exactly 50/50 splitter, the equal-intensity outputs can then be obtained .

On the whole, the configuration of the optical matrix is more flexible in multiplication of the output beams, and not highly dependent on the relatively larger manufacturing deviation on a single beamsplitter for generation of the equal-intensity optical pulses.

4.7 The conclusions of the optical matrix

In conclusion, a novel scheme for the generation of sequentially delayed optical pulses in a two-dimensional matrix is experimentally demonstrated. This matrix can be used in both cw and pulsed operations. The physical dimension of this matrix can be controlled for matching with the photodetector and switching arrays. It also has potential applications in the integrated optics. The required time delays among the optical elements can be precisely adjusted with no individual time jitter, and their polarization states are also maintained as that in the input pulse train. This optical matrix is suitable to be used in SDMA, TDMA and WDMA for high speed optical communications, parallel processing, and the waveguide or free-space optical interconnects under three proposed operation modes.

References

[1] J. W. Goodman, F. I. Leonberger, S. Y. Kung and R. A. Athale, "Optical interconnections for VLSI systems," *Proc. IEEE*, vol. 72, no. 7, pp. 850-866, 1984.

[2] M. R. Feldman, S. C. Esener, C. C. Guest and S. H. Lee, "Comparison between optical and electrical interconnections based on power and speed considerations," *Appl. Opt.*, vol. 27, pp. 1742-1751, 1988.

[3] J. Jahns and M. J. Murdocca, "Crossover networks and their optical implementation." *Appl. Opt.,* vol. 27, no. 15, pp. 3155-3160, 1988.

[4] A. Guha, J. Bristow, C. Sullivan and A. Husain, "Optical implementation for massively parallel architectures," *Appl. Opt.*, vol. 29, no. 8, pp. 1077-1093, 1990.

[5] A. D. Norte, A. E. Willner, W. Shieh and A. R. Tanguay, Jr., "Multiple-layer optical interconnections using through-wafer hollow-dielectric-waveguide vias," *IEEE Photon. Technol. Lett.*, vol. 6, pp. 851-854, 1994.

[6] A. C. Von Lehmen, T. C. Banwell, R. Cordell, C. Chang-hasnain, J. W. Mann, J. Harbison and L. Florez, "High speed operation of hybrid CMOS vertical cavity surface emitting laser array," *Electron. Lett.*, vol. 27, no. 13, pp. 1189-1191, 1991.

[7] A. E. Willner, C. J. Chang-Hasnain and J. E. Leight, "2-D WDM optical interconnections using multiple-wavelength VCSEL's for simultaneous and reconfigurable communication among many planes," *IEEE Photon. Technol. Lett.*, vol. 5, pp. 838-841, 1993.

[8] S. Kawai, "Free-space multistage optical interconnection networks using microlens arrays," *J. Lightwave Technol.*, vol. 9, pp. 1774-1779, 1991.

[9] The section of beamsplitters in the buyer's catalog of precision optical components, Optics for Research Inc., in Laser Focus World, p. 584, 1994.

[10] The catalog of dielectric beam splitters, Alpine Research Optics, 1994.

[11] O. Solgaard, M. Daneman, N. C. Tien, A. Friedberger, R. S. Muller and K. Y. Lau, "Optoelectronic packaging using silicon surface-micromachined alignment mirrors," *IEEE Photon. Technol. Lett.*, vol. 7, no. 1, pp. 41-43, 1995.

[12] R. T. Chen, H. Lu, D. Robinson, Z. Sun, T. Jannson, D. V. Plant and H. R. Fetterman, "60 GHz board-to-board optical interconnection using polymer optical buses in conjunction with microprism couplers," *Appl. Phy. Lett.*, vol. 60, pp. 536-538, 1992.

[13] E. Yoshida, T. Sugawa, Y. Kimura and M. Nakazawa, "A new femtosecond erbium-doped fiber laser with nonlinear polarization rotation," *Optical Amplifiers and Their Applications*, vol. 14, paper PD12, pp. 384–388, 1993.

[14] E. Desurvire, B. Tell, I. P. Kaminow, G. J. Qua, K. F. Brown-Goebeler, B. I. Miller and U. Koren, "High contrast GaInAs : Fe photoconductive optical AND gate for time-division demultiplexing," *Electron. Lett.,* vol. 24, pp. 396-397, 1988.

[15] T. C. She and C. Shu, "Optoelectronic exclusive-NOR gate operating at 200 Mbit/s," *IEEE Photon. Technol. Lett.,* vol. 6, pp. 712-714, 1994.

[16] C. Shu, X. -C. Zhang, E. S. Yang and D. H. Auston, "Optoelectronic generation of time-division multiplexed ultrafast bit stream on a coplanar waveguide," *Appl. Phys, Lett.*, vol. 57, no. 27, pp. 2897-2898, 1990.

[17] M. M. Rajadhyaksha and R. H. Webb, "Plate beamsplitter to produce multiple equal-intensity beams," *Opt. & Photon. News*, vol. 6, no. 5, engineering laboratory notes, 1995.

Chapter V Conclusions and Future Works

5.1 The conclusions

In serving a society of users in an optical network, one may use the multiple-access protocols for the multi-channel data communications. To date, the optical time-division multiple-access (TDMA) can support the ultrafast data communications with bitrate from several tens gigabit per second up to more than 100 gigabit per second [1,2], but the optical wavelength-division multiple-access (WDMA) can serve much more users [3]. Indeed, these two protocols may be used together for the future high-speed traffics. In this thesis, the proposed multiplying schemes called "Optical Loop Mirror Multiplexer" and "Optical Matrix" are concentrated on the developments of time-division multiplexing technologies for the future high-speed optical communications. It is worth to note that the optical matrix can be simultaneously operated in both TDMA and WDMA applications.

In the optical loop mirror multiplexer investigated in chapter III [4], the configuration with a parallel connection of several fiber loop mirrors has been constructed and experimentally demonstrated. This novel time-division multiplexer can generate the high-repetition-rate optical pulse trains with even outputs and is shown to has higher reliability in its multiplications. The amplitudes of the optical outputs can be adjusted by using the polarization controllers in the single-mode fiber loops and this configuration can be used in both single-mode and multimode setups. This multiplexer is suitable to be used as an all-optical clock multiplier, and will has potential applications in ultrahigh speed TDMA communications and in space-division multi-channel parallel processing. With the use of fiber switches, the configuration can be simply converted into a high speed optical bit pattern

generator. The mathematical series describing its operations is also derived. In our experiment, the output pulse train with 0.3 ns delay time between the neighboring pulses in the 16 optical outputs, and four spatial channels for optical parallel processing have been demonstrated.

In the optical matrix described in chapter IV, an array of optical channels or sequentially delayed optical pulses for high speed operations in two-dimensional array optoelectronic devices has been generated [5]. The required time delays among these optical elements can be precisely adjusted and its physical dimension can be controlled for matching with the photodetector and switching arrays. Each output pulse has the same state of polarization as the input pulse and there is no time jitter among the matrix elements. This optical matrix is suitable to be used in SDMA, TDMA and WDMA for high speed optical communications, parallel processing, and the waveguide or free-space optical interconnects under three proposed operation modes: multiplexing mode, independent mode and broadcasting mode. In our demonstration, eight spatially separated optical channels with 332 ps delay time have be generated.

The operation wavelength in our experiments for two proposed schemes is at 1.3 μm, because many existing optical networks are constructed with the standard optical fibers, not the dispersion-shifted fibers; but with simply employing the optical components at other operation wavelengths, these schemes can also be operated in the corresponding wavelengths as the physics in their operations remain unchanged.

5.2 The future works

The function of the OLMM is to generate the high-repetition-rate optical pulse train with even outputs, and the advantage of the optical matrix is in the generation of optical elements or spatially separated optical channels in two-dimensional array with precisely short delays. With the special properties and advantages in these developed schemes, a new time-division multiplexer can be constructed and is shown in figure 5-1. In this proposed configuration, the OLMM is used in the primary multiplying step for the parallel distribution of the multiplied

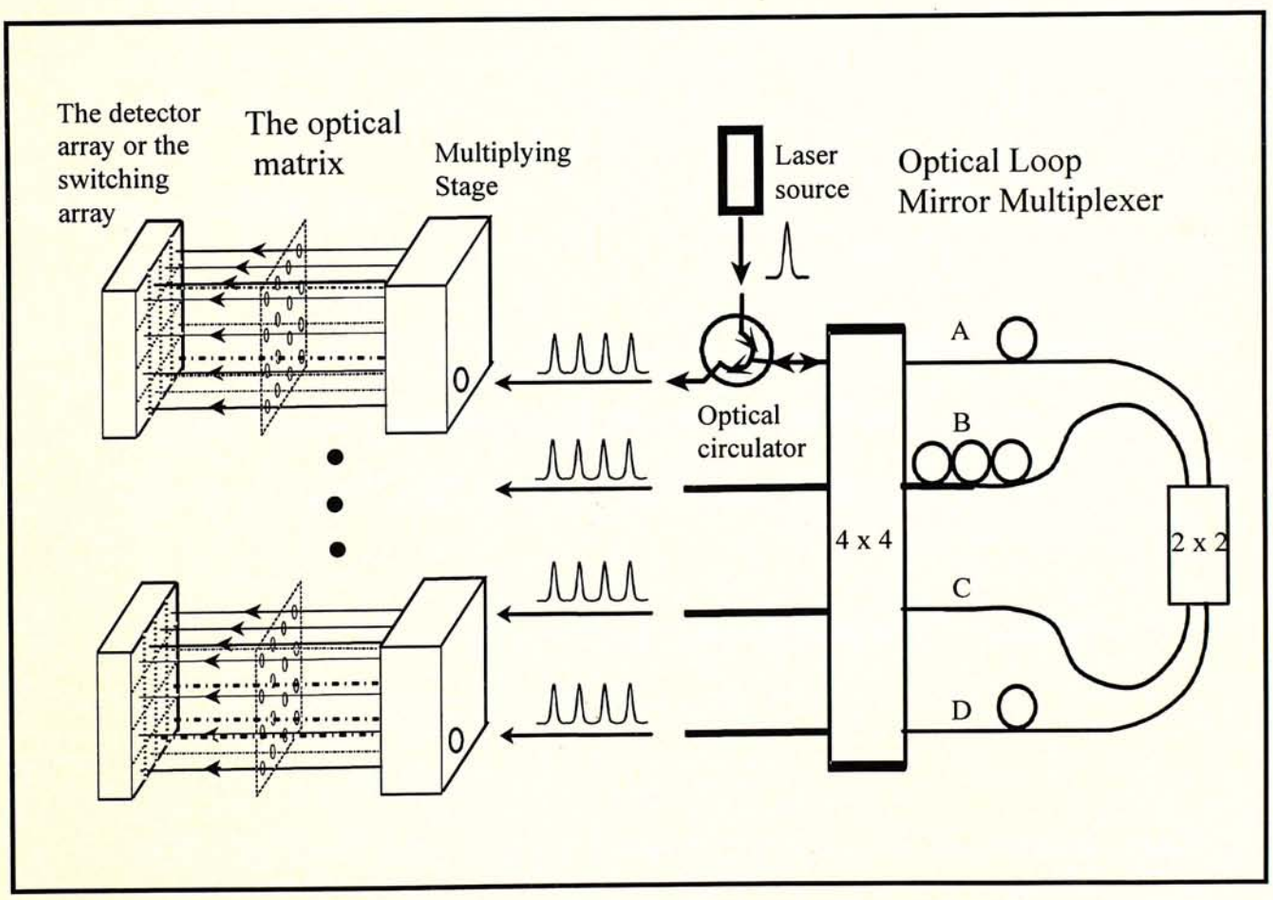

Figure 5-1 *The proposed time-division multiplexer composed by an optical loop mirror multiplexer and four optical matrixes. The 64 optical channels with repetition rate at least 4 times higher than the original inputs are generated.*

pulse trains, whereas four optical matrixes used in the secondary multiplying step are for the further multiplication of the parallel channels without time jitter. Thus, this new configuration is able to generate a large number of spatial channels with precisely time delays and can be used in high-speed optical space-division operations for a series of two-dimensional array devices. Note that the time delays of the optical channels generated in the secondary multiplying step can be further reduced if the optical matrixes are fabricated with the semiconductor materials. As shown in figure 5-1, 64 spatial channels can be generated and their repetition rate are at least four-times higher than the original input pulse train. It can be a alternative of the surface-emitting laser array for the future high-speed parallel processing and computational systems.

5.3 List of publications

1. K. S. Lee and C. Shu, "Novel scheme for multiplying the repetition rate of optical pulses by using optical loop mirrors," in *Conference on Lasers and Electro-Optics (CLEO'95)*, paper CME3, pp. 20-21, 1995.

2. K. S. Lee and C. Shu, "Optical loop mirror multiplexer," submitted to *IEEE Photon. Technol. Lett.*

3. K. S. Lee and C. Shu, "Optical matrix for two-dimensional array devices," in *Tenth International Conference on Integrated Optics and Optical Fibre Communication (IOOC'95)*, paper TuD2-4, pp. 79-80, 1995.

4. K. S. Lee and C. Shu, "Optical matrix for high-speed operation in two-dimensional array devices," submitted to *IEEE Photon. Technol. Lett.*

References

[1] M. Nakazawa, E. Yoshida, E. Yamada, K. Suzuki, T. Kitoh and M. Kawachi, "80 Gbit/s soliton data transmission over 500 km with unequal amplitude solitons for time clock extraction," *Electron. Lett.*, vol.30, no.21, pp.1777-1778, 1994.

[2] M. Saruwatari, "Ultrahigh-bit-rate 100-Gbit/s transmission technology," presented in *Conference on Lasers and Electro-Optics (CLEO'95)*, paper CTuN1, p.141, 1995.

[3] I. P. Kaminow and V. W. S. Chan, "Performance of an all-optical network testbed," in *tenth international conference on Integrated Optics and Optical fibre Communication (IOOC'95)*, paper ThC1-1, vol. 3, pp. 62-63, 1995.

[4] K. S. Lee and C. Shu, "Novel scheme for multiplying the repetition rate of optical pulses by using optical loop mirrors," in *Conference on Lasers and Electro-Optics (CLEO'95)*, paper CME3, pp. 20-21, 1995.

[5] K. S. Lee and C. Shu, "Optical matrix for two-dimensional array devices," in *Tenth International Conference on Integrated Optics and Optical Fibre Communication (IOOC'95)*, paper TuD2-4, pp. 79-80, 1995.

Appendices

The optical source for the researches in this thesis is a cw mode-locked neodymium-YAG solid-state laser. Its operation wavelength is 1.319 μm, the pulse width is about 100 ps, and the repetition rate is 82 MHz. The primary objectives of these appendices are to discuss the corresponding laser actions, to describe the practical operations of the commercial Nd:YAG laser used in our experiments, and to explain the mode-locking process.

Appendix 1 The 1.319 μm Nd:YAG laser system

A1.1 The laser action of the Neodymium-YAG solid-state laser

The Nd:YAG laser is one of the common solid-state lasers which is made by doping a rare earth element, neodymium, into a crystalline yttrium aluminum garnet ($Y_3A_{l5}O_{12}$) or YAG. The pure YAG is an optically isotropic crystal and its lattice characteristics is based on the cubic structure of garnets. The population of the yttrium ions (Y^{3+}) is about 3% in the YAG crystal, and the neodymium atoms can substitute some of them in order to form a Nd:YAG laser active medium. The number of substitutions, however, can not be very large because the size of neodymium is different from Y^{3+}, the crystal will become strained if a large amount of neodymium atoms are introduced. Typically, the neodymium is about 1% of the total number of atoms in a laser rod. With the substitutions, these active atoms are in the well-defined environment, so their energy levels are also well-defined and narrow in the YAG crystal lattice [1].

The neodymium atoms participate in the laser action as if they were triply ionized, Nd^{3+}, and its energy levels are broadened to a cluster of energy states in the host lattices. The YAG crystal is charge neutral and the three electrons of Nd^{3+} ions are bonded to the neighboring atoms of the host. The energy levels of neodymium in YAG is shown in figure A1-1, and the dominant laser transition is at $\lambda_0 = 1.0641$ μm from the $^4F_{3/2}$ upper level to the $^4I_{11/2}$ lower level at 300 °K. The laser transitions in Nd:YAG medium are primarily broadened by phonons at the room temperature, and the details in the cluster of energy states are shown in figure A1-1(b). Note that the weaker laser transitions are also possible from the same upper energy level to the cluster of states at energy level $^4I_{13/2}$ for four different

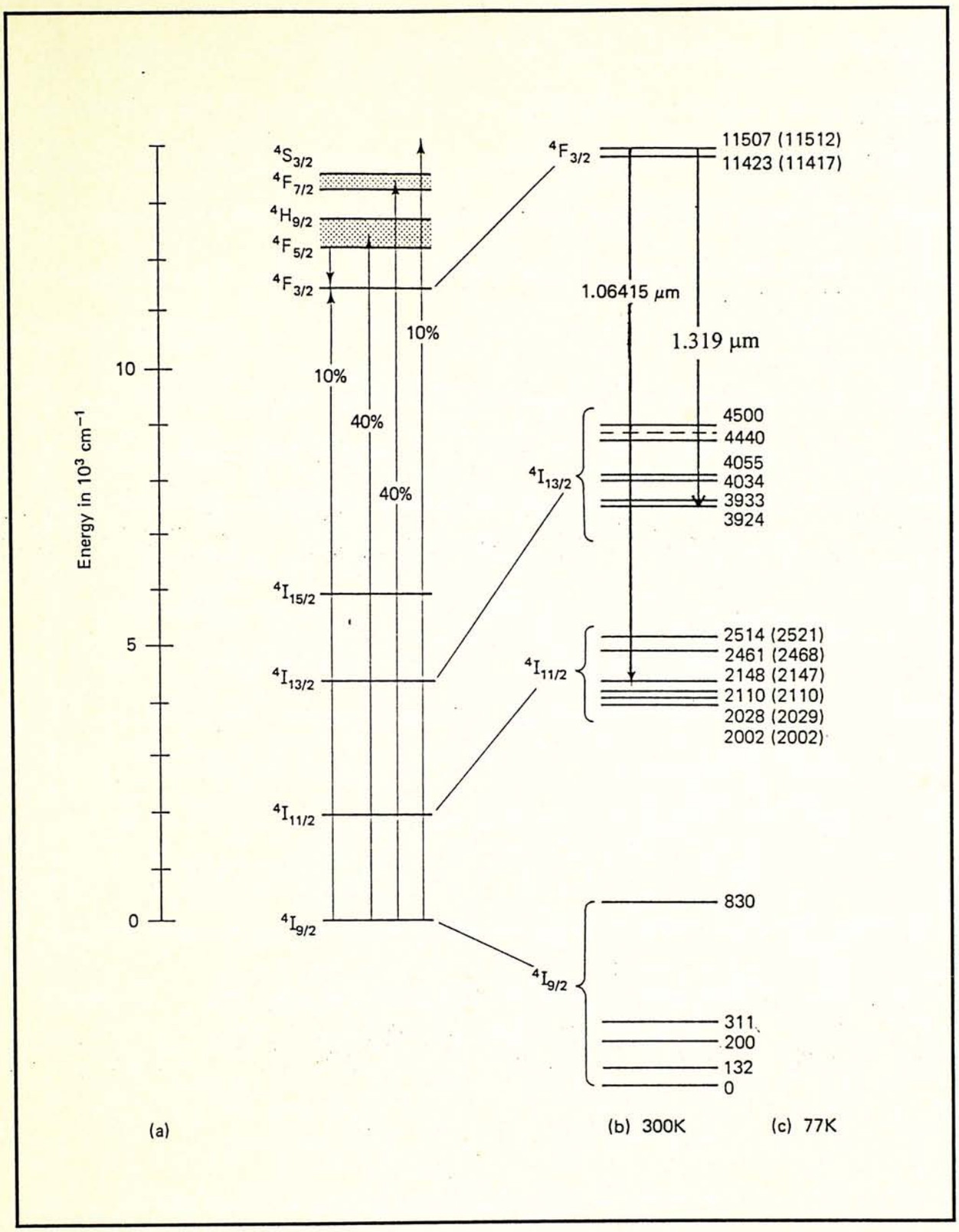

Figure A1-1 The energy levels for neodymium in YAG [1]. (a) The structure of YAG with pumping routes, in which the percentages refer to the optical pump with a broad spectrum. (b) The details of energy level at 300 °K. (c) The energy levels at 77 °K.

wavelengths between 1.319 μm and 1.358 μm [2], in which the transition for wavelength of 1.319 μm is desired in the optical fiber communications, the reasons have been explained in chapter I. Table I summarized all the possible laser transitions from the $^4F_{3/2}$ upper level in a Nd:YAG laser system. The required wavelength can be selected out by using a narrow band optical filter, such as etalon, in the laser cavity.

Laser transitions	Wavelengths (μm)
$^4F_{3/2} \rightarrow {}^4I_{9/2}$	0.89 — 0.95
$^4F_{3/2} \rightarrow {}^4I_{11/2}$	1.05 — 1.12
$^4F_{3/2} \rightarrow {}^4I_{13/2}$	1.30 — 1.36
$^4F_{3/2} \rightarrow {}^4I_{15/2}$	1.74 — 2.13

Table I *The possible laser transitions from the metastable $^4F_{3/2}$ level in a Nd:YAG active medium [1,2].*

In the optical pumping process, the typical routes are shown in figure A1-1(a). The approximately 10% of the optical energy can be directly absorbed by the upper manifold level of $^4F_{3/2}$, whereas, the remained energy will go to the higher energy levels but eventually be returned to the $^4F_{3/2}$ level. Therefore, the $^4F_{3/2}$ level has high population density of electrons. As the fluorescent lifetime of this level is about 255 μs which is much longer than that in the lower energy levels, the population inversion is possible to be achieved and the laser actions can be started.

The measured spontaneous lifetime for the laser transition at λ_0 is 550 μs [3]. After the laser action, the population density of electrons in the lower laser level of $^4I_{11/2}$ in which the transition lifetime of electrons to the ground level is about 30 ns is decayed quickly, the corresponding radiation is then strongly absorbed by the crystal and eventually converted into the heat. As the YAG has high thermal conductivity, the generated heat can be removed simply by conduction efficiently. The laser oscillation threshold of the Nd:YAG system is very low, so it can be operated under either continuous wave (CW) or pulsed modes [4]. Besides, as the absorption band in Nd:YAG active medium is narrow, the optical spectrum of the pump should be well-matched with it in order to obtain the high efficiency in energy transference. The krypton lamp and the recently developed high-power semiconductor lasers can be used for this purpose.

A1.2 The four-level laser system

For the purposes of analyzing the laser actions in the Nd:YAG system, a complicated set of energy levels, as shown in figure A1-1(b), can be simplified into the idealized four-level model, because it can provide a simple but accurate analytical mean for many real laser systems. In figure A1-2, the four-level laser model is shown. The energy level E_4 represents the combination of all energy levels lying above E_3 which is the metastable upper laser level. The levels E_2 and E_1 represent the lower laser level and the ground level in the system, respectively. All other energy levels present in the Nd:YAG active medium are ignored because they have no real function for the laser action. To analyze the laser transitions in the Nd:YAG system, a set of relevant rate equations for the four-level model should be used [2]. Assume that the optical pumping process produces a stimulated pump transition probability $W_{14} = W_{41} = W_p$ from level E_1 to level E_4, the rate equation at

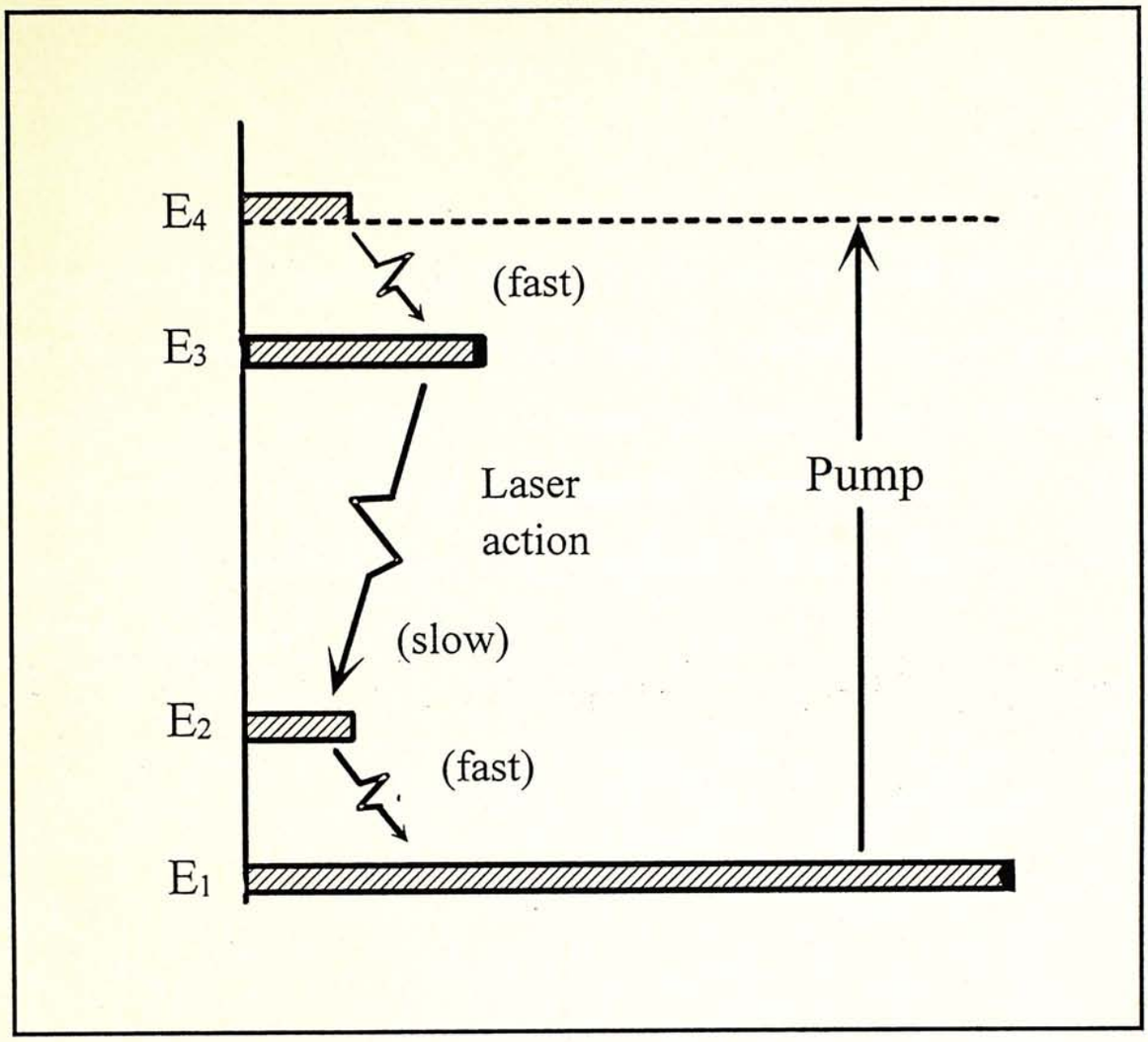

Figure A1-2 An idealized four-level laser system for Nd:YAG laser. E_3 and E_2 represent the upper and the lower laser levels, respectively.

level E_4 is

$$\frac{dN_4}{dt} = W_p(N_1 - N_4) - \frac{N_4}{\tau_4} \tag{1}$$

where N_4 and N_1 are the population densities of electrons in the excited level E_4 and the ground level E_1, respectively, and τ_4 is the lifetime for decay in level E_4 to all other lower energy levels. So, when $dN_4/dt = 0$, the steady state is achieved in level E_4 and the population density is given by

$$N_4 = \frac{W_p \tau_4}{1 + W_p \tau_4} N_1 \approx W_p \tau_4 N_1 \tag{2}$$

if the normalized pumping rate $W_p\tau_4 << 1$. The directly optical pump of electrons from the ground level to the upper laser level E_3 is often negligible in this model, because the absorption in level E_3 is weaker than that in level E_4 and the electron transition from level E_1 to level E_3 is much narrower than that in level E_4 which is made up with a group of strong absorption bands. Therefore the rate equations for levels E_3 and E_2 are

$$\frac{dN_3}{dt} = \frac{N_4}{\tau_{43}} - \frac{N_3}{\tau_3} \tag{3}$$

and

$$\frac{dN_2}{dt} = \frac{N_4}{\tau_{42}} + \frac{N_3}{\tau_{32}} - \frac{N_2}{\tau_{21}} \tag{4}$$

respectively, where τ_3 is the lifetime for decay in level E_3 to all other lower levels, τ_{ij} is the relaxation time for electron transition from energy level i to level j, and N_3, N_2 are population densities of electrons in the levels E_3 and E_2, respectively. Thus at the steady state of level E_3 ($dN_3/dt = 0$), its population density becomes

$$N_3 = \frac{\tau_3}{\tau_{43}} N_4 \tag{5}$$

In a good laser system, the relaxation rate of electron transition from level E_4 to level E_3 is very fast, and the upper laser level E_3 has a long lifetime for decay compared with that in level E_4, so $\tau_3 >> \tau_{43}$ and hence $N_3 >> N_4$.

By combining the equations (4) and (5), the population density in the lower laser level E_2 at its steady state is

$$N_2 = (\frac{\tau_{43}\tau_{21}}{\tau_{42}\tau_3} + \frac{\tau_{21}}{\tau_{32}})N_3 = \beta N_3 \tag{6}$$

where the parameter β is defined as

$$\beta \equiv \frac{\tau_{43}\tau_{21}}{\tau_{42}\tau_3} + \frac{\tau_{21}}{\tau_{32}} \tag{7}$$

Therefore, the population densities in levels E_2 and E_3 depends only on the parameter β which is a relaxation-time ratios, not a absolute values. If β is less than unity, then the steady-state result will be $N_2 < N_3$, which means that there is a population inversion between the upper laser level E_3 and the lower laser level E_2.

In general, for a good laser system, the electrons in level E_4 is relaxed primarily into upper laser level E_3, so that the relaxation time τ_{42} between levels E_4 and E_2 is infinite. Thus $\beta \approx \tau_{21} / \tau_{32}$ and the condition for the desired population inversion becomes

$$\beta = \frac{N_2}{N_3} \approx \frac{\tau_{21}}{\tau_{32}} << 1 \tag{8}$$

Besides, with a good inversion between levels E_3 and E_2, the electrons should be relaxed out from laser level E_2 down into the lower levels much faster than other relaxations from upper levels into level E_2. If the upper laser level has long lifetime (both the τ_{32} and τ_3 long) and the lower laser level has a short lifetime (τ_{21} short),

then the population inversion between levels 3 and 2 can be obtained, and the laser action can be initiated.

A1.3 The installation and operations of a 1.319 μm Nd:YAG laser

For the experiments in this thesis, our optical source is a 1.319 μm cw mode-locked Nd:YAG laser with repetition rate of 82 MHz, mode-locked pulse width of 100 ps and output peak power of 180 W. There are four main parts in this commercial laser system (Quantronix Model 4116E ML): the Nd:YAG optical configuration, the mode locker with RF driver unit, the logic control unit, and a main control unit. Their special functions and practical operations will be described individually as follows.

Nd:YAG optical configuration: A Nd:YAG crystal rod is used as the source of photons at wavelength of 1.319 μm in which the Yttrium Aluminum Garnet (YAG) crystal is the host materials for the active element of neodymium. The laser rod is optically pumped with a cylindrical krypton lamp (EG&G Electro-Optics Ltd.) and the emitted photons are directed into the optical cavity constructed by a pair of mirrors. The rear mirror is highly reflective and the front mirror is partially transmissive, thus the laser beam can be emitted from the front mirror at the left side of the system. The corresponding optical configuration is shown in figure A1-pI. The Nd:YAG crystal rod and the krypton lamp are already installed inside the white laser pot in which both of the crystal rod and the lamp are individually fitted into the glass enclosures aligned at the parallel plane of the pot and they are cooled by the continuously circulating deionized water. The lifetime of the Nd:YAG crystal rod is infinite and the operation period of the Krypton lamp is dependent on the supplied current. Figure A1-3 shows the lifetime of a krypton lamp, and figure A1-pII shows

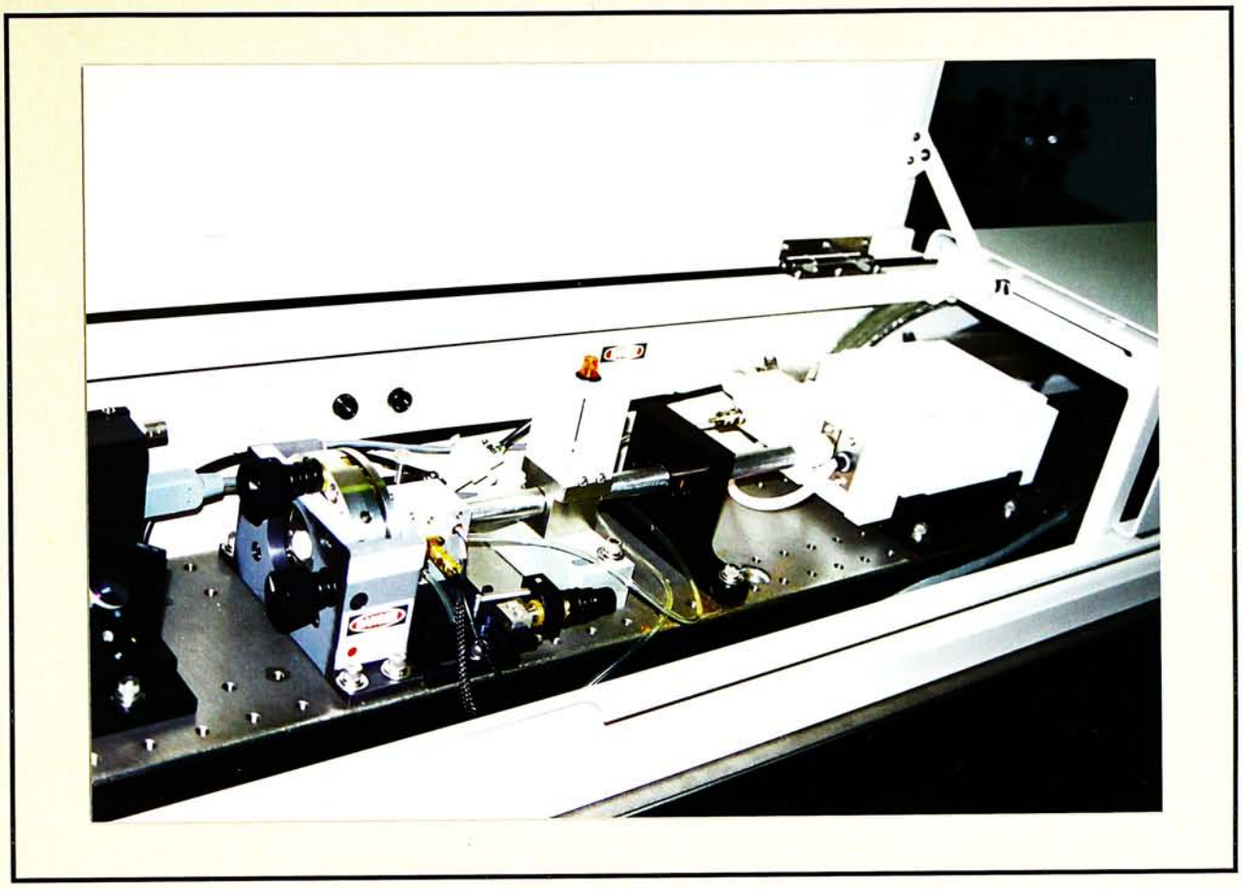

Figure A1-pI The optical configuration of the cw mode-locked 1.319 μm Nd:YAG laser. (Quantronix Model 4116E ML)
White box — Laser pot
Black mount — Variable aperture
Silver box (with indicator) — Electro-mechanical shutter
Silver box (without any indicator) — Acousto-optic mode locker
Silver mount with X and Y adjustments — Holder for the front mirror

the Krypton lamp used in our setup. The supplied current for the pumping lamp during our experiments is usually 29.5 amperes and the average laser output power is about 2 W. In the laser pot, an elliptical gold reflector with the highly polished surface is used to envelope the YAG rod and the lamp at its focuses, so that most of the light from the pump can be directed into the laser rod. In the first instillation of the system, distilled water should be used as the circulating primary water because some ions are need to be introduced for both the laser rod and the krypton lamp to stabilize and optimize their operations. Besides, both the front and the rear mirrors incorporate X and Y axis adjustments to facilitate the optical alignment for

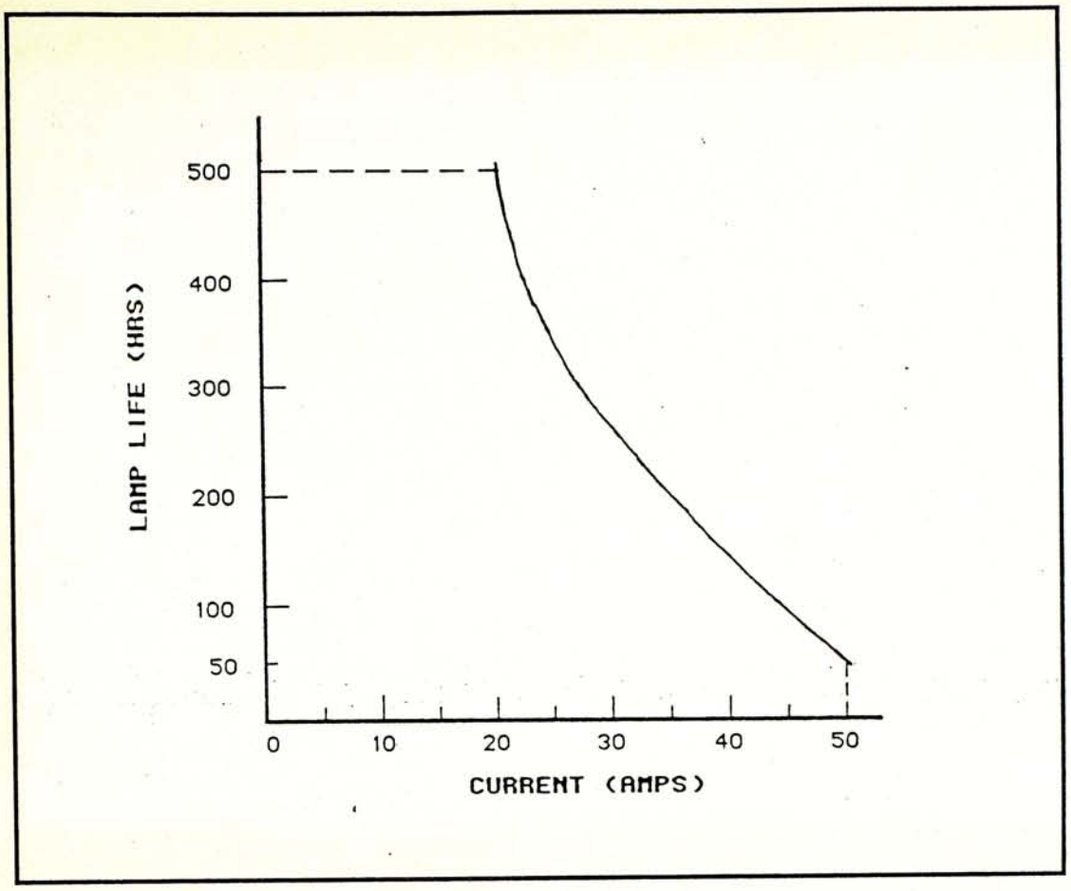

Figure A1-3 The nominal lifetime of the Krypton pumping lamp for Nd:YAG laser rod [5].

optimum laser performance. A variable aperture is fitted into the laser cavity and placed in front of the laser pot to establish the TEM_{00} mode operation in the laser output, and the X and Y axis adjustments are used to permit its correct position with respect to the central part of the laser beam in order to prevent the clipping, therefore the maximum power output is ensured. A polarizer installed inside the large black box in front of the rear mirror is simply a wedge mounted at the Brewster's angle, it can make the state of polarization in the TEM_{00} output beam linearly vertical. An electro-mechanical shutter installed inside the silver box with a small indicator is placed in the laser cavity to totally stop the lasing action when necessary. A partially reflective mirror is fitted in front of the laser output window in order to split a small portion of the light to a photodetector for feedback and power controls.

Figure A1-pII The Krypton lamp.

A etalon is also installed in the laser cavity to select the 1.319 μm laser oscillation from the Nd:YAG active medium and to suppress other possible laser actions. The output beam diameter is 0.9 mm and the angle of divergence is 2.4 mrad in our laser configuration.

Mode locker with the RF driver unit: For the generation of short optical pulses, the active mode locking is preferred in our 1.319 μm Nd:YAG laser system. The required theories have been discussed in appendix 2. This operation is achieved by using an acousto-optic mode locker together with a radio frequency driver unit. The acousto-optic modulator (Model 372) placed in the laser cavity, as shown in figure A1-pI, acts as a very fast optical switch and is located adjacent to the front mirror. Its modulation frequency is 41 MHz [6] and the matched cavity length is

182.9 cm, so the corresponding repetition rate of the output pulse train is 82 MHz. Moreover, the pulse width is dependent on the number of longitudinal modes in the laser cavity, for a Gaussian pulse profile with no frequency chirp, the pulse width Δt and frequency bandwidth Δv product is given by

$$\Delta t \cdot \Delta v = 0.5 \tag{9}$$

Therefore, the output pulse width can be reduced when larger optical bandwidth is obtained. The measured pulse width in our laser outputs is about 125 ps and the corresponding bandwidth is about 0.23196 Å. The measured optical bandwidth of the outputs is shown in figure A1-4, this measurement may be limited by the resolution of the optical spectrum analyzer. In the acousto-optical modulator, the acoustical wave produces a periodic variation in the refractive index of the crystal, and this result can scatter the incident laser beam. If the angle between the acoustical beam and the laser beam is adjusted to be the Bragg angle θ_B, the laser beam is then scattered and the low loss modulation can be achieved. This relationship can be determined by

$$\sin\theta_B = \frac{\lambda_o}{2\lambda_s} \tag{10}$$

where λ_o and λ_s are the optical and acoustical wavelengths, respectively. The acousto-optical interaction is polarization independent here. The required acoustical frequency for the mode locker is generated by the 372 RF driver unit with a impedance matched RG-174 cable [6]. This special cable is used to reduce the power reflection during the RF transmission. Our RF driver unit is shown in figure A1-pIII. The power monitor on it can continuously monitor the RF transference to the mode locker and the internal RF power generation is adjustable. The low

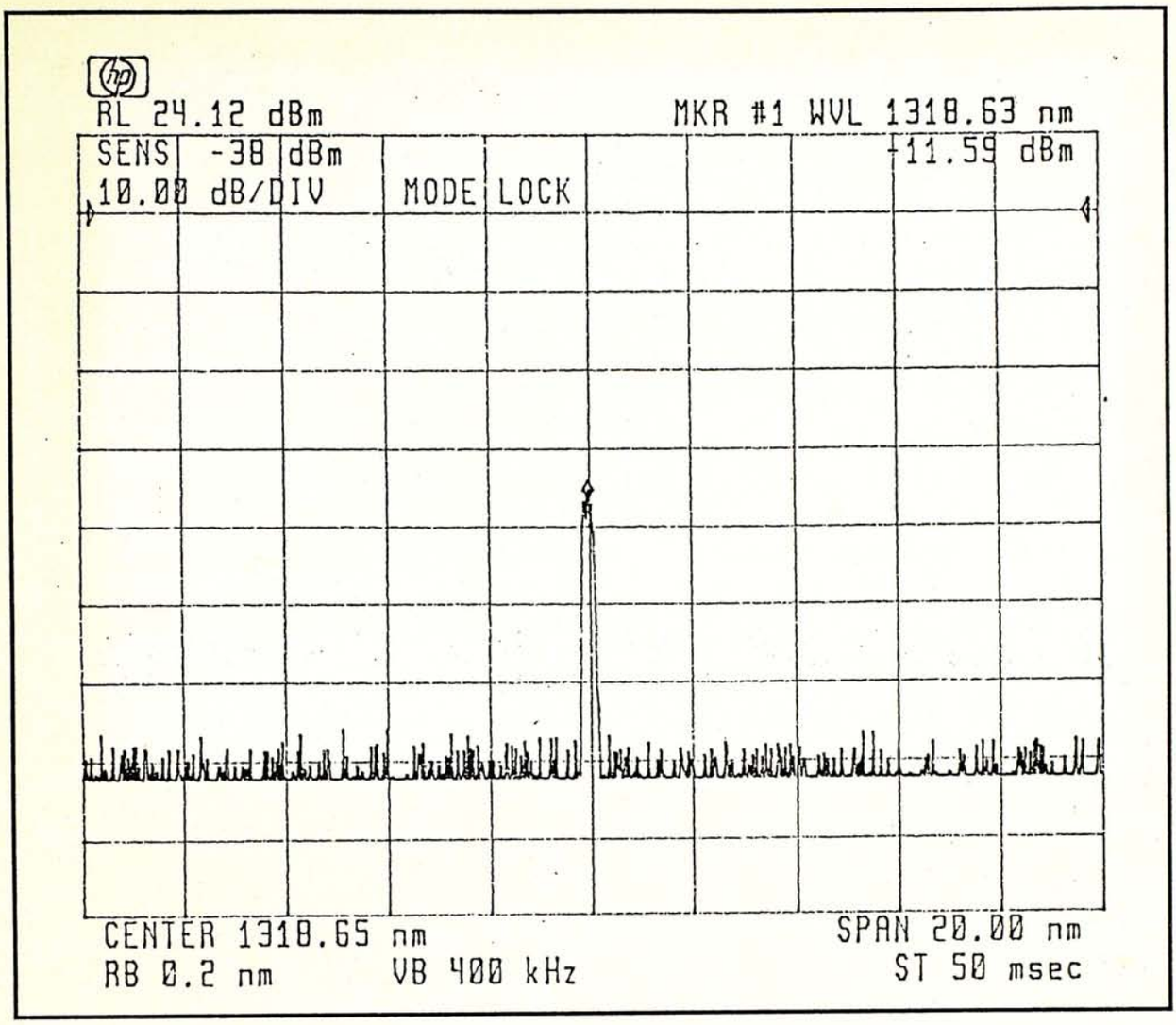

Figure A1-4 The measured bandwidth of the Nd:YAG laser with the active mode-locking operation.

reflection means that the acousto-optical modulator is received the high RF power, thus it can be effectively operated for the mode-locking process. An external RF frequencies can also be introduced to the mode locker through the driver unit for changing the modulation frequency in the mode-locking process, but the power level should not be exceeded 17.6 mW and no DC voltage can be applied. With a loop control, the driver unit can lock and control the temperature of the acousto-optical modulator, and four indicators can continuously show the situation of temperature control in the mode locker during the actual mode-locking process. Therefore, the operation conditions of the acousto-optic modulator will be stabilized

Figure A1-pIII The RF driver unit for the acousto-optic mode-locker. The output frequency is 41 MHz.

and the mode-locking process can be achieved effectively.

Logic control unit: This logic unit (Model 224 Logic Unit) consists of a power control unit and a primary cooling system, it is shown in figure A1-pIV. The function of the power control unit is to monitor and adjust the high voltage and the high current supplies of the laser pumping lamp [7]. To start the Krypton lamp, the high voltage igniter apply a 20 kV electrical pulse to its anode approximately every 4 seconds for a period of 20 seconds. This high voltage is sufficient to ionize the gas in the lamp and start its conduction. The arc across the lamp is sustained by the "boost voltage" of approximately 375 volts. When the lamp is conducting, the stable running voltage is 130 volts. In general, the first one or two voltage pulses

Figure A1-pIV The logic control unit, in which a power control unit and a primary cooling system are installed.

available during the 20 second triggering period can ignite the krypton lamp, but if all the five pulses fail to ignite it, the triggering sequence is automatically terminated. When it happens, the LASER switch on the "main control unit" must be turned off for at least five seconds, and turn it on again for the new triggering sequence. For controlling the current flow to the optical pump, a ammeter is located in the cathode return circuit of the lamp for continuously monitoring the supplied current. The threshold current of the lamp is at 25.5 amperes and the operation current is suggested to be 29.5 amperes. The external power supply for the whole "logic control unit" and the pumping lamp is from a three phase 208 V alternative voltage supply, which is stepped down from the 380 V main supply already installed in our laboratory. Besides the power control unit, the function of the primary

cooling system is to adjust and stabilize the temperature of the Nd:YAG laser rod, the krypton lamp and the mode locker. This system consists of a primary cooling route and a electronic feedback system. In the primary cooling route, as shown in figure A1-5, the cold water is drawn from the reservoir installed in the "logic control unit" by the water pump, one portion of it is directed to the laser pot and the mode locker after passing through the particle filter, whereas another portion is pumped back to the reservoir through the deionizer cartridge. The operation of the primary water flow is monitored by a flow switch which shuts down the whole laser system under improper flow conditions due to an obstruction or loss of coolant. A level switch mounted in the reservoir also shuts the system down if the water level is dropped below a predetermined point. An electro-mechanical solenoid is used to regulate the process of the heat exchange between the secondary cooling route and

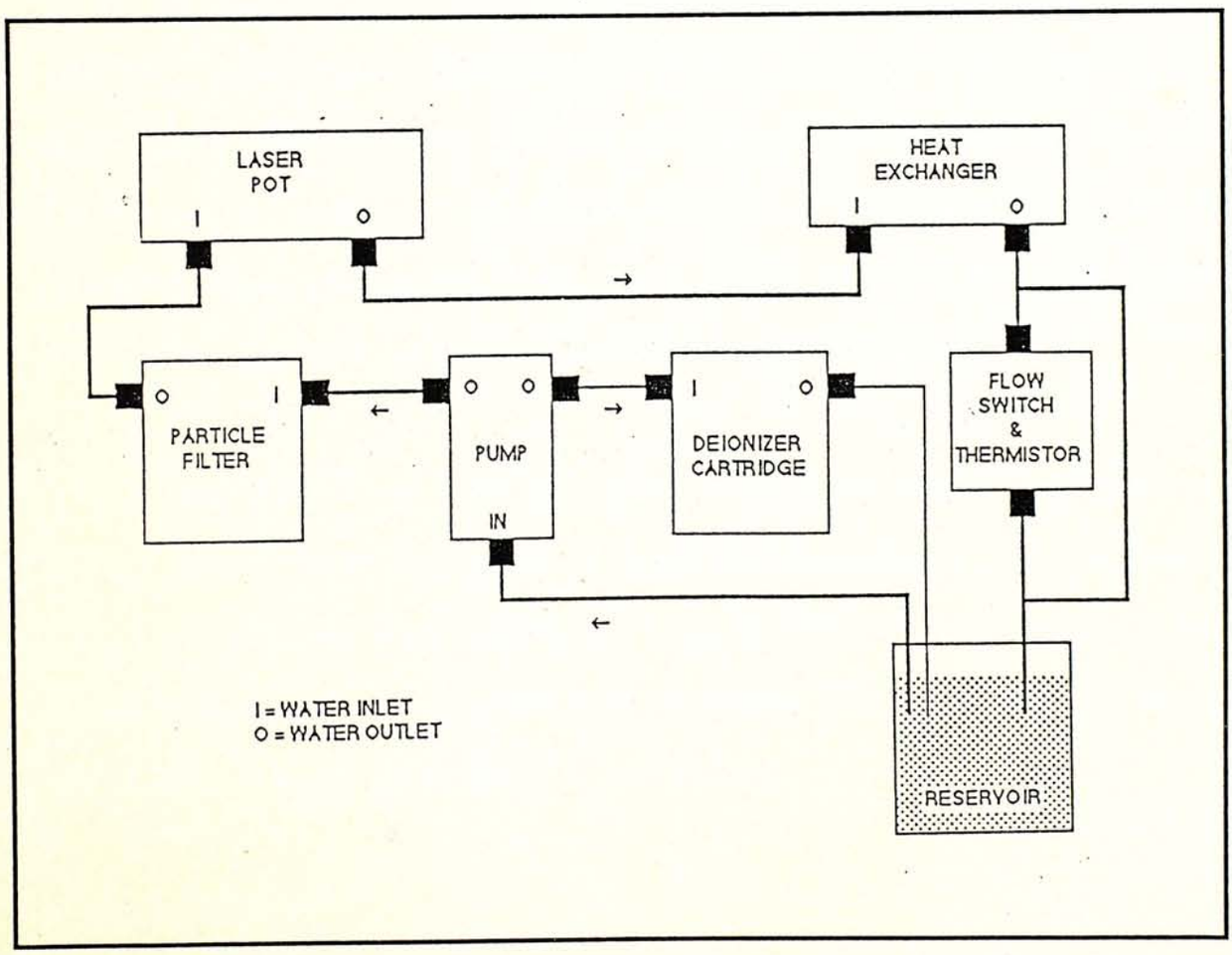

Figure A1-5 The primary cooling route in the logic control unit [7].

the heat exchanger. A thermistor installed in the flow path between the heat exchanger and the primary reservoir is used to monitor the primary water temperature. So, the thermostatic control in the solenoid is accomplished by a thermal logic unit which continuously receives the temperature signals of the primary water from the thermistor. The water temperature in the primary cooling route is already maintained between 25 °C and 30 °C with the thermal logic unit. When the temperature exceeds 30 °C, the system is automatically shut down. The heat in the primary water is finally exchanged to the secondary water. The secondary water refers to the outside water supply used to cool the primary water in the heat exchanger inside the "logic control unit". The secondary cooling route is comprised by a industrial chiller from Sam-chin water machines Ltd. (SC-010A) and a water filter. The temperature in the secondary water should be controlled in the range between 7 °C and 18.5 °C. The industrial chiller consists of a reservoir, a high efficiency water pump with bypassed outlet, a compressor with coolant, and a cooling fan. The maximum allowed inlet pressure in this cooling route is 5.6 kg/cm^2 and the minimum water flow rate is at 3 gallons per minutes. The heat generated from the Krypton lamp, the Nd:YAG rod and the mode locker is eventually removed by the cooling fan in the second cooling route.

Main control unit: On the control panel of this unit, a operation control knob, a shutter switch, and a set of data-input keys are designed. All operations and logic functions of the laser system can be controlled with it. The control unit is shown in figure A1-pV. The following procedures for the operations of the high-power Nd:YAG laser are suggested to be followed.

Figure A1-pV The main control unit of the Nd:YAG laser system.

The Nd:YAG laser system can be turned on by the following steps:

1. Turn on the chiller and adjust the water temperature between 10 °C and 18 °C, and wait for about 5 minutes,
2. Verify that the shutter switch on the main control unit is set to OFF position,
3. Switch the operation control knob clockwise to the CONTROLS position in order to switch on the "logic control unit" and the main power supply of the whole system, and wait for 5 second,
4. Set the same knob to the COOLER position in order to switch on the primary cooling system, and wait for 10 minutes,
5. Wear the laser protective goggles,

6. Switch the same knob to the LASER position in order to start the electrical triggering for the krypton lamp, both the indicators on the shutter case and the laser case will illuminate,
7. Turn on the shutter switch, and use the data-input keys on the control panel to adjust the supplied current of the krypton lamp to the desired level, (29.5 amperes is suggested here)
8. Wait at least 10 minutes to allow the temperature of the Nd:YAG laser rod becoming stable,
9. If necessary, open the front laser case and adjust the X and Y axis adjustments of the front mirror in order to obtain the maximum optical power,
10. If the mode locking operation is required, turn on the mode locker RF driver unit,
11. Wait until the RF power reflection is minimized,
12. Adjust the X and Y axis adjustments of the front mirror in order to get the maximum optical power.
13. If the pulse width is broadened and pulse time jitter is serious, tune the position of the wedge with a small knob at the rear part of the laser case,
14. Adjust the X and Y axis adjustments of the front mirror again to obtain the maximum optical power.

For switching off the laser system, the following steps should be followed.

1. Turn off the mode locker RF driver unit if applicable,
2. Set the shutter switch to the OFF position
   (The protective goggles may be taken off now)
3. Reduce the current of the krypton lamp to about 15 amperes,
4. Switch the operation control knob counterclockwise to the COOLER position,
5. Wait at least 10 minutes to allow the reduction of temperature of the Krypton lamp and the laser rod,
   (This additional step is based on our experience, it can make the electrical triggering of the krypton lamp fairly easy when the laser system is restarted.)
6. Switch the same knob to the CONTROLS position, and then
7. Turn off the laser by switching the same knob to the OFF position,
8. Turn off the chiller.

References

[1] J. T. Verdeyen, *Laser Electronics,* Prentice Hall, 1989.

[2] A. E. Siegman, *Lasers*, University science books, 1986.

[3] T. Kushida, H. M. Marcos and J. E. Geusic, "Laser transition cross section and fluorescence branching ratio for Nd^{3+} in yttrium aluminum garnet," *Phys. Rev.*, vol. 167, p. 1289, 1968.

[4] A. Yariv, *Optical electronics*, Saunders college publishing, 1991.

[5] Quantronix technical manual, series 100 lasers, p.4-3.

[6] Technical manual, *document number: 51A04818 for Quantronix closed loop mode locker driver system*, Neos Technologies Inc., 1993.

[7] Quantronix technical manual, model 416 lasers.

Appendix 2 Mode-locking in the Nd:YAG Laser

A2.1 The mode-locking technique

In the generation of the ultra-short optical pulses, the mode locking technique is more convenient and effective among all other optical methods. With Q-switching of the solid state lasers and gain-switching of the semiconductor laser diodes, the width of the generated pulses is from nanosecond to picosecond time scales. However, by using the mode-locking technique in the solid-state laser, the pulse width can be reduced to femtosecond time domain. To date, the shortest optical pulse generated by this technique is at 4.8 femtoseconds [1]. Therefore, the 1.3 μm or 1.55 μm lasers with mode-locking operation is a good optical source for high-speed communications.

The general equation to describe the n th mode electromagnetic field in a laser is

$$E_n(t) = A_n \exp j[(\omega_o + n\omega_c)t + \phi_n] \tag{1}$$

where A_n , ϕ_n and ω_c are the amplitude, phase term and mode spacing, respectively. The ω_c is equal to c/2L where L is the cavity length. The phase term is very important in the mode-locking process. With superposition of all modes in the laser cavity, the total electromagnetic field is [2]

$$E_T(t) = \sum_{-(N-1)/2}^{+(N-1)/2} A_n \exp j[(\omega_o + n\omega_c)t + \phi_n] \tag{2}$$

Assume that all N modes have the same amplitude ($A_n = A_o$), hence the total intensity is given by

$$I(t) = \frac{A_o^2}{2\eta}\left[\frac{\sin(N\omega_c t/2)}{\sin(\omega_c t/2)}\right]^2 \tag{3}$$

When $\omega_c t/2$ is an integral multiple of π and η is the wave impedance. This intensity is N^2 times the intensity per mode. As we have assumed N equal amplitude modes, the average power $P_{average}$ of the laser is N times the power per mode. Thus the pulse peak power is approximately N times of the average power and given by

$$P_{peak} = N \times P_{average} \tag{4}$$

The pulse train is produced with the repetition rate R of

$$R = 2L/c \tag{5}$$

where L is the cavity length. It is, indeed, the round trip time of photons. The pulse width is given by

$$\tau_p \approx \frac{1}{\Delta\nu} \tag{6}$$

where $\Delta\nu$ is the width of the laser gain spectrum or linewidth. Thus the pulse width will be reduced when the laser linewidth is broader. Note that there is no chirp obtained in the mode-locked pulses.

In practice, two basis techniques can be used for the mode-locking process, they are active mode locking and passive mode locking. In the former technique, both the electro-optic and acousto-optic modulators can be used in the laser cavity to modulate the intensity or the phase of the cavity modes; whereas in the later method, the saturable absorber is used in the laser cavity. For the laser source in our researches, the active mode locking is preferred.

In the cw 1.319 μm Nd:YAG laser, the intensity acousto-optic modulator is used for the mode-locking process. With a mode locker located adjacent to the front mirror or the output window in the optical cavity, the period of the modulation is exactly equal to the round trip time of the photons, so a small optical pulse can travel through both the mode locker and the output mirror during the low loss state of the modulator. As the result, the laser oscillation is permitted at this moment and the amplitude of such pulse can be grown to a stable value. With the sinusoidal modulation from the mode locker, this laser oscillation comprises the optical pulses travelling back and forth in the resonant cavity and pass through the modulator twice in each round trip at its minimum loss. So the optical outputs consist of the repetitive pulses with separation equal to the round trip time, and a portion of these pulses is reflected back to the optical cavity by the output mirror for laser oscillations in the following outputs. The proper modulation frequency f_o of the mock locker in this setup is one-half of the inverse of the round trip time T [3], the relationship is defined by

$$f_o = \frac{1}{2T} = \frac{c}{4L} \tag{7}$$

where L is the cavity length and c is the speed of light in free space. So the modulation frequency and the cavity length should be well-matched in order to

generate the stable outputs. In our mode-locked Nd:YAG laser, the modulation frequency is 41 MHz, the matched cavity length is 182.9 cm, and the repetition rate of the output pulses is 82 MHz.

References

[1] K. M. Yoo, W. Zhang, C. Y. Wang, Q. Xing and K. F. Lee, "Observation of 5-fs pulses from a self-Q-switched self-mode-locked Ti:sapphire laser," in the Pacific Rim Conference on Lasers and Electro-Optics (CLEO/Pacific Rim '95), paper PD1.8, 1995.

[2] J. T. Verdeyen, *Laser Electronics,* Prentice Hall, 1989.

[3] Quantronix technical manual, model 416 lasers.